NASA CR-175006
AiResearch 85-22592

IMPROVED SILICON NITRIDE FOR ADVANCED HEAT ENGINES

Annual Technical Report No. 1

September 26, 1984 - September 30, 1985

October 15, 1985

AIRESEARCH CASTING COMPANY
A DIVISION OF
THE GARRETT CORPORATION
Torrance, California

Prepared for

NATIONAL AERONAUTICS AND SPACE ADMINISTRATION

Lewis Research Center

Contract NAS3-24385

NASA

1. Report No.	2. Government Accession No.	3. Recipient's Catalog No.
NASA CR-175006		

4. Title and Subtitle	5. Report Date
IMPROVED SILICON NITRIDE FOR ADVANCED HEAT ENGINES	October 15, 1985
	6. Performing Organization Code

7. Author(s)	8. Performing Organization Report No.
H.C. Yeh, J.M. Wimmer, H.H. Huang, M.E. Rorabaugh, J. Schienle, K.H. Styhr	85-22592
	10. Work Unit No.

9. Performing Organization Name and Address	11. Contract or Grant No.
AiResearch Casting Company A Division of The Garrett Corporation Torrance, California 90509	NAS3-24385
	13. Type of Report and Period Covered
12. Sponsoring Agency Name and Address	Annual Technical Report 9/26/84 to 9/30/85
National Aeronautics and Space Administration Washington, D.C. 20546	14. Sponsoring Agency Code

15. Supplementary Notes

Project Manager, Marc R. Freedman
NASA - Lewis Research Center,
Cleveland, Ohio 44135

16. Abstract

The AiResearch Casting Company baseline silicon nitride (92% GTE SN-502 Si_3N_4 + 6% Y_2O_3 + 2% Al_2O_3) was characterized with methods that included chemical analysis, oxygen content determination, electrophoresis, particle size distribution (PSD) analysis, surface area determination, and analyses of degree of agglomeration and maximum particle size of elutriated powder. These analyses were conducted on as-received powder as well as on sized powder. Test bars were injection molded and processed through sintering at 0.68 MPa (100 psi) of nitrogen. The as-sintered test bars were evaluated by X-ray phase analysis, room and elevated temperature modulus of rupture (MOR) strength, Weibull modulus, stress rupture, strength after oxidation, fracture origins, microstructure, and density from quantities of samples sufficiently large to generate statistically valid results. A total of 452 test bars were injection molded to provide specimens for the various characterization tests. Of these, 216 were fully processed to provide specimens for the post-processing tests. A mean room temperature strength of 540 MPa (79.3 ksi) with a Weibull modulus of 7.9 was established as baseline using test bars with as-processed surfaces.

A series of small test matrixes were conducted to study the effects and interactions of processing parameters which included raw materials, binder systems, binder removal cycles, injection molding temperatures, particle size distribution, sintering additives, and sintering cycle parameters. Two half-replicated, fractional factorial (2^5), matrix-designed experiments were started as the first iteration of the MOR matrix study. The program goals of this first phase are to improve the test bar MOR values by 20 percent over all test temperatures and to achieve a doubling of the Weibull modulus.

17. Key Words (Suggested by Author(s))		18. Distribution Statement
Ceramics	Statistics	[redacted]
Injection Molding	Properties	
Silicon Nitride	Sinter/HIP	

19. Security Classif. (of this report)	20. Security Classif. (of this page)	21. No. of pages	22. Price*
Unclassified	Unclassified	141	

*For sale by the National Technical Information Service, Springfield, Virginia 22161

FOREWORD

Fabrication and processing of the ceramic specimens was conducted by the AiResearch Casting Company (ACC) at Torrance, California. Assistance with the statistical design of experiments and much of the characterization of materials and specimens was provided by the Garrett Turbine Engine Company (GTEC) Phoenix, Arizona, the major subcontractor.

The principal investigator at ACC was Dr. H. C. Yeh. Mr. David W. Richerson served as coprincipal investigator at GTEC until March 1985. Dr. James M. Wimmer assumed the role of coprincipal investigator at GTEC after March 1985. Mr. Karsten H. Styhr of ACC served as overall program manager. Mr. Marc R. Freedman of NASA Lewis Research Center is project manager. The significant contributions to experimental work and report preparation by Mike E. Rorabaugh, of ACC, and Henry H. Huang and Jim Schienle, of GTEC, are gratefully acknowledged.

TABLE OF CONTENTS

LIST OF ILLUSTRATIONS

LIST OF ILLUSTRATIONS (continued)

LIST OF ILLUSTRATIONS (continued)

LIST OF TABLES

EXECUTIVE SUMMARY

This document, submitted by AiResearch Casting Company (ACC), a division of The Garrett Corporation, is the first annual technical report for the improved silicon nitride for advanced heat engines program. The program is being conducted for the National Aeronautics and Space Administration (NASA) under contract no. NAS3-24385. Garrett Turbine Engine Company (GTEC) is the major subcontractor to this program. This report covers the period September 26, 1984 through September 30, 1985.

The objective of the program is to establish the technology base required to fabricate silicon nitride components that have the strength, reliability, and reproducibility necessary for actual heat engine applications.

The program consists of seven major tasks. The Task I technical effort, baseline characterization, was completed in the first nine months of the program. Current efforts are in Tasks II and VII.

Task I

The major objective of Task I was the complete characterization of the ACC baseline silicon nitride (92% GTE SN-502 Si_3N_4 + 6% Y_2O_3 + 2% Al_2O_3) and the modulus of rupture (MOR) of test bars fabricated by an ACC baseline injection molding process. The characterization methods included chemical analysis, oxygen content determination, electrophoresis, particle size distribution (PSD) analysis, surface area determination, and analyses of degree of agglomeration and maximum particle size of elutriated powder. These analyses were conducted on as-received powder as well as on sized powder. MOR test bars were injection molded and processed through sintering at 0.68 MPa (100 psi) of nitrogen. The as-sintered test bars were evaluated by X-ray phase analysis, room and elevated temperature MOR strength, Weibull modulus, stress rupture, strength after oxidation, fracture origins, microstructure, and density from quantities of samples sufficiently large to generate statistically valid results.

A total of 452 test bars were injection molded to provide specimens for the various characterization tests. Of these, 216 were fully processed to provide specimens for the post-processing tests.

A total of 108 test bars were strength tested at room temperature, 1066°, 1232°, and 1399°C (1950°, 2250°, and 2550°F). The mean strength at room temperature for 66 bars was 540 MPa (79.3 ksi), with a Weibull modulus of 7.9. The mean strengths at 1066°, 1232°, and 1399°F were 420, 320, and 140 MPa (61.1, 47.1, and 21.7 ksi), respectively.

Static oxidation test data on room temperature strength showed that test bars exposed for 200 hours to air in the temperature range of 388° to 1296°C (730° to 2365°F) had a slight strength degradation after oxidation.

Task II

Task II, which was initiated at the completion of Task I, consists of a series of test matrixes designed to establish the optimum materials and processing parameters so that the initial program goal of improving test bar properties will be achieved. Two matrixes (test Matrixes II-1 and II-2) were designed based primarily on information obtained from Tasks I and VII. These two matrixes, which are to be completed in the first seven months of Task II, define a total of 32 experiments, evaluating 6 variables at 2 levels. Continued Task II efforts will include additional matrix experiments and smaller optimization experiments which will be designed using all new available information over the 18-month Task II effort.

In Matrix II-1, powder preparation and powder/binder mixing were initiated using Starck H-1 Si_3N_4 powder with 6 percent Y_2O_3 and 1 percent and 2 percent Al_2O_3. Sufficient material was prepared to make the 1500 test bars required to complete Matrix II-1. Processing was completed through the dewax cycle on 640 test bars during this report period.

Matrix II-2 is similar to Matrix II-1 except that Denka 9FW powder is being evaluated. Mixing is complete and injection molding has been initiated.

Task VII

Task VII is being conducted continuously throughout the program, both to perform screening experiments on advanced materials and processing and to identify critical variables affecting strength and reliability. Task VII includes a series of iterations between experimental design, fabrication, characterization, and analysis. Data from these experiments will provide input for additional Task II optimization experiments.

The first two statistically designed test matrixes involved alternate raw materials and alternate binder systems. Subsequently, Matrixes 3, 4, 5, 6, and 7 (binder removal cycle, molding temperature, particle size distribution, sintering additives, and sintering cycle parameters) are being investigated.

Significant portions of Task VII, primarily involving alternate binder systems, binder removal cycles, and sintering/hot isostatic pressing parameter investigations, are being conducted on internal ACC funding, on a cost-share basis. The results concerned with the demonstration of improved properties and reliability are available in this NASA program. However, some compositional and processing detail will remain proprietary to ACC.

INTRODUCTION

This document, submitted by AiResearch Casting Company (ACC), a division of The Garrett Corporation, is the first annual technical report for the improved silicon nitride for advanced heat engines program. The program is being conducted for the National Aeronautics and Space Administration (NASA) under contract no. NAS3-24385. Garrett Turbine Engine Company (GTEC) is the major subcontractor to this program. This report covers the period September 26, 1984 through September 30, 1985.

The objective of this program is to develop the technology base required to fabricate silicon nitride components that have the strengths, reliability, and reproducibility necessary for actual heat engine applications.

The master program schedule is presented in figure 1. The program consists of two phases of process development. Both phases will be completed in 60 months. Phase I includes fabrication, evaluation, and optimization of test bars. Phase I is divided into four tasks. The objectives of these tasks are:

Task I - Characterize the baseline sintered silicon nitride.

Task II - Use statistically designed matrix experiments to achieve material and process improvements as demonstrated by a 20-percent increase in strength and a 100-percent increase in Weibull modulus.

Task III - Characterize the improved material and process.

Task VII - Perform screening experiments on advanced materials and processing for input to Task II statistically designed experiments.

Phase II includes the fabrication and evaluation of a large complex shape that will be potentially useful in an actual gas turbine engine application. Phase II is divided into four tasks; the objectives of these tasks are:

Task IV - Evaluate the improved process (from Task III) in the fabrication of a large shape and identify critical process variables requiring further improvement due to the scale-up in size.

Task V - Use statistically designed matrix experiments to achieve material and process improvements.

Task VI - Characterize the improved material and process.

Task VII - Continue screening experiments, especially those related to the requirements of the large size.

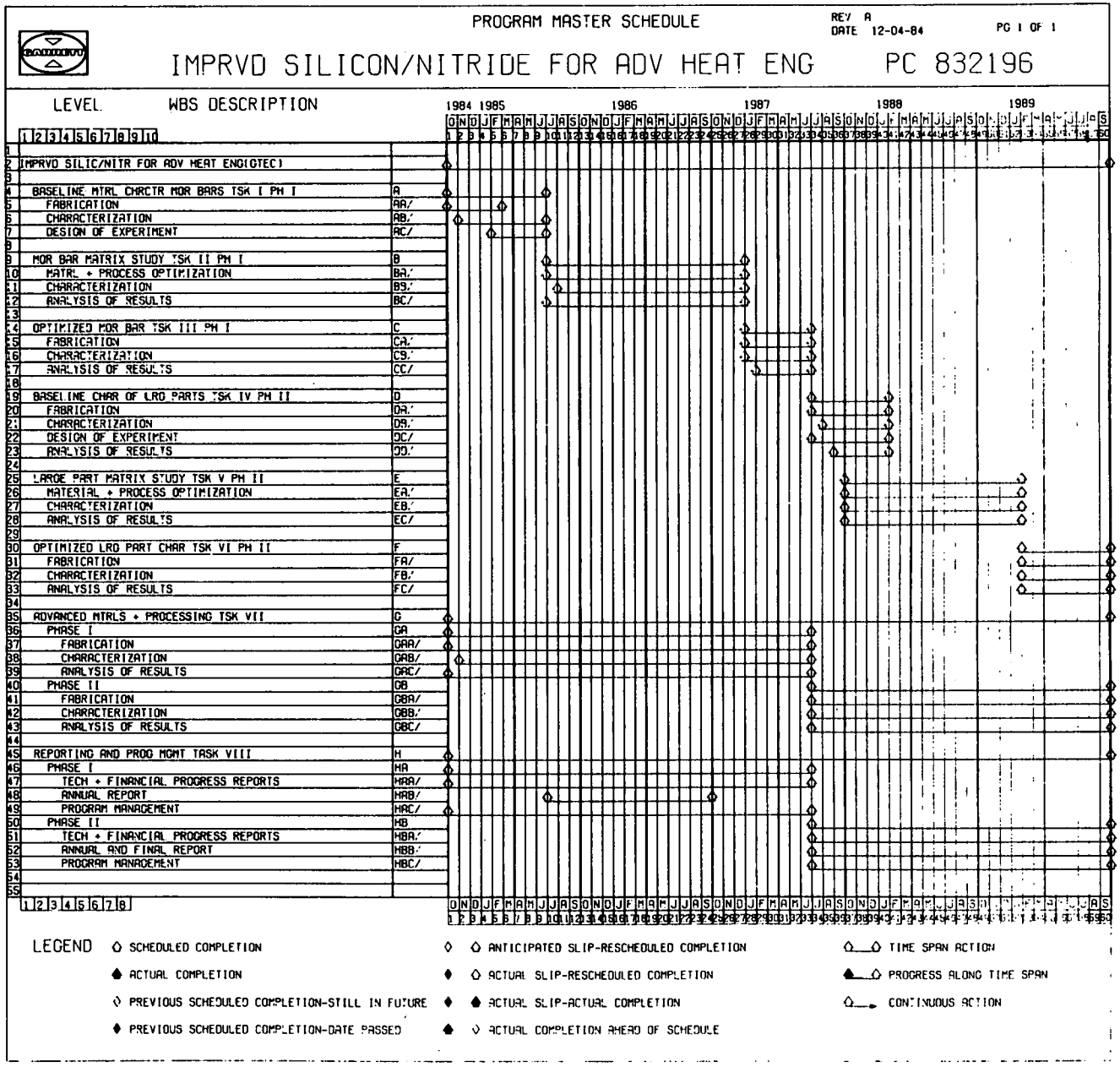

Figure 1.--Master program schedule.

More than 40 variables have been identified for study. Experiments are being performed in a series of iterations between experimental design, processing, characterization, and analysis. Critical variables are being identified in these experiments. Interactions between variables will be identified and studied by using statistically designed matrix experiments.

During the first year of this five-year program, Task I of Phase I was completed as scheduled. It is reported in its entirety in this report. Tasks II and VII were both initiated in this first year. Progress reports are included for both tasks along with those results and conclusions that are available for Task VII.

A technical paper, "Processing Study of Injection Molding of Silicon Nitride for Engine Applications," was prepared and presented at the 1985 SAE Aerospace Technology conference and exposition, October 14-17, in Long Beach, CA. A copy of this paper, which is based upon the program, is included as Appendix A.

EXPERIMENTAL WORK

Task I - Baseline Materials Characterization

The ACC baseline fabrication process selected for study in this program is direct injection molding of test bars to net shape. The material selected as baseline is a silicon nitride composition consisting of 92 percent GTE SN-502 Si_3N_4, 6 percent Y_2O_3 and 2 percent Al_2O_3. The Task I logic chart (fig. 2) suggests that the multi-step fabrication process may be conveniently divided into four subtasks:

(1) Characterization of starting raw materials and baseline milled batch powders

(2) Preparation of injection molding mix, injection molding, and evaluating test bars

(3) Dewax and sintering of test bars.

(4) Post-process characterization and statistical and fractographic analysis

The extensive and very diverse nature of the experimental equipment and procedures suggests that each of the subtasks be reported as separate, sequential experiments.

Subtask I - characterization of starting raw materials and baseline mix batch powders.--This subtask concerns the measurements of the characteristics of all starting raw materials, remeasurement to determine the degree of change by preparation and mixing processes, and evaluation of powder blend quality for further preparation into an injection molding mix.

Materials tested: One lot of GTE SN-502 silicon nitride powder, lot SN-107, was set aside for this program. The yttrium oxide used in Task I was Molycorp 5600 Y_2O_3, lot 1406. The aluminum oxide used was Union Carbide, Linde A, 0.3 μm Al_2O_3, lot 0923402.

Test apparatus: Particle size analysis was performed at ACC on a Leeds and Northrup Microtrac. Comparative analysis was also done on a sedigraph at the University of Florida and an electrozone particle size analyzer, Elzone, at Particle Data Laboratories, Ltd., Elmhurst, Illinois. Electrophoresis, zeta potential, and pH measurements were also done at the University of Florida using equipment developed at the university specifically for these purposes. Air classification was done at ACC using a Donaldson Acucut Classifier, model A12. The scanning electron microscope used at GTEC was an ETEC Autoscan. Oxygen analysis was measured by a neutron activation method at IRT Corp., San Diego, California. Chemical analysis was done by semi-quantitative emission

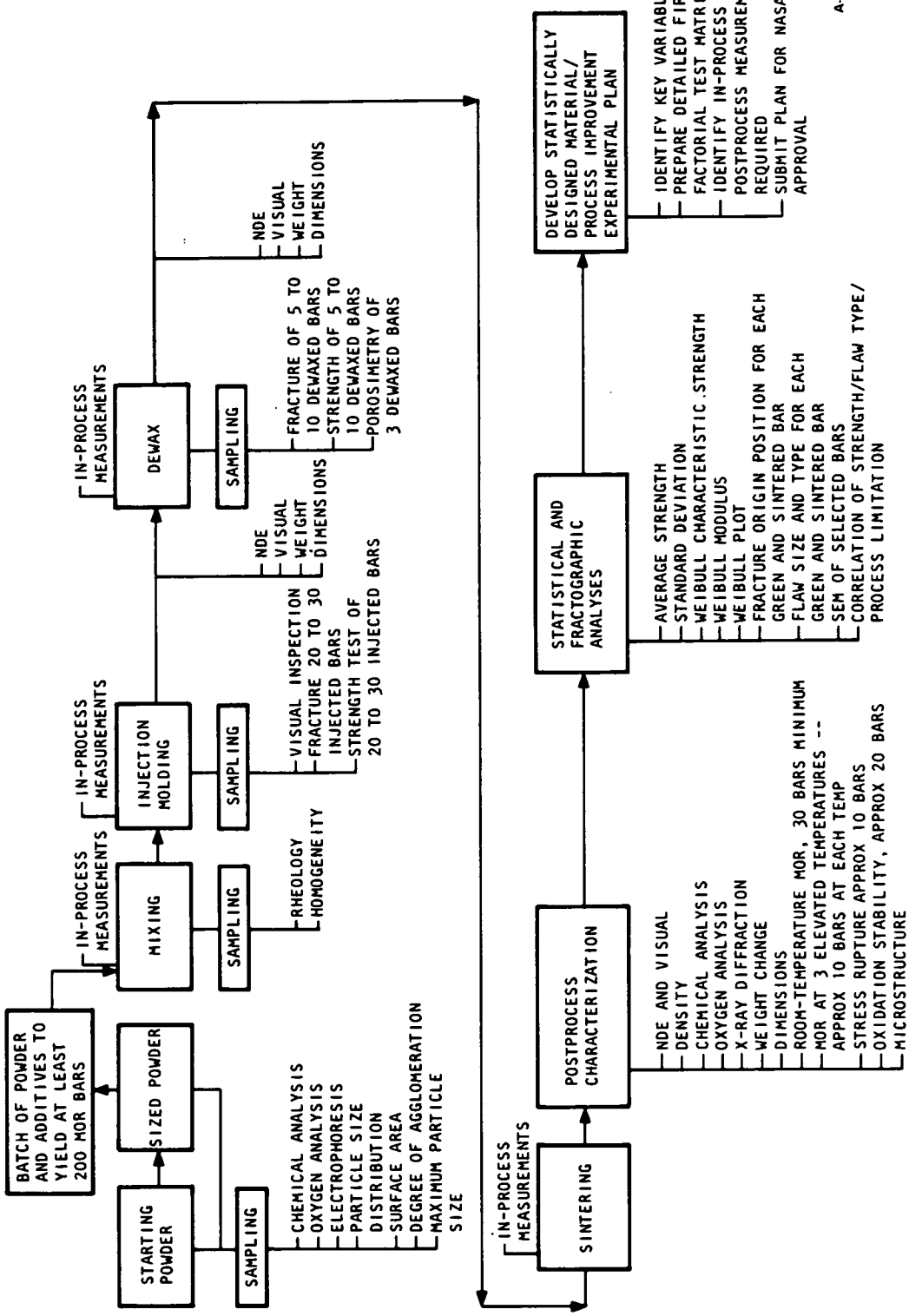

Figure 2.--Task I logic chart.

spectrography at Ledoux and Co., Teaneck, New Jersey. Surface area measurements were done by the Brunauer-Emmett-Teller method by Porous Materials, Inc., Ithaca, New York. Agglomeration studies, homogeniety determination, and maximum particle size measurements were done at GTEC using elutriation, ultrasonic dispersion in deionized water, optical microscope (40 times magnification) scanning electron microscope (SEM), and energy-dispersive X-ray analysis methods. Tap density of powders was determined by ASTM B527-7D using a 100-ml glass cylinder. Ball milling (and mixing) was done in a Norton rubber-lined, two-gallon steel jar mill using 5930 g of 15.9-mm-(5/8-in.)-dia Si_3N_4 milling media.

Test procedure and selected results: The baseline Si_3N_4 powder is supplied by GTE Sylvania, grade GTE SN-502. To ensure uniform particle size distribution (PSD) throughout the drum of SN-502 lot 107, samples were taken from the top, middle, and bottom of the drum. Figure 3 shows that the PSD curves of the three samples were practically coincident with each other as measured by the L/N microtrac particle size analyzer at ACC.

The Si_3N_4 powder was first air classified to remove the major portion of large, dense particles and agglomerates. Figure 4 shows the particle size distribution results of air-classified SN-502 powder (lot 107). Although there was a systematic shift in PSD from coarse to filter fine, it was evident that the PSD's of the three fractions of the air-classified powder overlapped extensively. This overlap is attributed to the needle-like nature of the as-received SN-502 powder. The weight percent of the coarse, fine, and filter-fine fractions of the powder after air classification were: 17.7, 69.4, and 12.9 percent, respectively. The coarse fraction was discarded and the fine and filter-fine fractions were recombined, in the appropriate ratio (69.4 to 12.9), to form the batch material.

The ACC baseline powder milling procedure employed the following elements:

- Rubber-lined, two-gallon capacity steel jar (Norton No. 2)
- 5930 g of Si_3N_4 milling media, 15.9-mm (5/8-in.) dia
- 800 g of 92% Si_3N_4 + 6% Y_2O_3 + 2% Al_2O_3
- 24 hr milling at 52 rpm jar speed

Two powder samples were taken from each of three locations in each mill jar--the lid edge, bottom end corner, and the center of the jar--to ensure particle size distribution reproducibility throughout the mill jar.

The sample preparation method employed by ACC for particle size distribution measurements used a chemical dispersant and a high-energy, ultrasonic probe. This dispersant, Colloid 226/35 (produced by

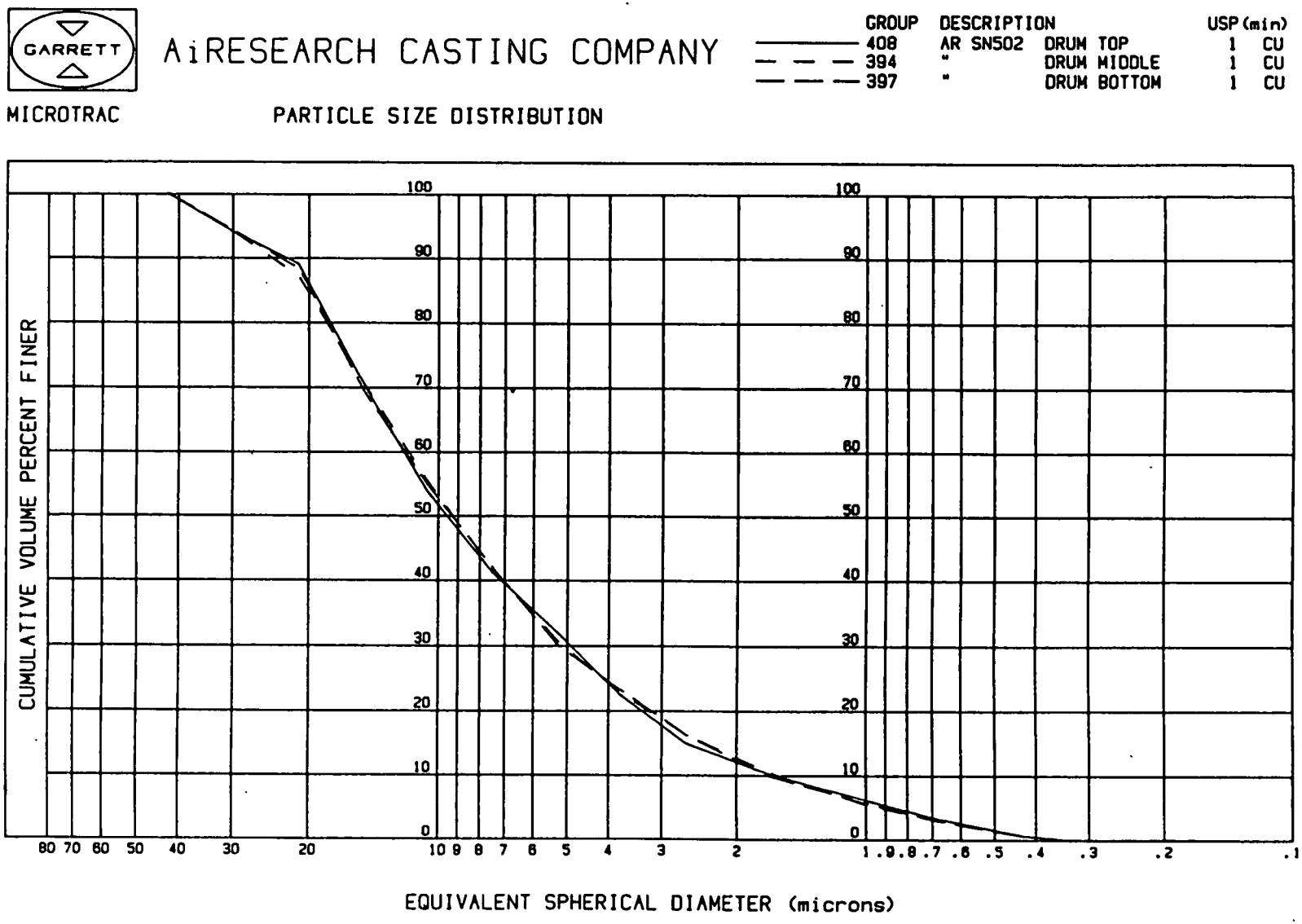

Figure 3.--Particle size distributions of powders sampled from the top, middle, and bottom of a GTE SN-502 Si_3N_4 drum (lot SN 107).

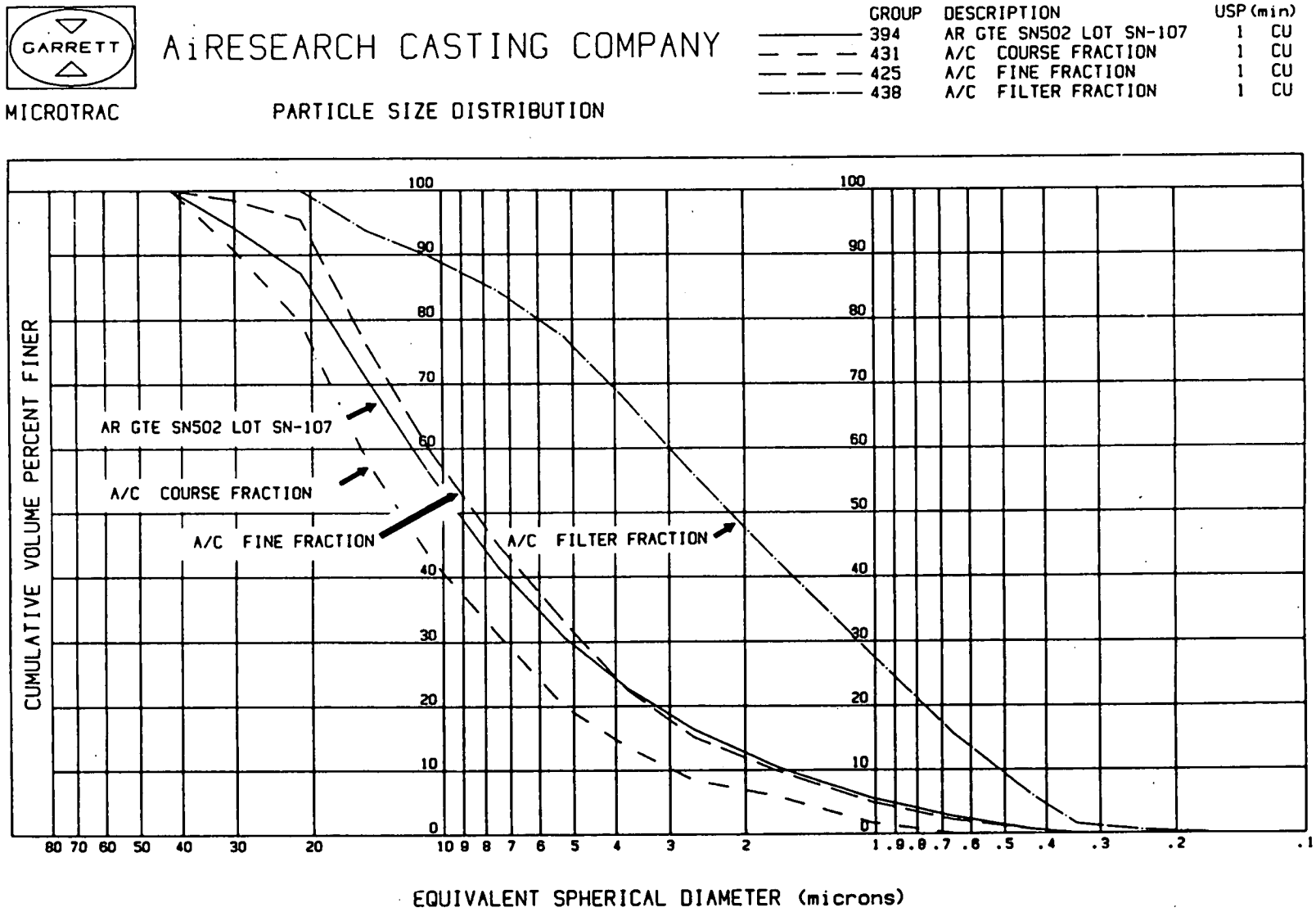

Figure 4.--Particle size distributions of air-classified GTE SN-502 Si_3N_4 powder.

Colloids, Inc., Newark, NJ), is an anionic dispersant and was used at a concentration of 1 drop in 15 ml of deionized water. To this solution was added a nominal 0.06 g of the powder to be tested. A 3/4-in. sapphire-tipped ultrasonic probe was then inserted into the solution and driven at full power using a 375-watt sonicator power supply (manufactured by Heat Systems-Ultrasonics, Inc., Farmingdale, NY). Dispersion was performed in a 15-ml plastic beaker. The plastic beaker provided 100 percent delivery of the sample without rinsing because of its non-wetting behavior with water; it also reduced risk of damage to the sapphire tip. A sonication time of 1 minute was sufficient for complete deagglomeration of milled powders. Longer sonication times were required for the as-received powders and the samples also required cooling.

The procedures described below were used by the University of Florida for measuring particle size distribution of the starting powders by the X-ray sedigraph method.

(1) AR GTE SN-502 Si_3N_4 lot SN-107

In this procedure, 3.0 g of Si_3N_4 powder and 50.0 g of deionized water were combined and sonicated for two minutes. The suspension pH was then adjusted to approximately 9 using ammonium hydroxide solution. This was followed by two 15-minute periods of sonication with pH adjustment (to 9) after each sonication period. The suspension was stirred for an additional 25 minutes and the pH was readadjusted (to 9), if necessary. Just prior to the sedigraph run, the suspension was sonicated for an additional 5 minutes. Sonication was done using a Heat Systems Model W-375 with cup horn attachment. Unless noted otherwise, the power output setting was 6 (maximum output is 10). Sedigraph run no. 1 (fig. 5) was made from 28-0.2μm. Approximately two hours after the start of this run, the suspension was resonicated (about 10 minutes) and the pH was readjusted to 9. This suspension was then used for sedigraph run no. 2 which was run from 50.-0.2μm.

(2) AR Molycorp 5600 Y_2O_3 lot 1406

In this procedure, 1.1 g of Y_2O_3 powder and 50.0 g of deionized water were mixed. The sample preparation procedure for sedigraph run no. 3 (fig. 6) was the same as used in sedigraph run no. 1, except that the pH was adjusted to 10. The procedure for sedigraph run no. 4 was the same as used in sedigraph run no. 2, except that the pH was adjusted to 10.

(3) AR U.C. Linde A 0.3 m Al_2O_3 lot 0923402

For this procedure, 4.0 g of Al_2O_3 and 50.0 g of deionized water were mixed. The pH was adjusted to 4 with hydrochloric acid solution. The rest of the procedure for sedigraph run no. 5 (fig. 7) was the same as for sedigraph run no. 1, except that the sonication powder output setting was 7. After run no. 5, the suspension was aged 40 hours and used for sedigraph run no. 6 (fig. 8). Just prior

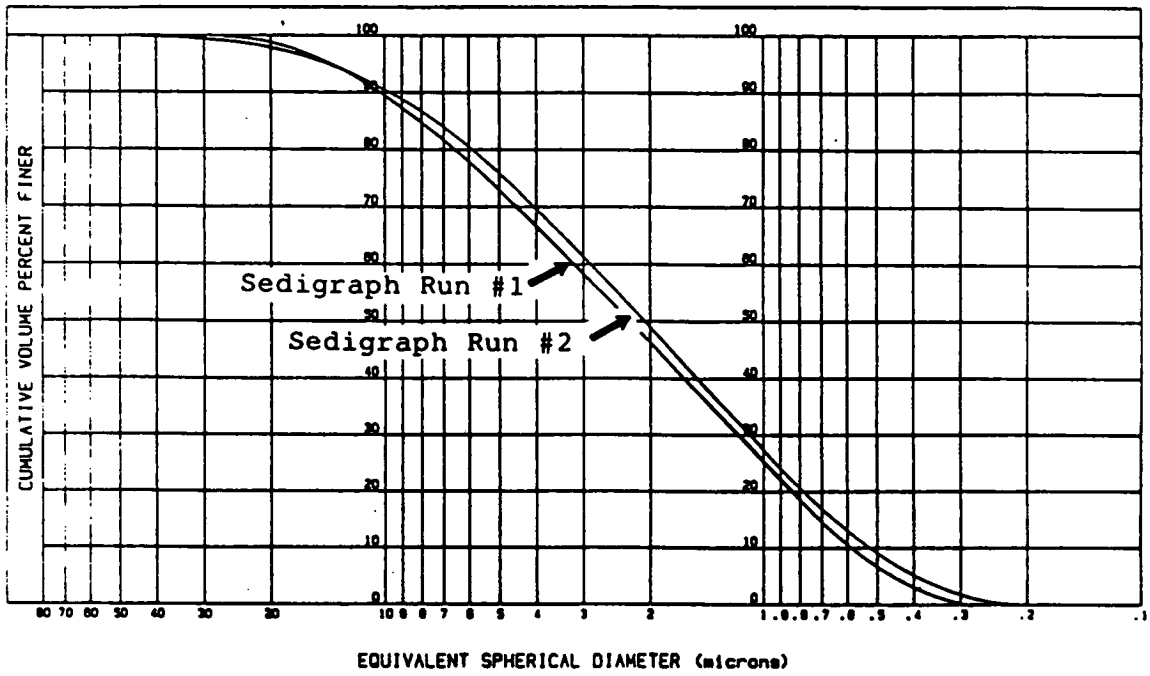

Figure 5.--Particle size distribution of as-received GTE SN-502 Si_3N_4 X-ray sedigraph.

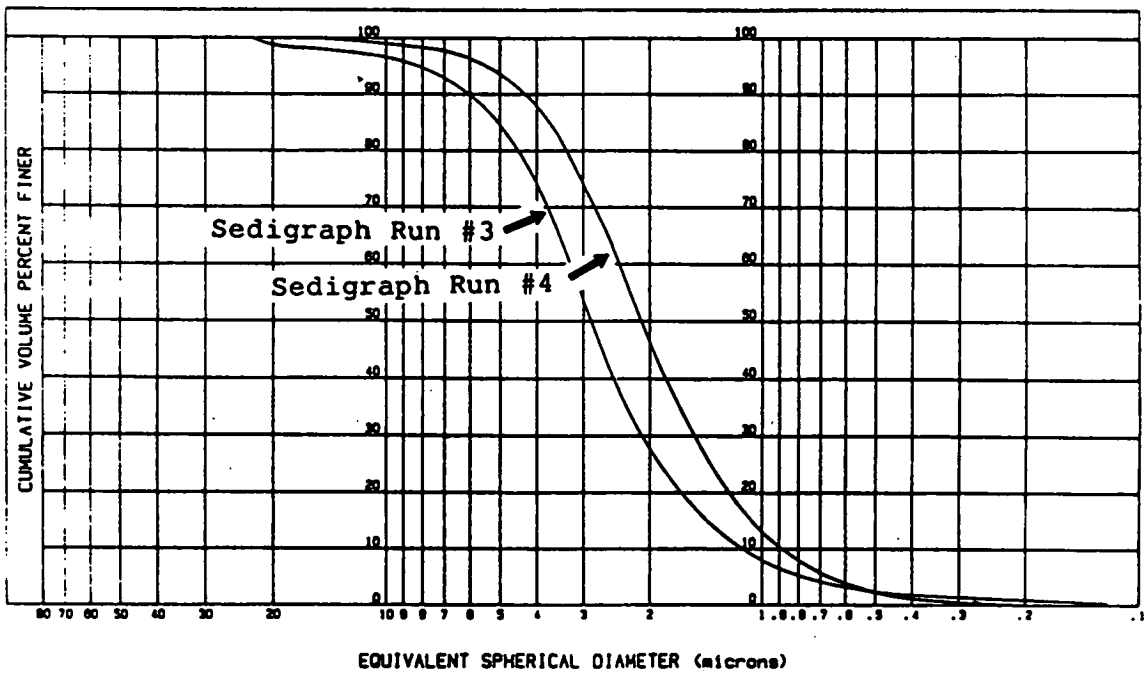

Figure 6.--Particle size distribution of as-received Molycorp Y_2O_3 X-ray sedigraph.

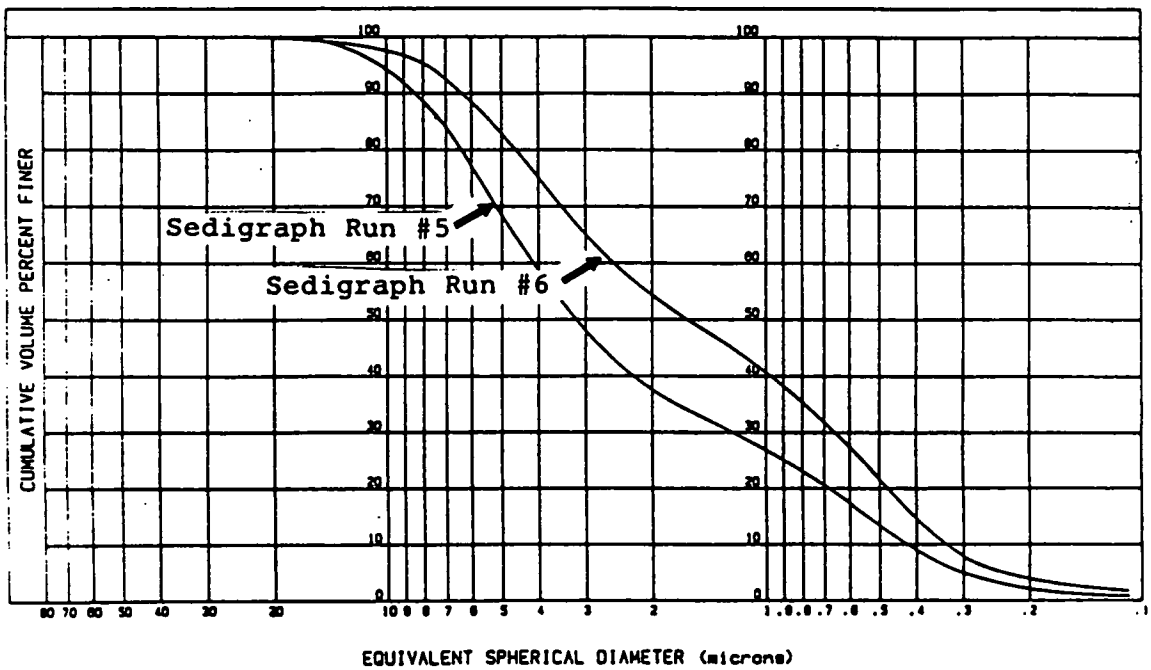

Figure 7.--Particle size distribution of as-received Linde Al_2O_3 X-ray sedigraph.

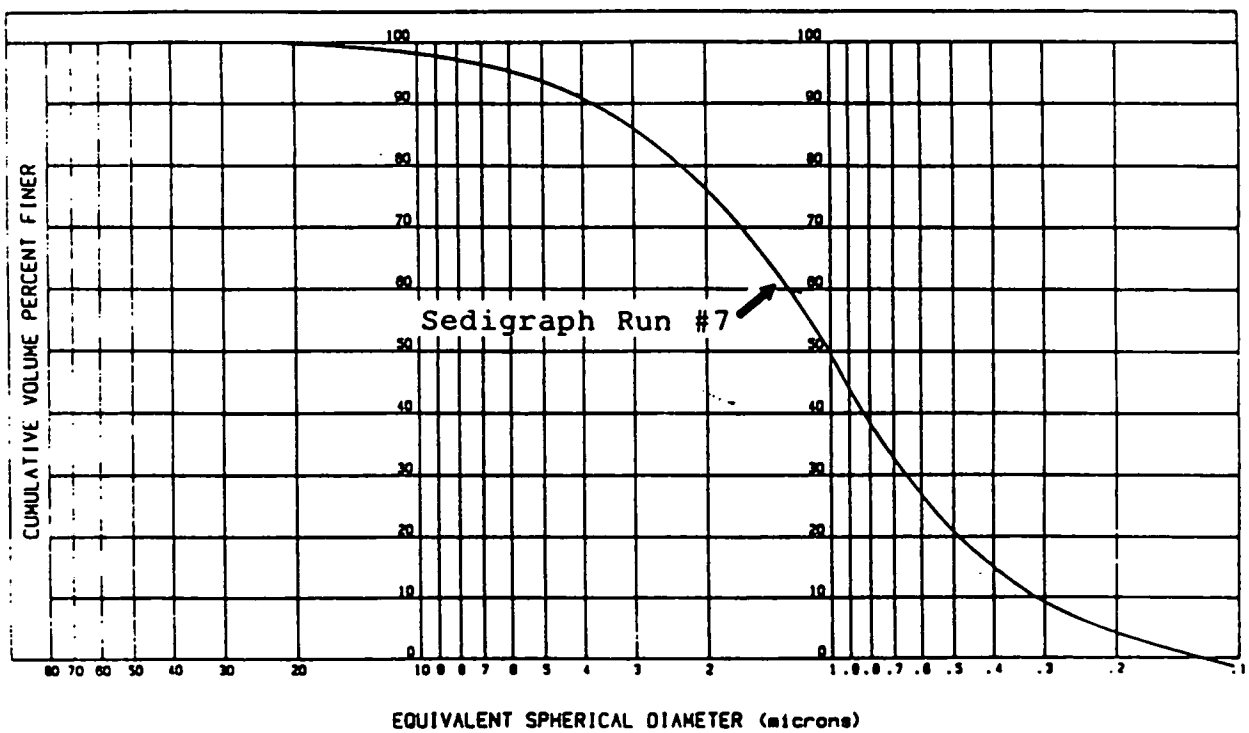

Figure 8.--Milled baseline powder X-ray sedigraph.

to run no. 6, the suspension was sonicated (two 15-minute sonications at power output setting 5) and the pH was readjusted to 4.

(4) M94-5 (Si_3N_4 + Y_2O_3 + Al_2O_3)

In this procedure, 2.9 g of powder and 50.0 g of deionized water were mixed. The sample preparation procedure for sedigraph run no. 7 (fig. 8) was the same as used in sedigraph run no. 1 (fig. 6), except that the pH was adjusted to 10.5.

Particle Data Laboratories, Ltd. of Elmhurst, IL, dispersed the powders in methanol for electrozone measurements. Si_3N_4, Y_2O_3, and the milled powder were dispersed with 8-percent LiCl. The Al_2O_3 sample was dispersed using sodium pyrophosphate. All samples were sonicated.

All particle size data is plotted in figures 9 through 12 for PSD data from the Microtrac, Sedigraph, and Elzone analyzers. PSD data were obtained for as-received Si_3N_4, Y_2O_3, and Al_2O_3 and for the milled mixture by each measurement technique. Data from the Microtrac on all four powders are shown in the above order in figures 3, 10, 11, and 12. Data from the sedigraph on all four powders in the above order are shown in figures 5, 6, 7, and 8. All data from the Elzone are shown in figure 9.

A comparison of the data from the different measurement techniques shows good agreement between Microtrac and Elzone for as-received Si_3N_4 (fig. 3 and 9), Y_2O_3 (fig. 9 and 10), and Al_2O_3 (fig. 9 and 11). A good agreement is also shown between Microtrac and Sedigraph for the milled powders (fig. 8 and 12). As shown in figures 10 and 11, sample preparation appears to be very significant for variations in sonication time at ACC, and in figures 6 and 7 for variation in sample aging and sonication time at the University of Florida.

Electrophoresis measurements were made at the University of Florida prior to the sedigraph particle size distribution measurements. The sample preparation procedure used for the electrophoresis measurements was essentially the same as that used for the X-ray sedigraph runs. After sonication and pH adjustment, the suspension was centrifuged (15,000 rpm) to obtain a clear supernatant liquid. The conductivity of this liquid was measured. A small amount (about 0.01 cc) of the original (reserved) suspension was mixed with 40 cc of the supernatant liquid. This suspension was used for the electrophoresis measurements. Measurements were made for two samples at each pH. Approximately 20 individual readings were collected and averaged per sample. The results are given in table I and illustrated in figure 13. These data were used to determine the pH values that would most effectively disperse the powders for the particle size measurements.

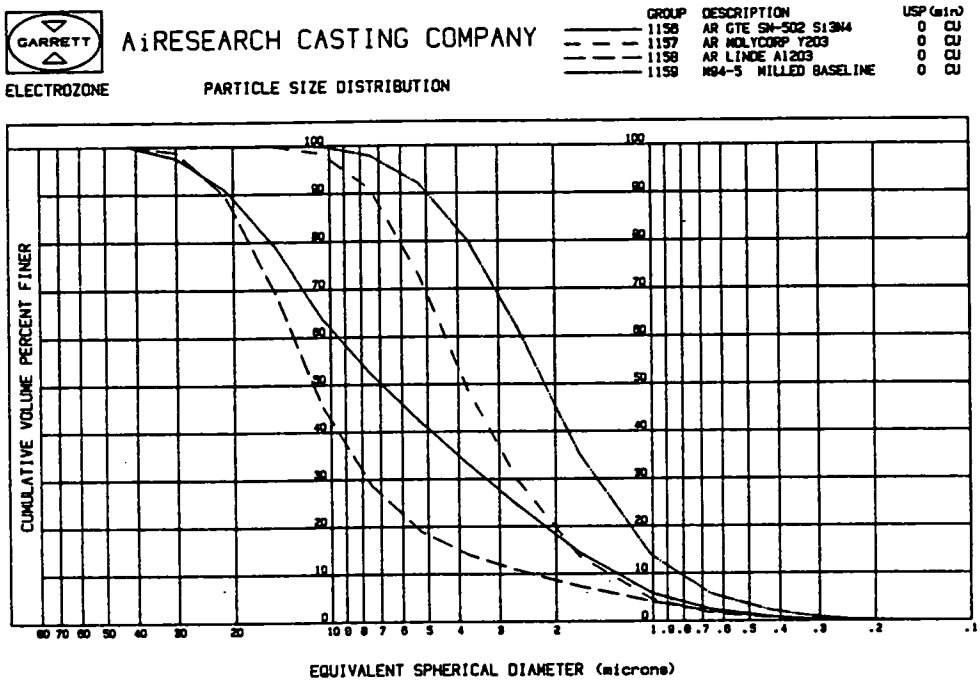

Figure 9.--Particle size distribution of as-received and milled powder Particle Data, Inc., electrozone analyzer.

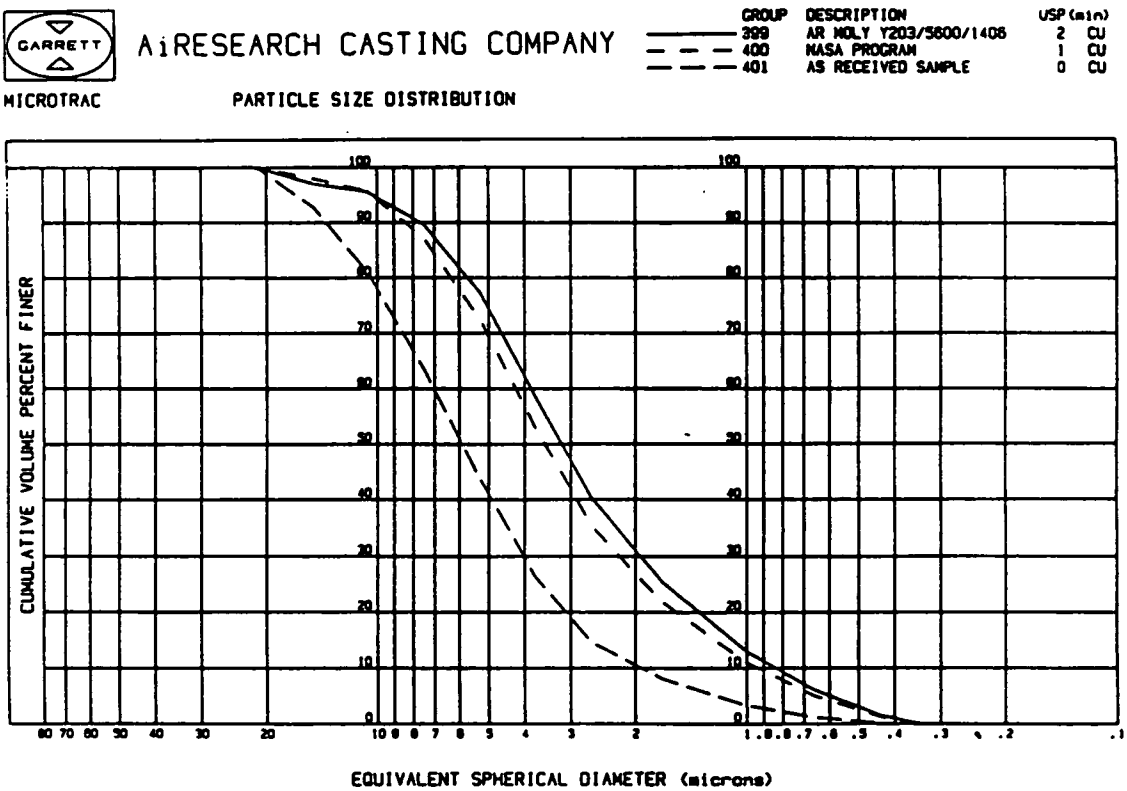

Figure 10.--Particle size distribution of as-received Molycorp Y_2O_3 L&N Microtrac.

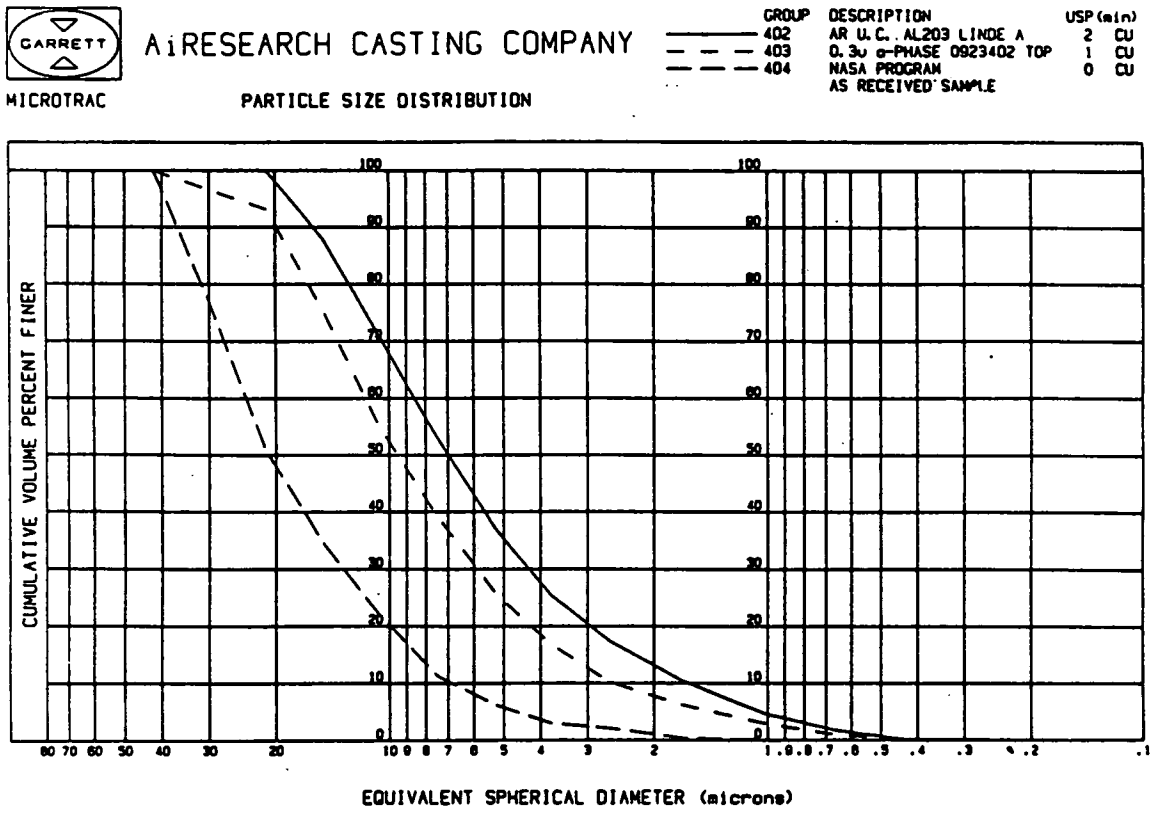

Figure 11.--Particle size distribution of as-received Linde Al_2O_3 L&N Microtrac.

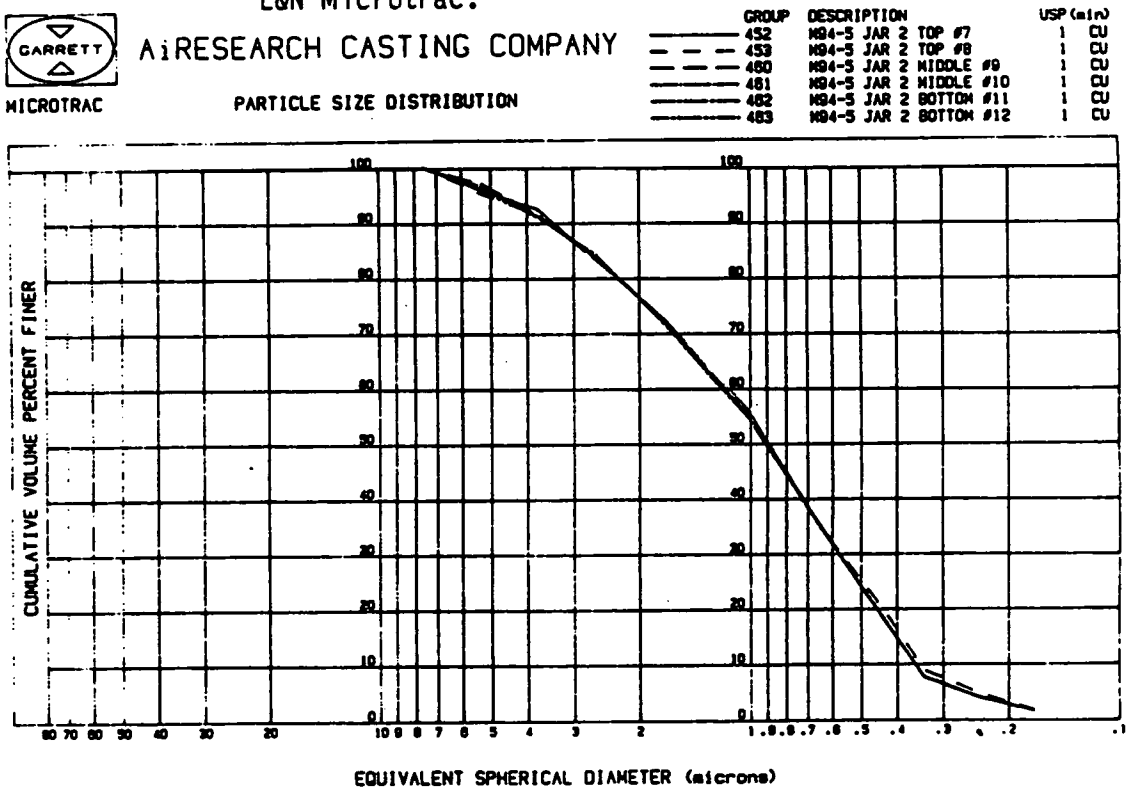

Figure 12.--Milled baseline powder L&N Microtrac.

TABLE I.--ELECTROPHORESIS AND CONDUCTIVITY RESULTS

Material	pH	Zeta potential (mv)			Conductivity ($ohm^{-1}m^{-1} \times 10^4$)
		Sample 1	Sample 2	Average	
Si_3N_4 lot SN-107	3.6	+45	+37	+41	178
Si_3N_4 lot SN-107	6.0	-27	-28	-28	25
Si_3N_4 lot SN-107	8.1	-49	-52	-50	39
Si_3N_4 lot SN-107	10.3	-66	-69	-67	365
Y_2O_3 lot 1406	7.0	+32	+39	+36	7
Y_2O_3 lot 1406	8.0	+36		+36	19
Y_2O_3 lot 1406	9.0	-22	-25	-24	89
Y_2O_3 lot 1406	10.4	-46	-45	-45	240
Al_2O_3 lot 0923402	4.0	+77	+81	+79	373
Al_2O_3 lot 0923402	5.6	+60	+59	+59	62
Al_2O_3 lot 0923402	10.0	-35	-37	-36	439
Al_2O_3 lot 0923402	10.6	-46	-49	-48	631
M94-5 (Si_3N_4 + Y_2O_3 + Al_2O_3)	10.6	-59	-59	-59	548

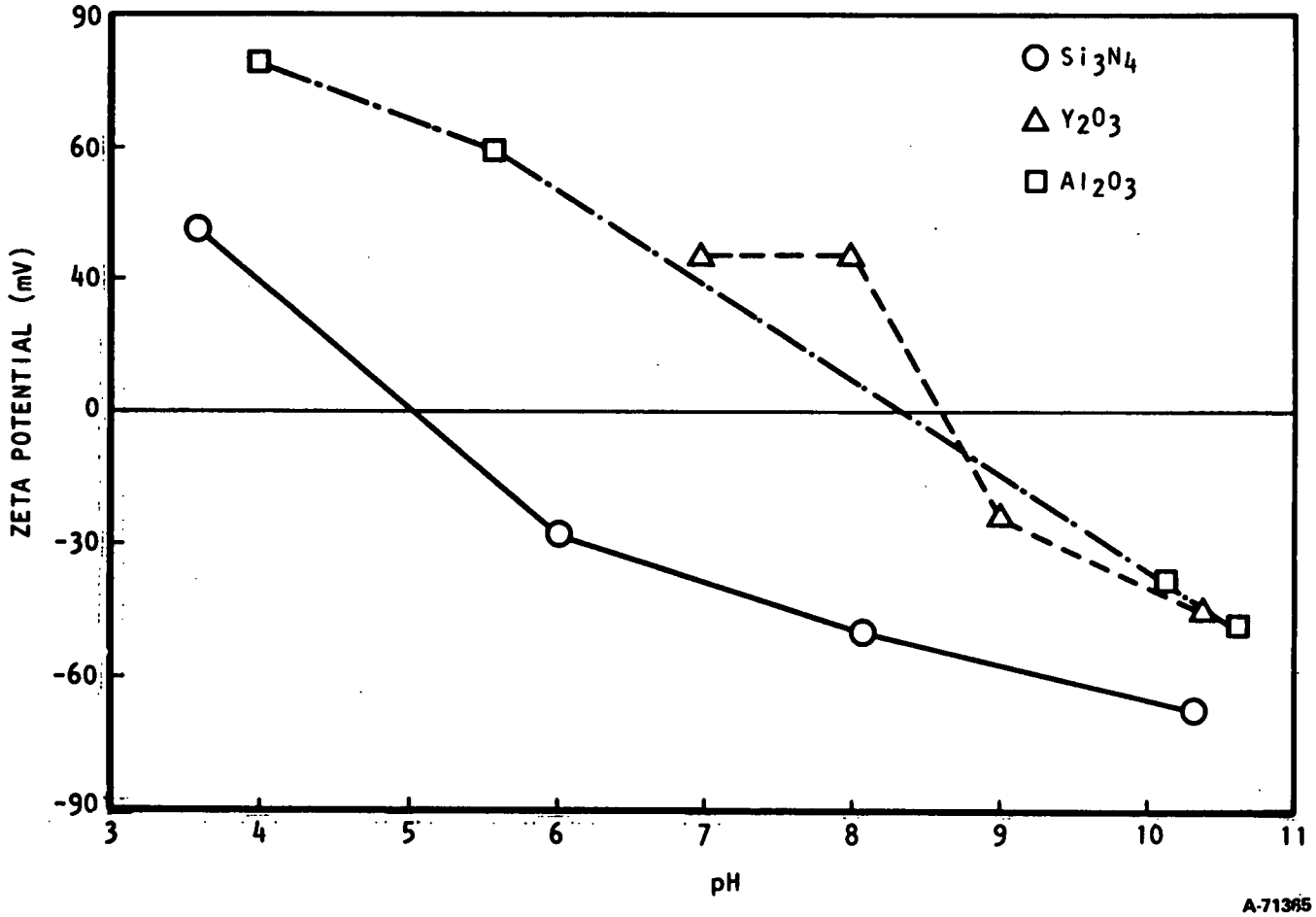

Figure 13.--Electrophoresis measurements of Si_3N_4. Y_2O_3, and Al_2O_3.

Test results and discussion: The chemical analysis of the as-received GTE SN 502, lot 107, the Y_2O_3, and Al_2O_3 are listed in table II. Table III lists the neutron activation oxygen analysis results of the as-received and the as-milled powders. The oxygen content of the as-received SN-502 is reasonable. The oxygen contents of Y_2O_3 and Al_2O_3 are lower than the calculated values based on the chemical formulas. The oxygen content of the milled powder is in agreement with the batch composition. The surface area measurements as measured by the BET method are listed in table IV.

The as-received GTE SN-502 powder was evaluated optically and found to be very coarse and nonhomogeneous. The bulk of the powder was beige in color, but contained numerous white particles and black particles, typical of GTE SN-502 powder. White particles and black particles were carefully hand-separated for inspection by energy dispersive X-ray analysis (EDX). Chemically, the white particles were essentially indistinguishable from the beige particles. The black particles contained metallic impurities. The EDX spectral plots are illustrated in figure 14.

The coarse particles are as large as 750 µm in diameter and appear to be agglomerates of many very fine particles. Some of the agglomerates are relatively soft, but most are quite hard. Individual agglomerates were hand sorted and examined by SEM. Others were washed and concentrated by a sequence of elutriations in deionized water. Samples of both the concentrated coarse fraction and the fine fraction from the supernatant were prepared on slides, gold coated, and examined at GTEC by SEM.

Coarse particles or agglomerates which settled after one elutriation in deionized water and were further washed during a second elutriation are shown in figure 15. As shown in figure 15a, these range in size to over 500 µm. All are soft and can be deformed, although the ease of deformation varies substantially between "particles." Examination at high magnification (fig. 15b) shows that these "particles" are actually agglomerates of much finer particles, some of which have a high aspect ratio (which will subsequently be referred to as whiskers). The whiskers appear to be less than 1 µm in diameter and up to about 40 µm long. The particles appear to be equiaxed and under 1 µm, but with a tendency to agglomerate into short chain-like structures (fig. 15c).

A sequence of elutriations was conducted on as-received GTE SN-502 Si_3N_4 powder using ultrasonic agitation prior to settling. Figure 16 illustrates, at various magnifications, agglomerates retained in the deionized water after brief settling. Individual agglomerates varied substantially. The one shown in figure 16 consisted largely of needle-like material, whereas particles predominated in agglomerate shown in figure 16d. Note that many of the needles interpenetrate. This reticulation contributes to the strong tendency of the as-received GTE SN-502 powder to form large agglomerates.

TABLE II.--CHEMICAL ANALYSIS - BASELINE MATERIALS
SEMIQUANTITATIVE EMISSION SPECTROGRAPHY

Impurity	Si_3N_4	As-received Y_2O_3	Al_2O_3	Milled mixture
Al	0.004[1]	0.001	H	L-M[2]
Ca	ND[3]	ND	ND	0.001
Fe	0.004	ND	0.001	0.005
Ga	ND	ND	0.001	ND
K	<0.001	<0.001	0.005	<0.001
Li	<0.001	<0.001	<0.001	<0.001
Mo	0.02	ND	ND	0.02
Na	<0.001	<0.001	0.003	<0.001
Si	H	0.001	0.008	H
Y	ND	H	ND	M-H

[1]Percentage

[2]L = low, M = medium, H = high

[3]ND = not detected

TABLE III.--OXYGEN CONCENTRATION OF POWDER

	Weight, %		Deviation (± %)
	Measured	Theoretical	
As-received SN-502	2.18	---	0.046
As-received Y_2O_3	20.30	21.30	0.250
As-received Al_2O_3	45.30	47.10	0.560
As-milled baseline	4.66	---	0.073

TABLE IV.--TASK I BET SURFACE AREA
AS-RECEIVED POWDERS FOR BASELINE BARS

GTE SN-502 lot SN-107	Si_3N_4	5.26 sq m/g
Molycorp 5600	Y_2O_3	6.51 sq m/g
Linde A	Al_2O_3	13.13 sq m/g

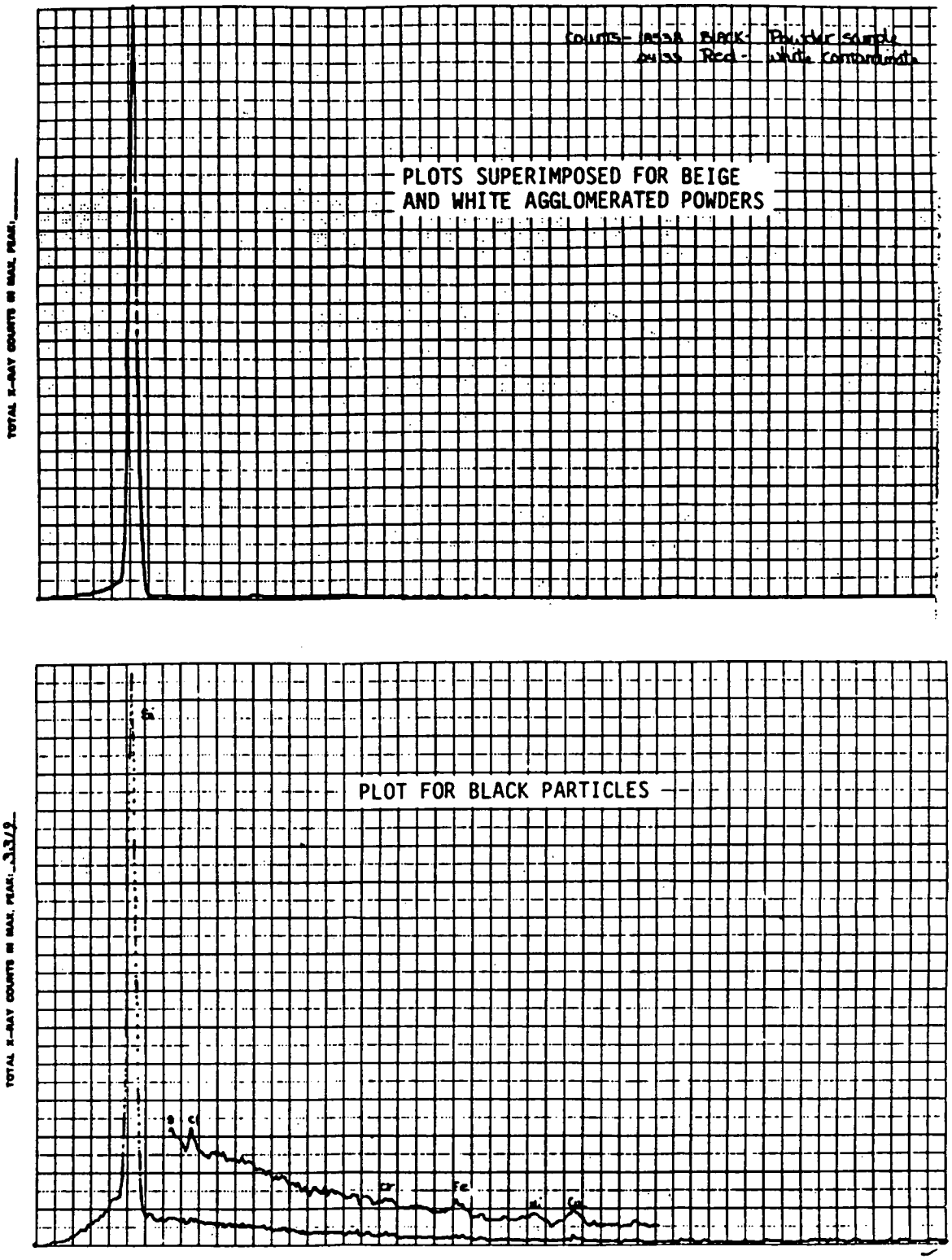

Figure 14.--EDX results of coarse particles separated from GTE SN-502 as-received powder.

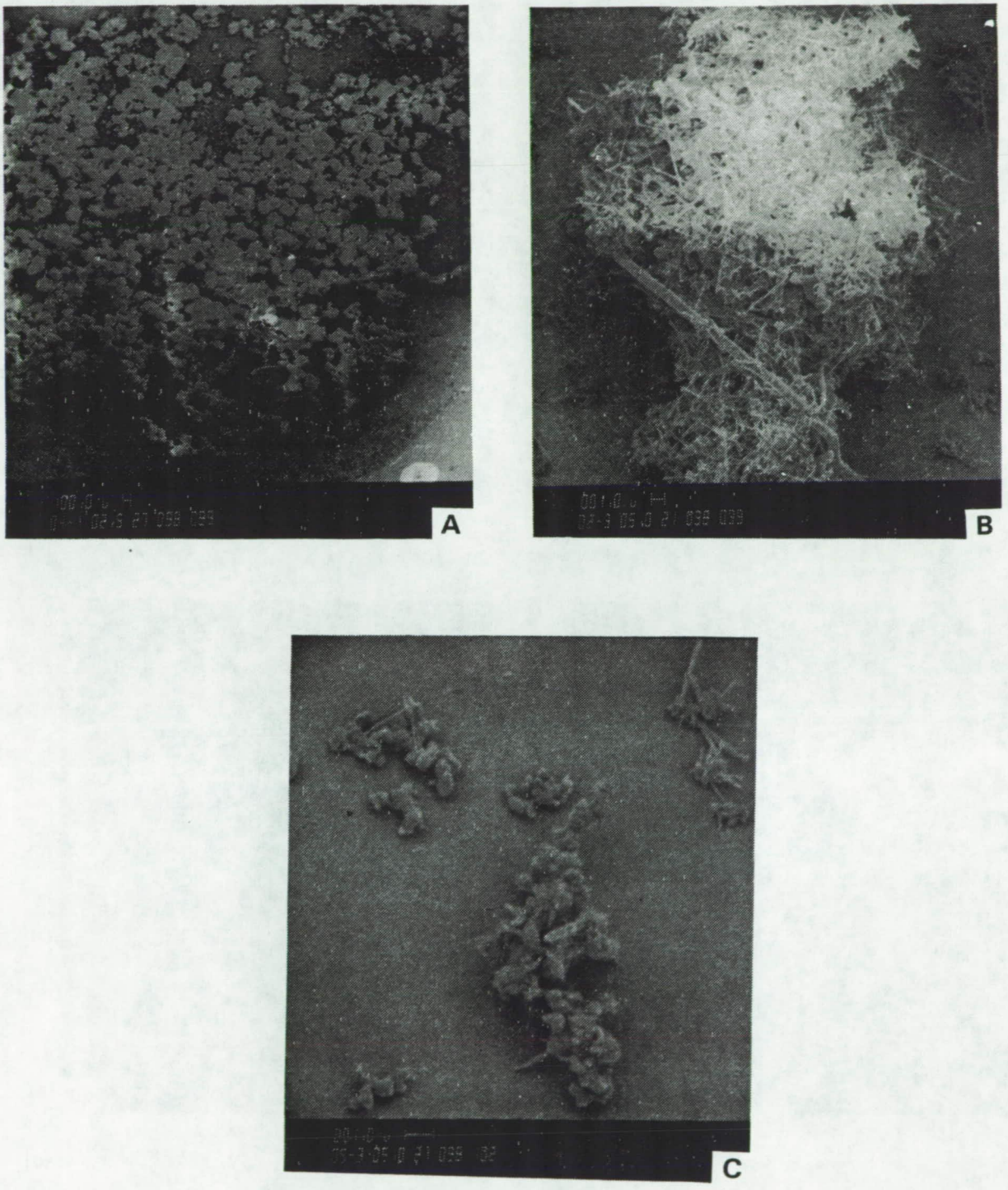

Figure 15.--SEM photomicrographs of as-received GTE SN502 Si_3N_4 powder.

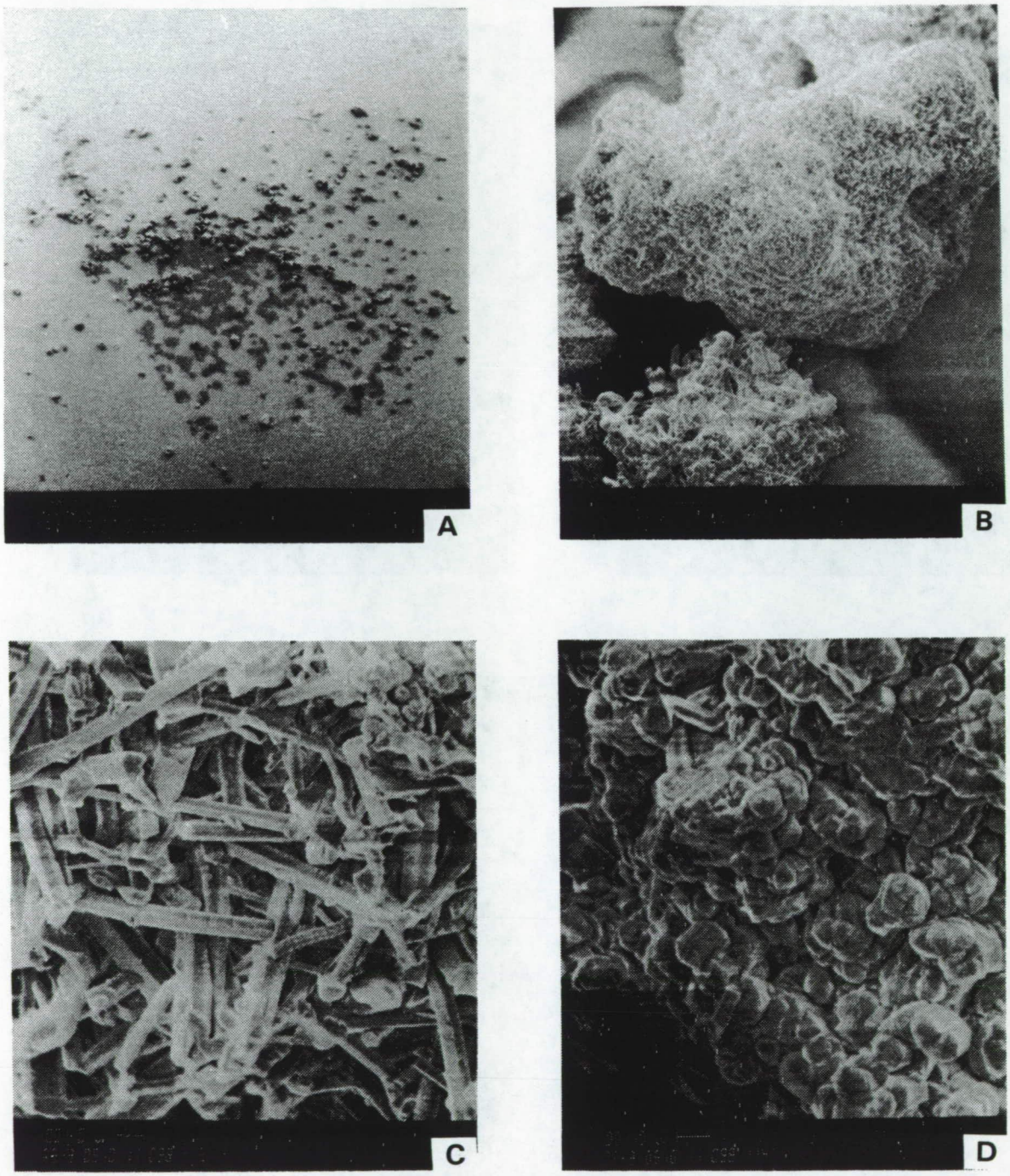

Figure 16.--SEM photomicrographs of fraction of GTE SN-502 powder from the liquid after ultrasonic agitation and elutriation.

The as-received Y_2O_3 powder was visually more homogeneous than the GTE Si_3N_4 powder and appeared to be free of large agglomerates. No significant coarse fraction was isolated by elutriation. Typical SEM views of the powder are shown in figure 17. Particle size ranges up to 12 μm and is typically 1 to 5 μm. Particles are angular with a fractured appearance and contrast sharply with the rounded particles and elongated whiskers of the GTE SN-502 Si_3N_4. Some Y_2O_3 particles contain cracks and laminar porosity.

The as-received Al_2O_3 powder also was visually more homogenous than the GTE Si_3N_4 powder, but unlike the Y_2O_3 it did form agglomerates during elutriation. As shown in figure 18, the agglomerates are much smaller than the typical SN-502 Si_3N_4 ones and contain no whiskers. The Al_2O_3 particles appear to be equiaxed and about 0.2 μm across. However, they are agglomerated into highly porous networks with a low coordination number for individual particles.

The results of examinations of as-received powders verify the need to process the powders before they can be suitable for fabrication of test bars.

Typical morphology of the baseline milled powder is shown in figure 19. Most of the particles are less than 1 μm diameter but some were observed up to 5 μm. The particles are generally equiaxed and angular. Many, however, have retained some of the needle-like shape of the as-received powder, but with reduced aspect ratios (maximum after milling is about 6 to 1).

No settling of coarse particles was observed in elutriation. SEM and elutriation indicate large agglomerates identified in the as-received powder were effectively reduced in air-classifying and milling.

The absence of settling in the elutriation experiments confirms the preliminary findings of a tap density test. Samples taken from the top, middle, and bottom of the drum of SN-502, lot 107, had tap densities of 0.171 g/cc, 0.171 g/cc, and 0.172 g/cc, showing little indication of a significant density gradient.

Subtask 2 - preparation of injection molding mix, injection molding, and evaluation of test bars.--This subtask described the processes of preparing a suitable injection molding mix from Subtask 1 powder blends, the molding of a group of test bars in suitable equipment and tooling, and the evaluation of the molded (green) shapes prior to further processing.

Materials tested: The solids content of the molding mix is the air-classified and dry ball-milled composition that was characterized in Subtask 1. The binder is LN-205-208* at 15.5 weight percent and is commercially available.

*J.F. McCaughin, Rosemead, California

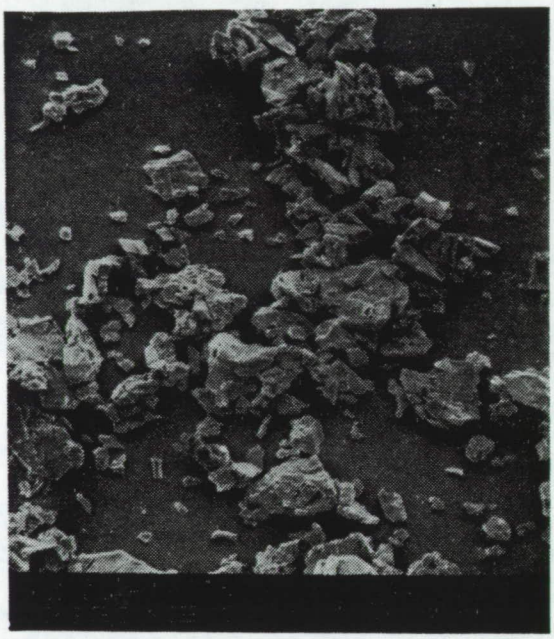

F-48907

Figure 17.--SEM photomicrographs of the as-received Y_2O_3 powder.

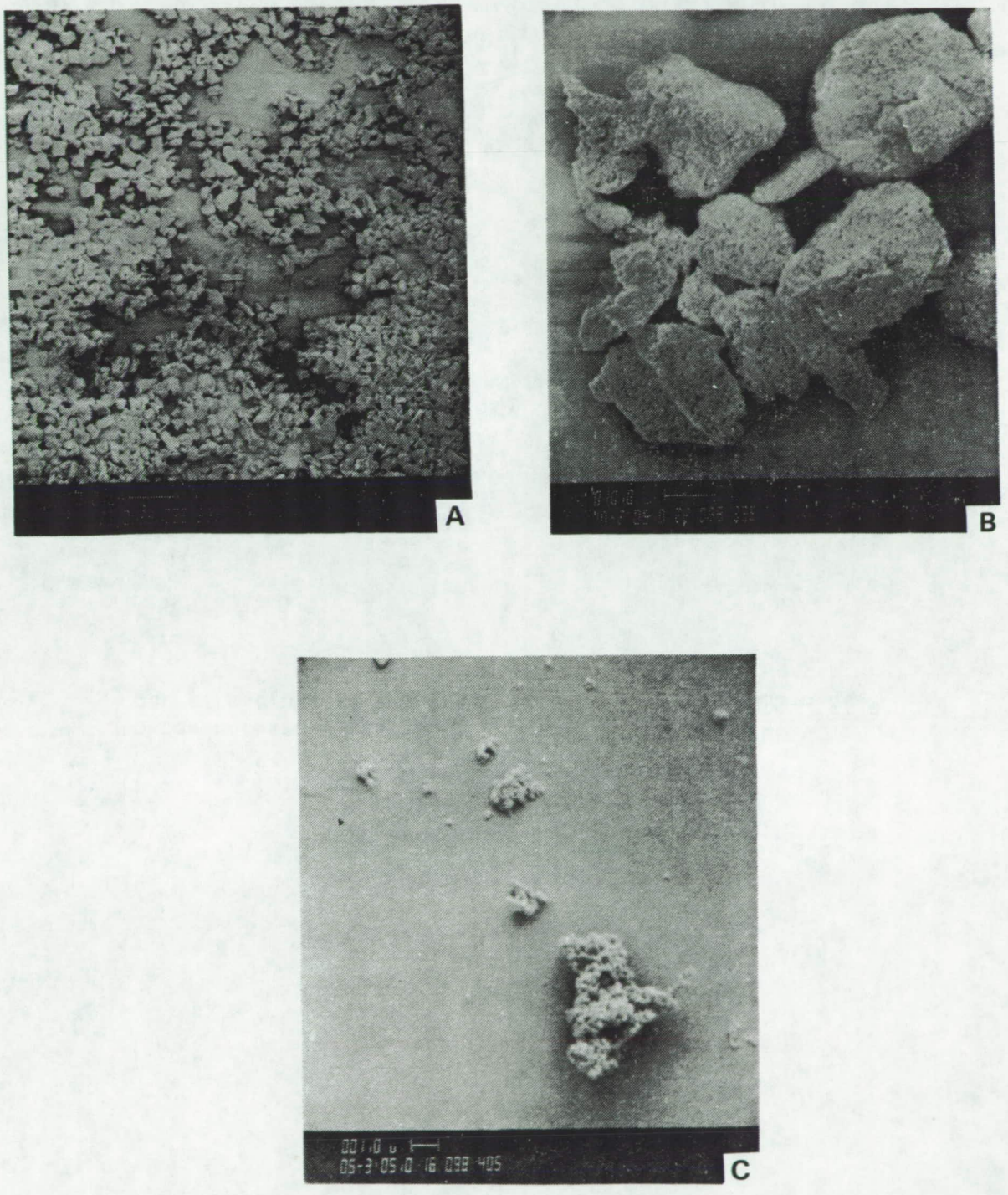

F-48902

Figure 18.--SEM photomicrographs illustrating the characteristics of the as-received Al_2O_3 powder.

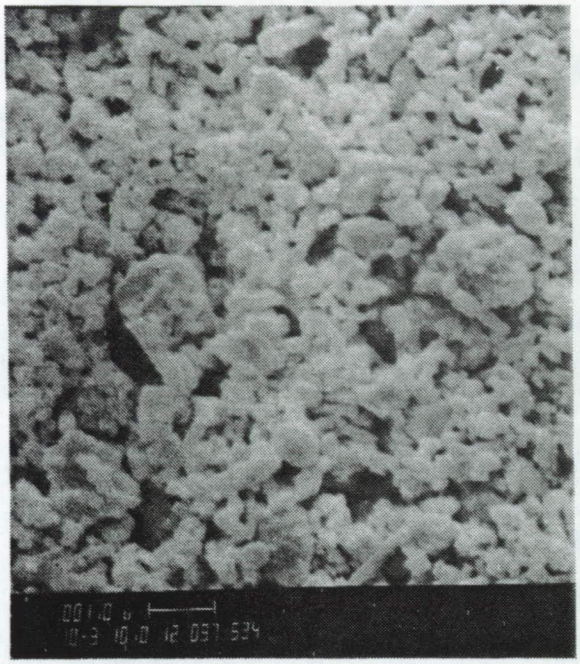

F-48908

Figure 19.--SEM photomicrograph showing the particle size and shape distribution of milled Task 1 baseline powder.

Test apparatus: Mixing was done in a heated sigma mix. The cooled mixed material was pelletized in a Polymer Machining Co. pelletizier. Injection molding was accomplished using ACC's Arburg 2.2 screw-meter-feed, plunger injection molding machine. The test bar die is a four-cavity tool, each cavity yielding a 3.18 by 6.35 by 50 mm (1/8 by 1/4 by 2 in.) test bar after sintering to full density. Green strength was measured using an Instron model 1125.

Test procedures: The overall procedure for Task I is block diagrammed in figure 20. After mixing and pelletizing, the molding mix was placed in the hopper of the Arburg and the following baseline parameters set.

Temperature of mold	32°C (90°F)
Temperature of nozzle	77°C (170°F)
Temperature of nozzle zone	77°C (170°F)
Temperature of feed zone	66°C (150°F)
Injection speed	4 (on dial scaled from 0-5)
Injection pressure	9.6 MPa (1400 psi)
Clamp time	110 sec
Injection time	61 sec

A total of 452 baseline test bars were injection molded using the four-cavity tool. Each cavity in the tool is numbered and complete traceability is maintained by recording which cavity created each bar. All bars are then numbered sequentially. All of the bars were X-rayed for internal flaws such as pores or laminations. The visual (40 times magnification) evaluation was completed on all sintered bars. Of the first five shots (20 bars), all bars were fractured and evaluated. In the next five shots, every fifth bar was fractured. All four bars in the tenth, twentieth, and thirtieth shot were submitted to GTEC for green modulus of rupture (MOR) values. Table V presents the visual evaluation with respect to the type and degree of defect observed.

A computer-generated random number sequence was used to select the individual tests bars for sequencing into the four parallel processing cycles and reference matrix for Task VII.

Test results: Flexure strength testing was conducted on as-injected, green test bars at GTEC. The results are presented in table VI, and a typical load-deflection curve is shown in figure 21. Also included in table VI are the results of visual inspection of fracture surfaces.

The point of fracture initiation was easily visible and occurred at the tensile surface for each specimen. Four features noted on the fracture surfaces are:

(1) All specimens contained a dispersion of very small black particles that were visible at 40 times magnification.

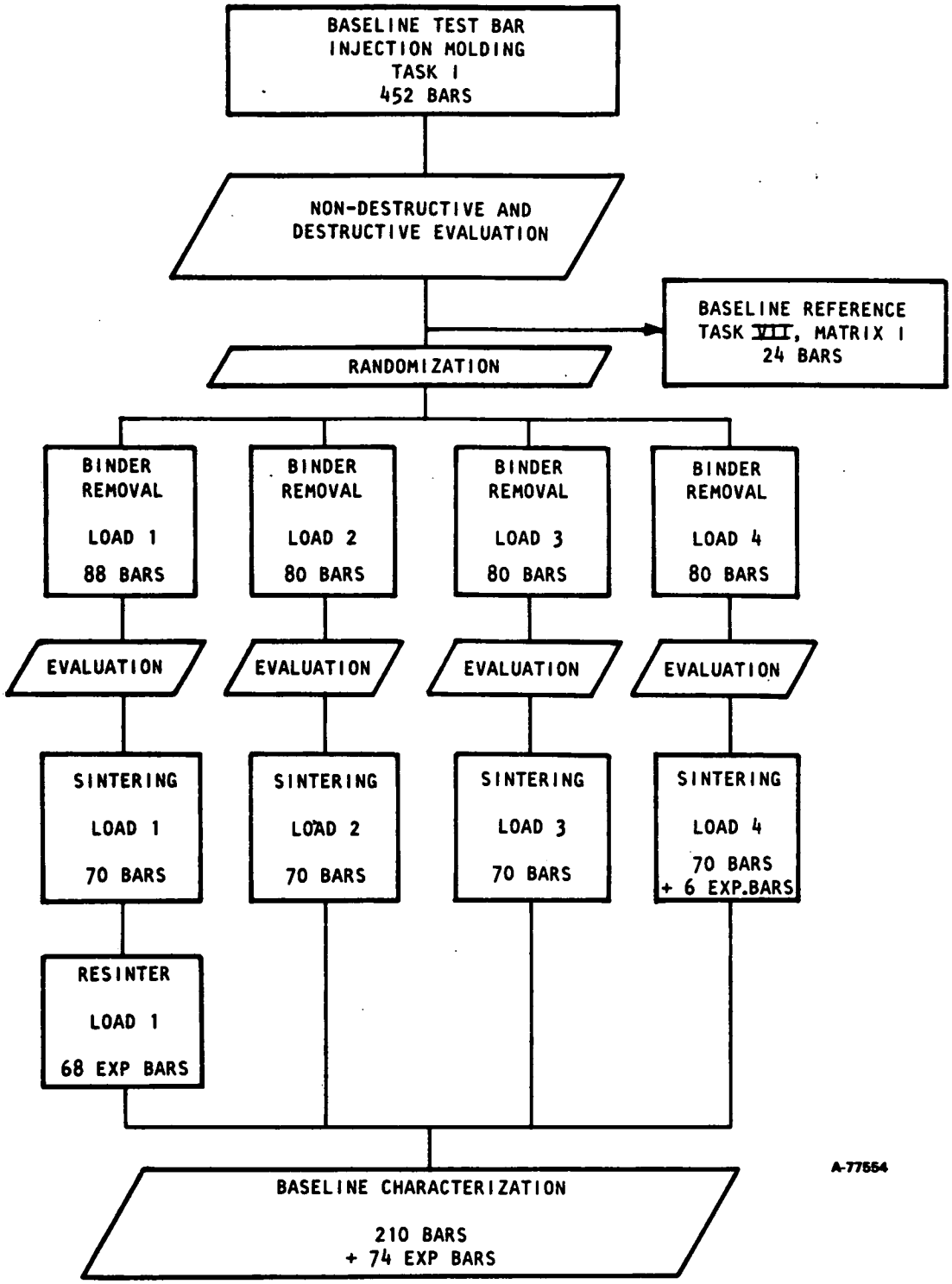

Figure 20.--Processing and evaluation history of baseline test bars.

TABLE V.--VISUAL EVALUATION OF BASELINE TEST BARS

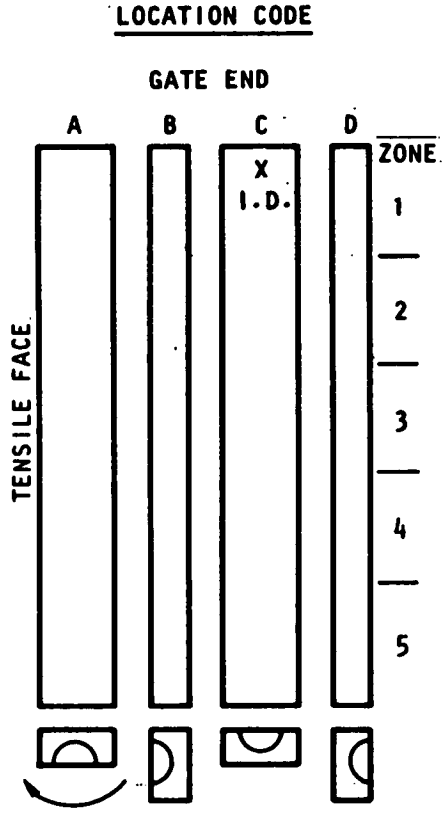

FLAW DESCRIPTION *	DESCRIPTION CODE		
	FLAW TYPE	LEVEL	LOCATION
LIGHT FLOWLINES ON TENSILE FACE NEAR INGATE	FL	0	A1
SLIGHT SURFACE POROSITY OVER MOST OF BAR	SPL SPR	0 1	A1, A5
SCRATCHES FROM HANDLING	SC	0	------
OCCURRING FROM TOOL DAMAGE	--	-	------

CODE

FLAW TYPE	LEVEL
FL - FLOW LINE	0 - NOTICEABLE AT 30X MAG.
SPL - SURFACE POROSITY LINEAR	1 - MORE THAN DESIREABLE
SPR - SURFACE POROSITY DUE TO EXCESS MOLD RELEASE	2 - POSSIBLE EFFECT ON PROPERTIES
SPC - SURFACE POROSITY CIRCULAR	3 - DEFINITE EFFECT ON PROPERTIES
SC - SCRATCHES	
P - PIT	

*UNLESS OTHERWISE STATED, ALL BARS EVALUATED CONTAIN THESE FLAWS. ONLY FEATURES OTHER THAN THESE WILL BE RECORDED.

A-71364

TABLE VI.--FOUR-POINT FLEXURE STRENGTH RESULTS FOR INJECTED BASELINE TEST BARS

Sample number	Failure load	MOR (ksi)	Failure origin	Observations
37	6.4	1.09	TF	Black inclusion; nodules
38	6.2	1.05	TF	----------
39	6.8	1.16	TF	Nodules; comma
40	6.8	1.16	TF	----------
77	7.0	1.19	TF	----------
78	6.8	1.16	TF	----------
79	7.0	1.19	TF	Comma
80	7.0	1.19	TF	Large void or pullout at origin
117	6.6	1.12	TF	Large nonspherical nodule
118	6.4	1.09	TF	Nodules; exaggerated hackle
119	6.8	1.16	TF	----------
120	6.8	1.16	TF	----------
197	6.8	1.16	TF	Nodules
198	6.6	1.12	TF	----------
199	6.8	1.16	TF	----------
200	6.4	1.09	TF	----------
277	6.8	1.16	TF	Exaggerated hackle; no core
278	7.0	1.19	TF	----------
279	6.8	1.16	TF	Large comma
280	6.6	1.12	TF	Nodule
357	5.8	0.99	TF (corner)	Possible flaw at origin
358	6.2	1.05	TF (corner)	----------
359	6.4	1.09	TF	Large comma
360	6.6	1.12	TF	----------
397	6.6	1.12	TF	Possible crack
398	6.6	1.12	TF	Void or pullout away from origin
399	No test	---		Specimen dropped
400	5.8	0.99	TF	----------
437	6.2	1.05	TF	----------
438	6.6	1.12	TF	----------
439	6.0	1.02	TF	----------
440	6.0	1.02	TF	Large nodule

Mean MOR: 7.6 MPa (1.11 ksi)
Standard deviation: 0.4 MPa (0.06 ksi)
Weibull characteristic: 7.8 MPa (1.14 ksi)

Weibull slope: 21.7

Inner span: 1.91 cm (0.75 in.)
Outer span: 3.81 cm (1.50 in.)

Specimen width: 0.80 cm (0.315 in.)
Specimen thickness: 0.37 cm (0.145 in.)
Load rate: 0.5 mm (0.02 in.) per minute
*TF = tensile face

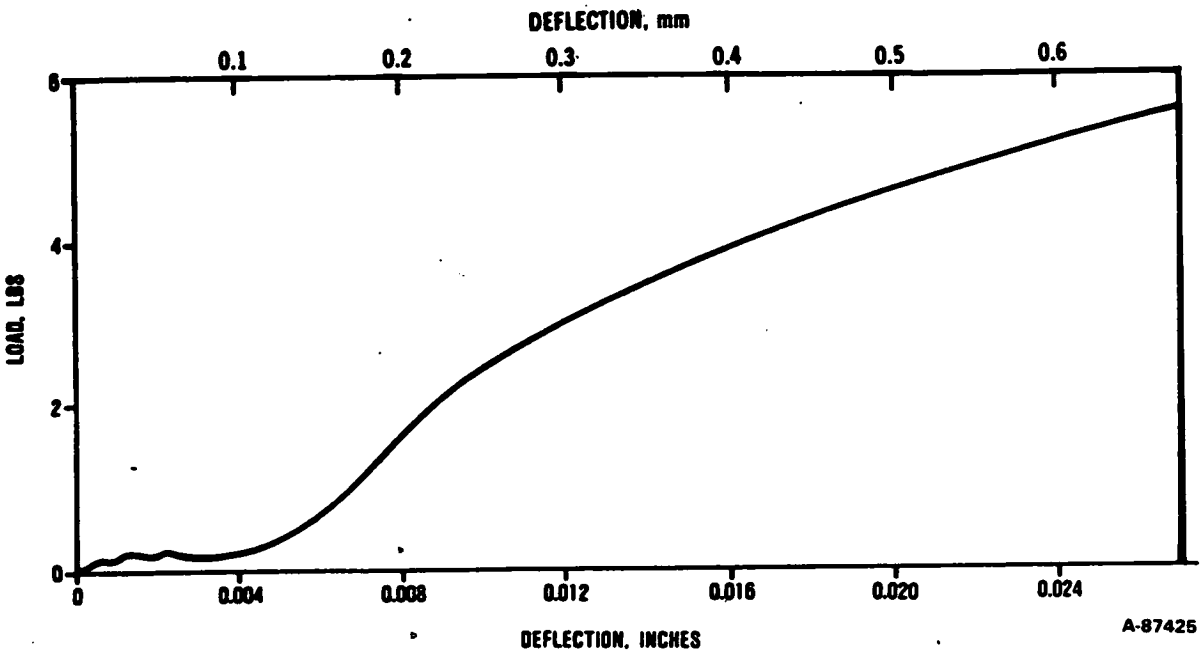

Figure 21.--Typical load-deflection curve for an as-injected specimen strength tested in four-point flexure.

(2) Many of the specimens had a distinct comma-shaped feature extending from the fracture origin into the material; further examination by SEM will be described subsequently.

(3) Some specimens had roughly spherical raised "nodules" on one fracture surface with a matching depression in the other fracture surface.

(4) Each specimen showed a slight perturbation in the fracture path symmetrically around the core of the test bars. This suggests the presence of a residual stress in the test bar, probably due to the more rapid cooling of the surface (compared to the interior) during injection molding.

Figure 22 shows SEM photomicrographs (for specimen no. 117) which are typical of most of the specimens tested. Figure 22a shows the complete fracture surface. All of the faint surface lines emanate from the small sunburst pattern on the lower surface of the specimen near the lower left corner. This side of the specimen was in tension during the fracture test, and the "sunburst" is the likely fracture origin. Figure 22b illustrates this region at higher magnification. The apex of the sunburst is shown at still higher magnification in figure 22c and is compared with a typical microstructure (figure 22d) from the interior of the specimen. Other than some possible porosity, no clearly defined discontinuity is evident to distinguish the fracture origin region from the general microstructure.

Figure 23 illustrates the fracture surface features for specimen no. 118. This specimen contained a distinct "comma" feature at the origin and several "nodules" on the fracture surface, well away from the origin. No discontinuity is apparent at (or adjacent to) either the "comma" or "nodule" features.

Figure 24 shows a large flake-like feature at the fracture origin of specimen no. 80. Figure 24a illustrates the overall fracture surface with the flake-like feature at the origin on the tensile face. The higher magnification view in figure 24b reveals possible linear discontinuities at the origin. However, the green strength of this specific test bar was within the same statistical range as the other specimens, i.e., 8.2 vs 7.6 MPa (1.19 vs 1.11 ksi) with a standard deviation of 0.4 MPa (0.06 ksi).

Optical and SEM examinations indicate that the Task I baseline injection-molded test bars are uniform and do not have major visible defects. Defects that are hidden by the binder material may be present, but further examination after binder removal will be necessary.

Test bars also have been evaluated by optical microscopy up to 1000 times magnification. Particle packing appears uniform except for occasional shiny inclusions and black regions, less than 10 μm, shown in figure 25. These features were present on the as-molded surface and were

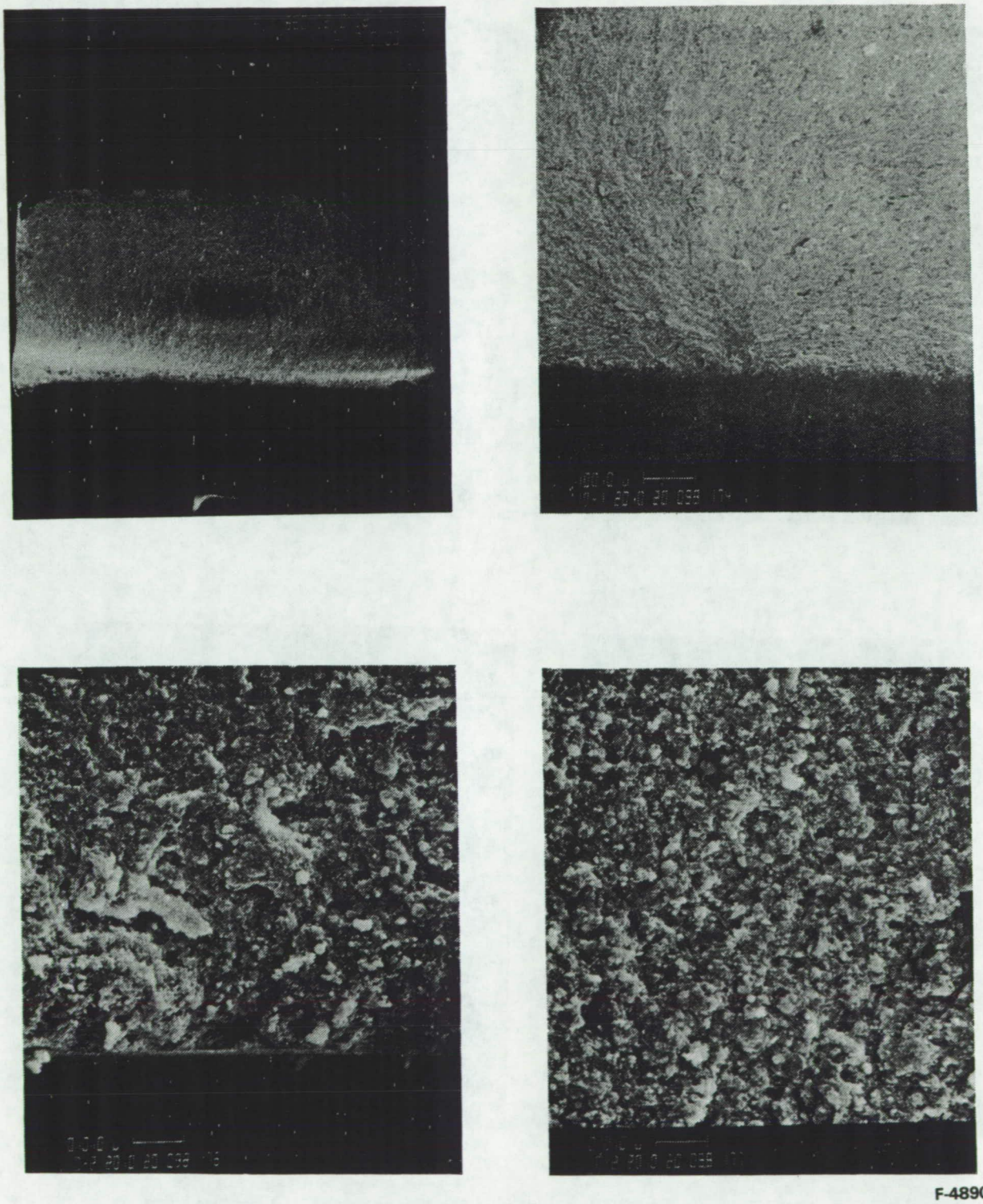

F-48906

Figure 22.--Scanning electron photomicrographs illustrating the fracture surface and origin for specimen no. 17.

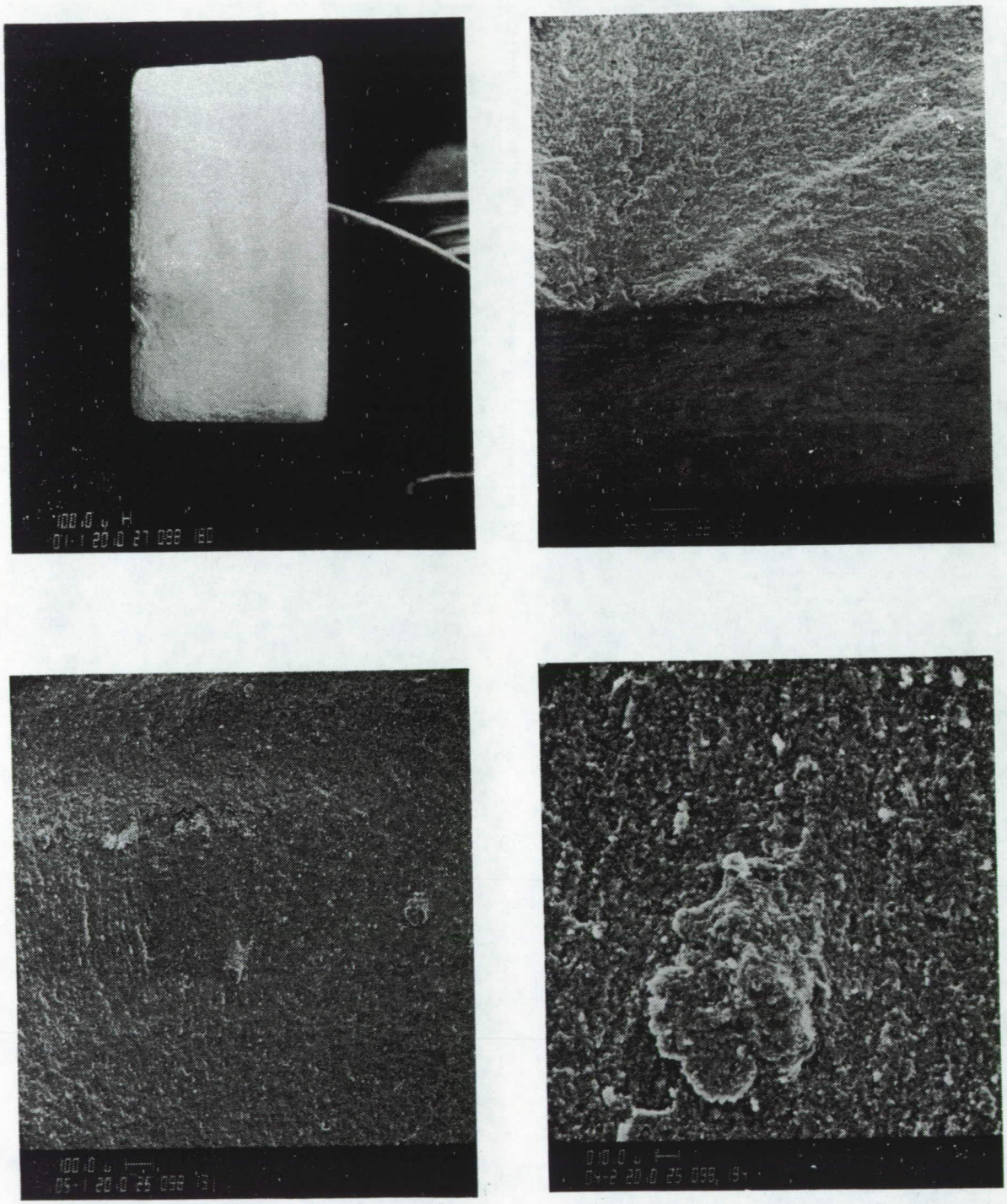

F-48904

Figure 23.--Scanning electron photomicrographs illustrating the fracture surface features for specimen no. 118.

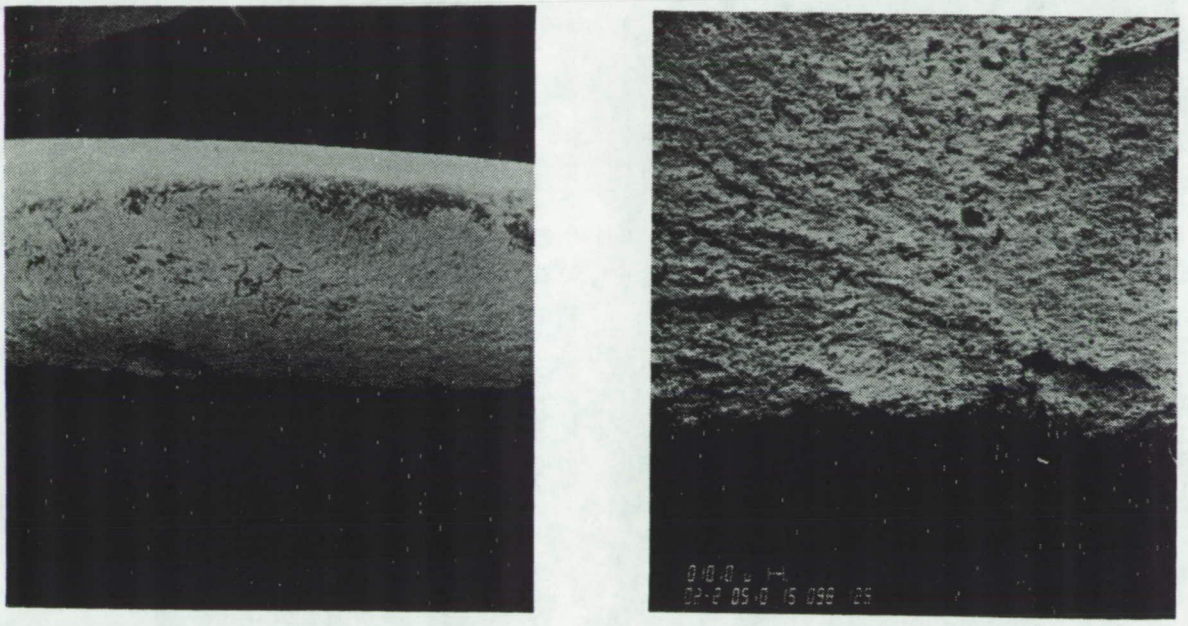

F-48903

Figure 24.--Scanning electron photomicrographs of the fracture surface of as-injected Si_3N_4 specimen no. 80.

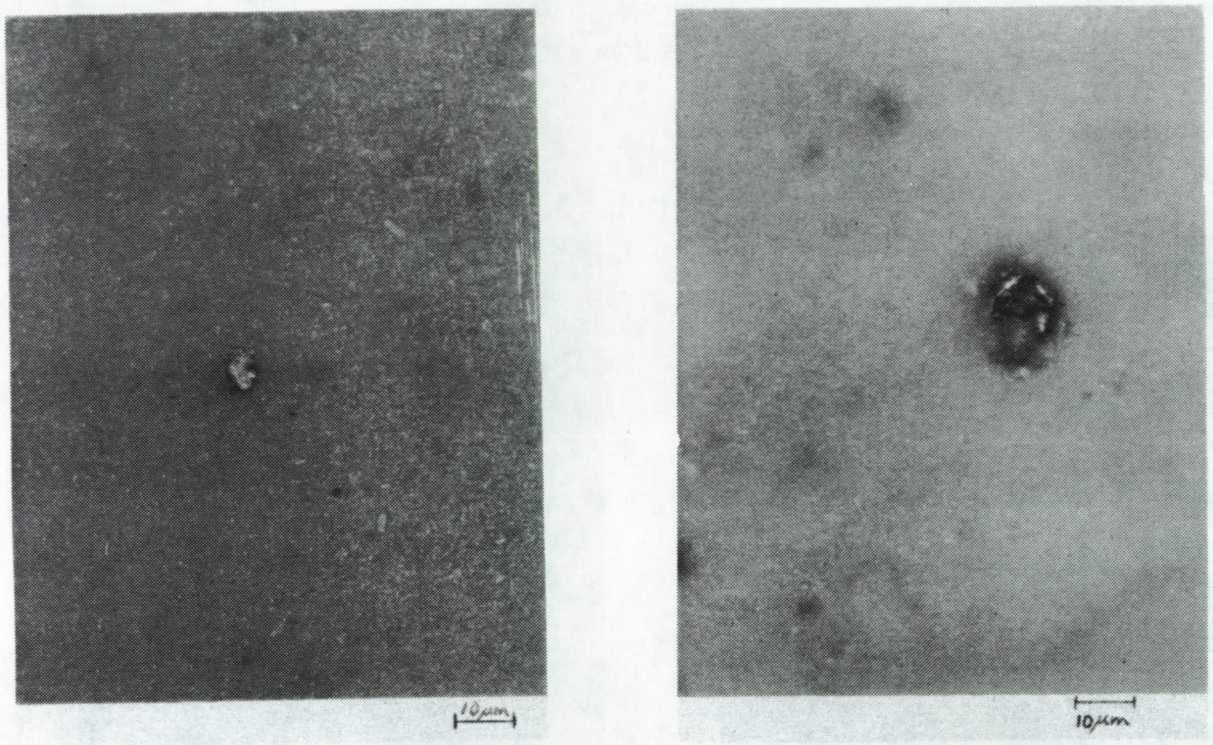

F-48910

Figure 25.--Optical micrographs of as-injected test bar no. 119.

revealed in the interior by etching the surface with a solvent. The black regions were identified as porosity by dark field illumination. Figure 25a also shows some elongated particles similar to SEM photomicrographs of the as-received powder.

Chemical analysis of the inclusions by energy dispersive X-ray using the SEM was tried but not completed. SEM requires an electrically conductive surface to prevent charge buildup. Carbon coating was not successful in preventing charging. Gold coating resulted in damage to the surface, evident at high magnification (5000 times), disguising the original features.

Subtask 3 - dewax and sintering of test bars.--This subtask describes the thermal and environmental treatments needed to remove the injection molding binder system and to densify the green shape into a dense, high-strength ceramic material.

Materials tested: The bulk of the 452 injection-molded test bars that were fabricated in Subtask 2, except those selected for destructive evaluation.

Test apparatus: ACC dewax chamber BE-I, a front-load, temperature, atmosphere, vacuum, or pressure furnace capable of precisely programmable thermal cycles. The ACC vacuum induction sintering furnace capable of 0.68 MPa (100 psi) N_2 overpressure and 2000°C. Optical and electron optical previously described at GTEC.

Test procedure: The overall procedure for Task I is block diagramed in Figure 20. As previously mentioned, a computer-generated random number sequence was used to locate each numbered test bar in three of the four dewax runs and each of the four sintering runs in a manner conducive to statistical analysis. Variables considered in the arrangement are position within the furnace, mold cavity (in the multicavity molding die), and test bar serial number.

The sintering plan included the following features.

- Four identical sintering runs with 70 bars in each run
- Bars sintered in each run would represent one binder removal cycle
- Some known defective bars included to observe possible flaw healing during sintering
- The positioning of bars to allow statistical analysis of injection molding cavity, location in binder removal, sintering layer, and location on the supporting plate in sintering

Test results: A total of 328 bars of Task I baseline material were dewaxed (processed through binder removal) in four dewax runs. The first

run included the first 88 bars that had been injected into the four-cavity injection molding tool. The specimens were distributed in a 30.5 by 30.5 cm (12 by 12 in.) dewax tray. In order to obtain additional information on the effect of the sequence of injection molding, the remaining as-injected bars were randomized over three subsequent dewax runs (80 bars per run) according to the matrix in figure 26. Figure 27 shows typical test bar arrangement and identification in these three dewax runs.

The percent weight loss after dewax was recorded for each bar. The data for each individual run have been statistically analyzed to detect whether the molding cavity, dewax location, and injection sequence have any effect on weight loss. To detect difference in two groups of data, a t test was performed on computer. An example of computer output is shown in table VII. In the output, the t test as well as the mean, the standard deviation, the standard error of mean (S.E.M.), and the histogram, are calculated. Three comparisons are computed: (1) t test with separate variances, (2) t test with pooled variances, and (3) F test for variances. The P-values shown in the output for these three statistics correspond to two-sided tests of significance (i.e., test in equality in either direction). If the P-value approaches one, the two groups are equal. The lower the P-value, the higher the probability that the two groups are different. Values of P below 0.10 are usually considered significant. The results are summarized in tables VIII and IX. The results indicated that:

(1) The bars injected into cavity no. 3 are different in dewax weight loss from those injected into the other cavities (lower percent weight loss).

(2) The dewax locations have no significant effect on dewax weight loss.

A typical dewaxed bar was analyzed by SEM and EDX. Figure 28a, an X-ray image for yttrium, shows the dispersion of yttrium throughout the matrix with some very localized high concentrations. A back-scatter electron image, figure 28b, shows that these high concentrations may be large individual particles of Y_2O_3.

Some flaw healing appears to occur during sintering. Optical inspection indicated that in many samples surface roughness was reduced and sharp discontinuities were rounded. The effect of these changes on measured strength was not determined. Internal defects that had been identified with X-ray radiography prior to sintering showed no significant change resulting from the Task I sintering.

Sintering data of all four sintering runs, including one interrupted run which was subsequently resintered, have been analyzed. The data included percent weight loss, sintered test bar density, sintering tray layer, and test bar location on each sintering tray. A schematic showing the kiln furniture (made of slip-cast reaction-bonded Si_3N_4) used in all

	Load 2						Load 3						Load 4					
Mold Cavity 1	Sequence 1			Sequence 2			Sequence 4			Sequence 2			Sequence 3			Sequence 2		
	Dewax Loc. 1 6	Dewax Loc. 2 9	Total 15	Dewax Loc. 1 2	Dewax Loc. 2 3	Total 5	Dewax Loc. 1 6	Dewax Loc. 2 9	Total 15	Dewax Loc. 1 2	Dewax Loc. 2 3	Total 5	Dewax Loc. 1 6	Dewax Loc. 2 9	Total 15	Dewax Loc. 1 2	Dewax Loc. 2 3	Total 5
	Total Cavity 1 This Load 20						20						20					
Mold Cavity 2	Sequence 2			Sequence 1			Sequence 3			Sequence 1			Sequence 4			Sequence 1		
	6	9	15	2	3	5	6	9	15	2	3	5	6	9	15	2	3	5
	20						20						20					
Mold Cavity 3	Sequence 3			Sequence 4			Sequence 1			Sequence 4			Sequence 2			Sequence 4		
	6	9	15	2	3	5	6	9	15	2	3	5	6	9	15	2	3	5
	20						20						20					
Mold Cavity 4	Sequence 4			Sequence 3			Sequence 2			Sequence 3			Sequence 1			Sequence 3		
	6	9	15	2	3	5	6	9	15	2	3	5	6	9	15	2	3	5
	20						20						20					

Figure 26.--Test matrix.

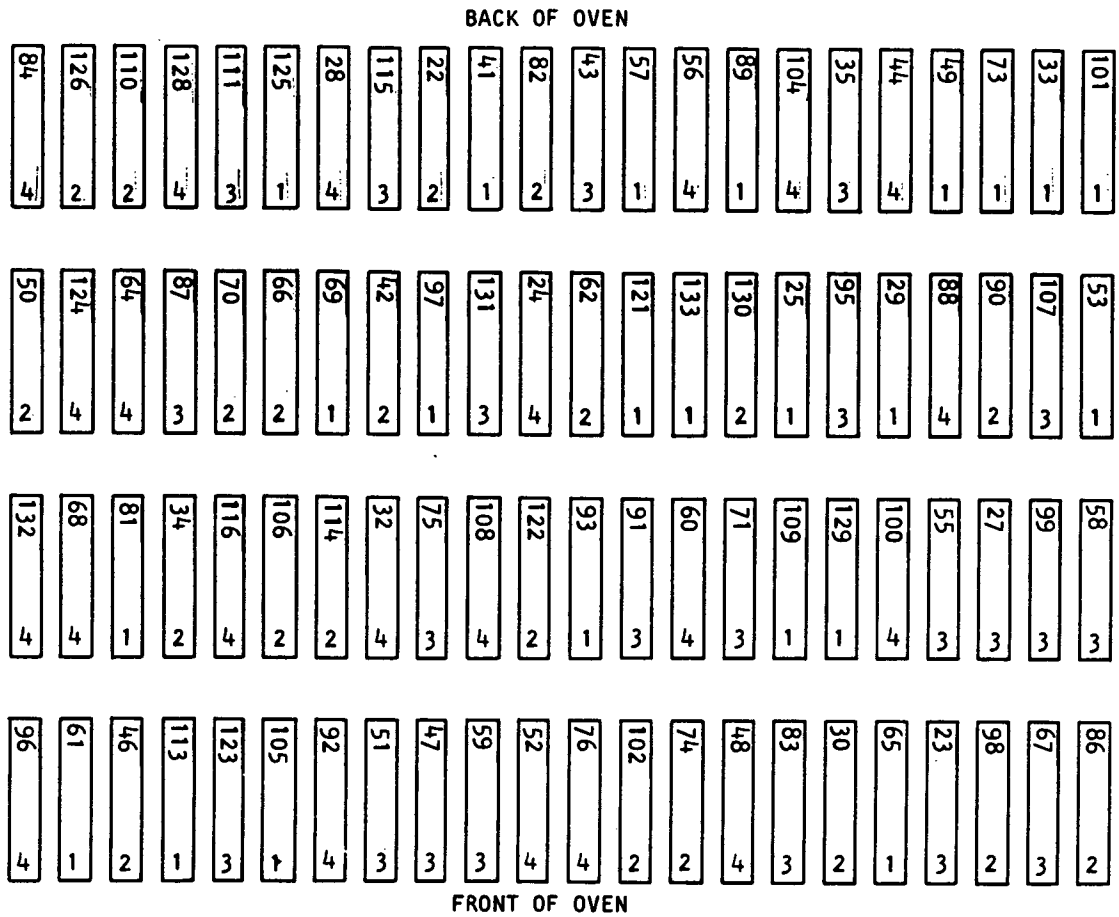

Figure 27.--Detail of test bar arrangement in binder removal oven. Numbers on the top of the bars indicate part sequence number. Numbers on the bottom of the bars indicate cavity location in mold tool.

TABLE VII.--T TEST RESULTS

LOAD 2 DEMAX LOCATION

DIFFERENCES ON SINGLE VARIABLES

****
* LOC1 * VARIABLE NUMBER 2
****

STATISTICS		P-VALUE	DF
T (SEPARATE)	.58	.5685	37.9
T (POOLED)	.58	.5685	38
F(FOR VARIANCES)			
LEVENE	.01	.9304	1, 38

GROUP	3 BACK	4 FRONT
MEAN	15.3000	15.2750
STD DEV	.1338	.1410
S.E.M.	.0299	.0315
SAMPLE SIZE	20	20
MAXIMUM	15.5000	15.6000
MINIMUM	15.0000	15.1000

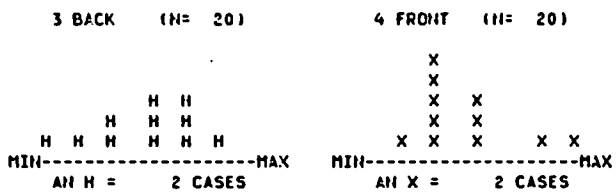

TABLE VIII.--MOLDING CAVITY (DEWAX)

MOLDING CAVITY (DEWAX)

LOAD 1 ($\bar{x}$ = 15.37, σ^2 = 0.061)			LOAD 2 ($\bar{x}$ = 15.28, σ^2 = 0.01167)			LOAD 3 ($\bar{x}$ = 15.364, σ^2 = 0.0463)			LOAD 4 ($\bar{x}$ = 15.474, σ^2 = 0.0416)		
CAVITY	$\bar{x}$	σ^2	CAVITY	$\bar{x}$	σ^2	CAVITY	$\bar{x}$	σ^2	CAVITY	$\bar{x}$	σ^2
1	15.438	0.1936	4	15.305	0.1146	4	15.320	0.0364	1	15.516	0.0525
2	15.382	0.2015	1	15.29	0.0912	2	15.275	0.0598	4	15.495	0.0299
4	15.364	0.2128	2	15.285	0.1137	1	15.255	0.0384	3	15.450	0.0248
3	15.30	0.1817	3	15.245	0.1146	3	15.205	0.0505	2	15.44	0.0592

GROUP	P-VALUE	GROUP	P-VALUE	GROUP	P-VALUE	GROUP	P-VALUE
1,3	0.022	4,3	0.1060	4,3	0.095	1,2	0.293
2,3	0.169	1,3	0.1778	1,4	0.295	1,3	0.329
1,4	0.236	2,3	0.2747	2,3	0.359	2,4	0.375
3,4	0.297	2,4	0.5827	1,3	0.467	3,4	0.429
1,2	0.356	1,4	0.6495	2,4	0.521	1,4	0.752
2,4	0.773	1,2	0.8789	1,2	0.777	2,3	0.789

FOUR MATERIAL

MATERIAL (2)

CAVITY	$\bar{x}$	σ^2
1	15.348	0.0649
4	15.190	--
2	15/175	0.0649
3	15.114	0.0547

MATERIAL (4)

CAVITY	$\bar{x}$	σ^2
4	15.48	0.02839
1	15.46	
2	15.41	
3	15.348	0.0649

MATERIAL VII

CAVITY	$\bar{x}$	σ^2
1	15.18	
2	15.18	
4	15.04	
3	15.04	

MATERIAL

4	15.427	0.02823
2	15.217	0.06505
I	15.20	0.07368
VII	15.110	0.03042

TABLE IX.--(DEWAX) LOCATION

(DEWAX) LOCATION

LOAD 1			LOAD 2			LOAD 3			LOAD 4			FOUR MATERIAL MATERIAL 1 + 2		
LOCATION	$\bar{X}$	σ^2	LOC.	$\bar{X}$	σ^2	LOC.	$\bar{X}$	σ^2	LOC.	$\bar{X}$	σ^2	LOC.	$\bar{X}$	σ^2
Back	15/46		Top	15.308	0.00447	Front	15.325	0.01987	Bottom	15.567	0.04968	Top	15.289	0.0661
Top	15.44		Back	15.30	0.01789	Top	15.30	0.03455	Back	15.525	0.0409	Back	15.208	0.0708
Front	15.286		Front	15.275	0.01987	Bottom	15.30	0.01455	Front	15.384	0.0436	Bottom	15.189	0.0536
Bottom	15.283		Bottom	15.245	0.01273	Back	15.27	0.02221	Top	15.358	0.0372	Front	15.173	0.0662
GROUP		P-VALUE	GROUP		P-VALUE	GROUP		P-VALUE	GROUP		P-VALUE	GROUP		P-VALUE
Back-Front		0.0024			0.5685			0.238			0.0394			
Bot. Top		0.0377			0.1305			1.0			0.023			
Bot. Back		0.0034			0.259			0.539			0.602			
Bot. Front		0.957			0.578			0.599			0.0329			
Top Back		0.758			0.816			0.64			0.0289			
Top Front		0.038			0.375			0.692			0.728			
LOCATION	$\bar{X}$	σ^2	LOCATION	$\bar{X}$	σ^2	LOCATION	$\bar{X}$	σ^2	LOCATION	$\bar{X}$	σ^2	LOCATION	$\bar{X}$	σ^2
Center	15.379	0.219		15.289	0.126		15.189	0.290		15.604	0.191		15.221	0.209
Circumf.	15.371	0.193		15.27	0.0794		15.304	0.1521		15.458	0.209		15.241	0.352
		P-VALUE			P-VALUE			P-VALUE			P-VALUE			P-VALUE
		0.858			0.402			0.0625			0.3436			0.718

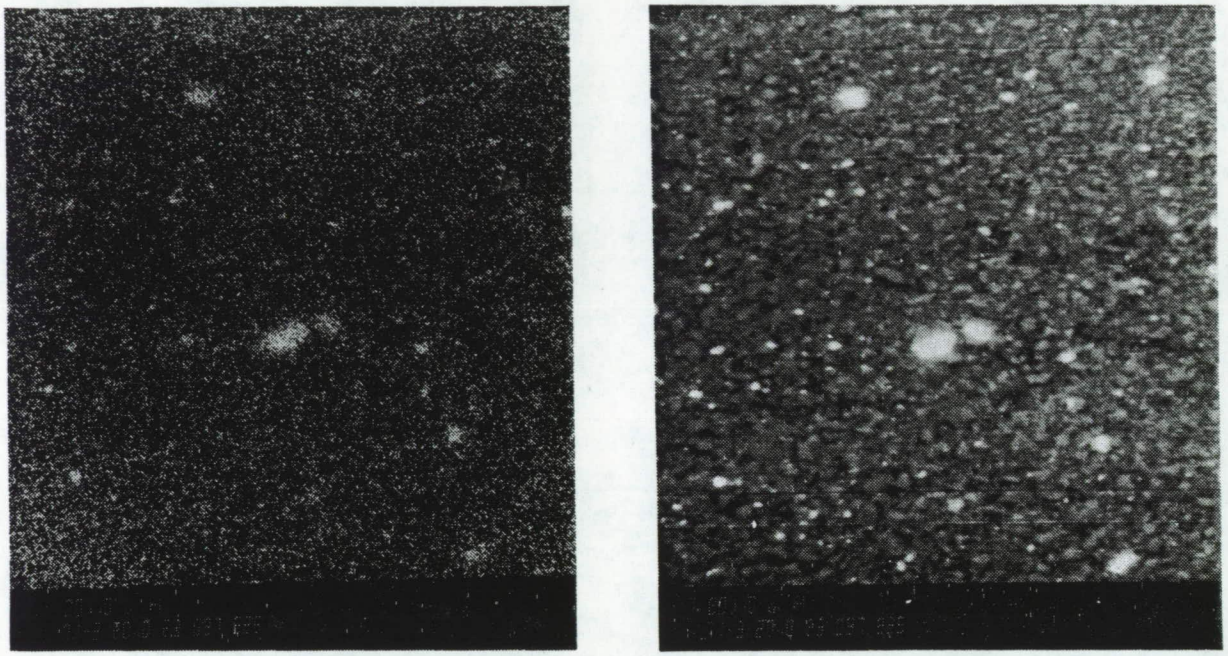

F-48905

Figure 28.--SEM examination of the surface of a test bar after dewax: (A) x-ray image for yttrium (B) back scatter electron image.

the sintering experiments is presented in figure 29. The tray location of the test bars is indicated by location codes A, B, C, and D as shown in figure 30. The purpose of the analysis was to determine whether the sintering tray layer level and the location within each tray have any effect on test bar weight loss and sintered density.

The results are shown in tables X through XV. The tables include the mean values of weight loss (percent) and density (g/cc) for each location on different layers and the P value between the two groups to be compared. The P value is the probability that the mean of two groups, X and Y, will be equal. The value of P is a function of the means, standard deviations, and sample sizes of two groups.

The following conclusions were drawn from the test results.

(1) On the same layer, location A produces the lowest weight loss. The bars in location A exhibit an average 0.315 percent less weight loss than the bars in other locations.

(2) The statistically significant differences test indicated, with a 99-percent confidence, that the difference between location A and other locations is significant.

(3) Except for location A, there was no difference in weight loss between locations.

(4) In the same location, layer level has an effect on weight loss. Layer 3 (top) produces the highest weight loss and layer 1 (bottom) the least.

(5) The statistically significant difference test indicated, with 90-percent confidence, that the difference in weight loss between layers 1 and 2 is not significant, but the differences between layers 1 and 3 and layers 2 and 3 are significant.

(6) There is no difference in sintered test bar density between locations on the same or different layers.

(7) Statistical difference tests indicated that differences do exist in weight loss and density, with more than 95-percent confidence in most cases. The average difference from run to run is more than 0.15 percent for weight loss but less than 0.03 percent for density.

Subtask 4 - post-process characterization and statistical and fractographic analysis.--Subtask 4 includes the measurements of strength (MOR) at selected temperatures and after exposure to oxidation, the stress rupture data, probability of failure data, and determination and analysis of origin of failure during testing.

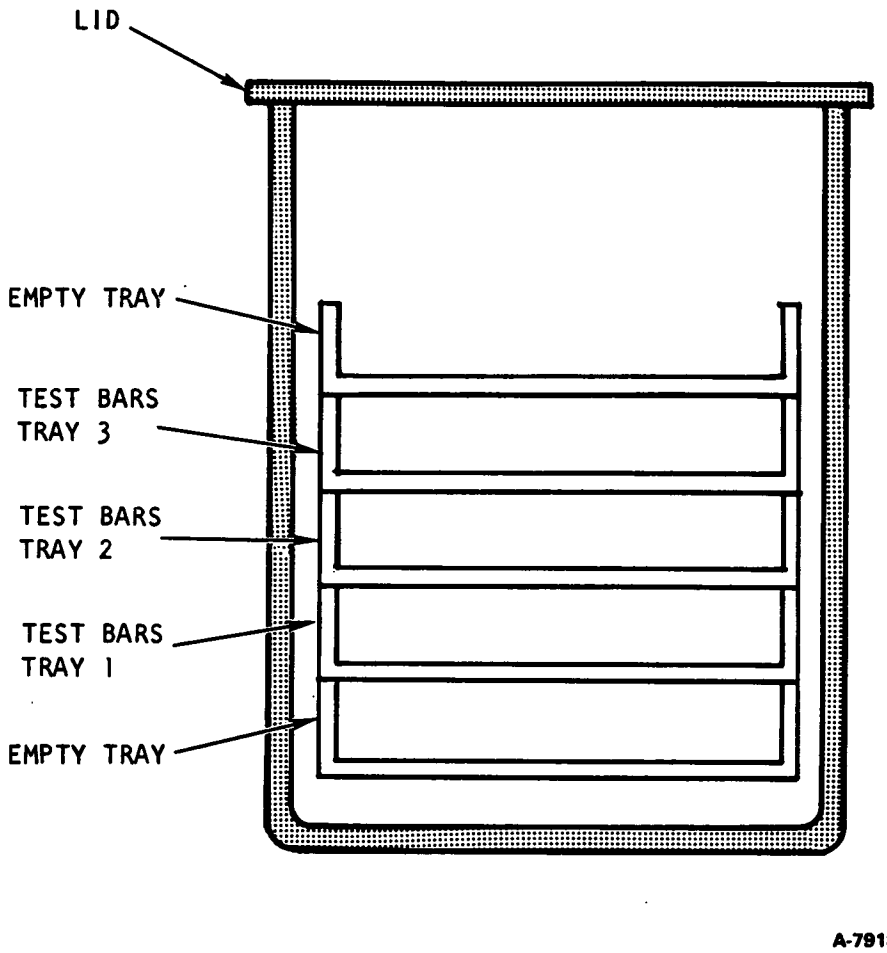

Figure 29.--Schematic showing the cross section of the reaction-bonded silicon nitride sintering kiln furniture.

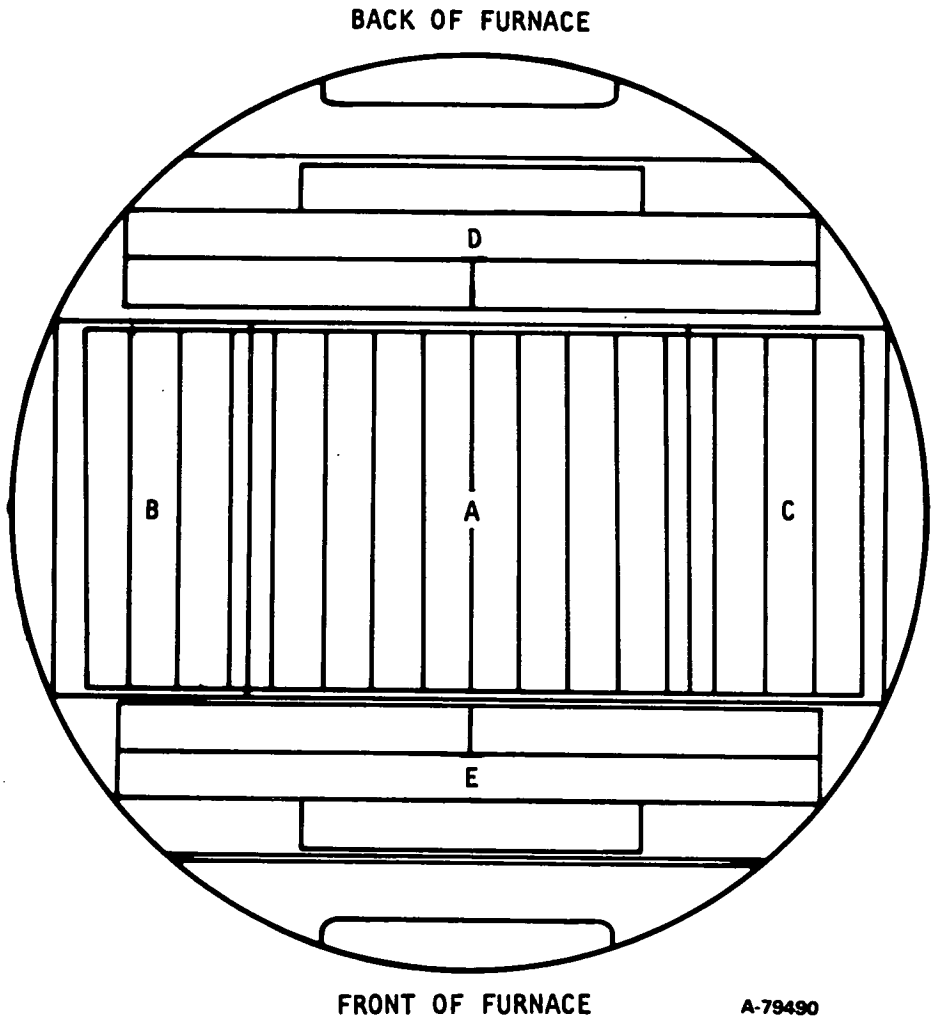

Figure 30.--Test bar location codes on sintering tray.

TABLE X.--SINTERING DATA: BASELINE MATERIAL TASK I, LOAD 1

All Layer			Separated Layer					
Location	$\bar{X}$ % Weight Loss	$\bar{X}$ g/cc Density	Location	$\bar{X}$ % Weight Loss	$\bar{X}$ g/cc Density	Significant Diff. Test	P-Value Weight Loss	P-Value Density
A	1.291	3.226	A1*	1.025	3.220	A1 - A2	0.957	0.337
B	1.867	3.233	A2	1.028	3.216	A1 - A3	0.000	0.004
C	1.678	3.229	A3	1.857	3.243	A2 - A3	0.000	0.0004
D	1.787	3.225	B1	1.567	3.230	B1 - B2	0.834	0.491
E	1.540	3.225	B2	1.633	3.223	B1 - B3	0.0379	0.0668
			B3	2.40	3.247	B2 - B3	0.0735	0.0352
Center*	1.291	3.226	C1	1.30	3.227	C1 - C2	0.643	0.374
Circumf.*	1.740	3.227	C2	1.43	3.220	C1 - C3	0.0194	0.116
			C3	2.30	3.24	C2 - C3	0.0383	0.075
Significant Difference Test of the Mean Groups	P-Value Weight Loss	P-Value Density	D1	1.780	3.224	D1 - D2	0.410	0.724
			D2	1.380	3.222	D1 - D3	0.387	0.346
			D3	2.20	3.230	D2 - D3	0.000	0.650
A - B	0.0003	0.242	E1	1.280	3.214	E1 - E2	0.259	0.108
A - C	0.040	0.647	E2	1.380	3.228	E1 - E3	0.107	0.034
A - D	0.0075	0.848	E3	1.960	3.232	E2 - E3	0.161	0.373
A - E	0.124	0.756						
B - C	0.462	0.461	Circumf. 1	1.493	3.223	Circumf. 1 - Circumf. 2	0.730	0.785
B - D	0.757	0.0813						
B - E	0.162	0.121	Circumf. 2	1.437	3.224	Circumf. 1 - Circumf. 3	0.000	0.0026
C - D	0.680	0.393						
C - E	0.559	0.419	Circumf. 3	2.306	3.235	Circumf. 2 - Circumf. 3	0.000	0.0004
D - E	0.162	0.121						
Center - Circumf.	0.001	0.553						

*Center location is the location A. Circumferential location is B + C + D + E
*Number 1, 2, 3, is layer 1, 2, 3
*P Value is the probability the two groups to be equal

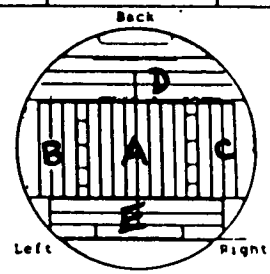

TABLE XI.--SINTERING DATA: BASELINE MATERIAL TASK I, LOAD 2

All Layer			Separated Layer					
Location	$\bar{X}$ % Weight Loss	$\bar{X}$ g/cc Density	Location	$\bar{X}$ % Weight Loss	$\bar{X}$ g/cc Density	Significant Diff. Test	P-Value Weight Loss	P-Value Density
A	0.404	3.195	A1*	0.437	3.20	A1 - A2	0.593	0.796
B	0.467	3.198	A2	0.414	3.190	A1 - A3	0.0938	0.037
C	0.511	3.199	A3	0.357	3.193	A2 - A3	0.0395	0.067
D	0.493	3.201	B1	0.400	3.20	B1 - B2	0.288	0.725
E	0.540	3.193	B2	0.500	3.197	B1 - B3	0.435	0.374
Center*			B3	0.50	3.197	B2 - B3	1.0	1.0
Circumf.*			C1	0.533	3.210	C1 - C2	0.579	0.158
			C2	0.467	3.190	C1 - C3	1.00	0.274
			C3	0.533	3.197	C2 - C3	0.579	0.374
			D1	0.380	3.198	D1 - D2	0.0125	0.565
			D2	0.500	3.20	D1 - D3	0.0004	0.856
			D3	0.600	3.20	D2 - D3	0.056	0.636
			E1	0.520	3.196	E1 - E2	0.346	0.403
			E2	0.500	3.190	E1 - E3	0.065	1.00
			E3	0.600	3.196	E2 - E3	0.0133	0.621
			Circumf. 1	0.456	3.20	Circumf. 1 - Circumf. 2	0.255	0.929
			Circumf. 2	0.493	3.20	Circumf. 1 - Circumf. 3	0.018	0.629
			Circumf. 3	0.550	3.19	Circumf. 2 - Circumf. 3	0.099	0.664
Significant Difference Test of the Mean Groups	P-Value Weight Loss	P-Value Density						
A - B	0.101	0.504						
A - C	0.008	0.413						
A - D	0.007	0.186						
A - E	0.000	0.771						
B - C	0.461	0.837						
B - D	0.587	0.075						
B - E	0.065	0.509						
C - D	0.721	0.768						
C - E	0.463	0.443						
D - E	0.165	0.232						
Center - Circumf.	0.0002	0.705						

*Center location is the location A. Circumferential location is B + C + D + E
*Number 1, 2, 3, is layer 1, 2, 3
*P Value is the probability the two groups to be equal

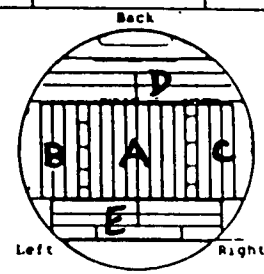

TABLE XII.--SINTERING DATA: BASELINE MATERIAL TASK I, LOAD 3

All Layer			Separated Layer					
Location	$\bar{X}$ % Weight Loss	$\bar{X}$ g/cc Density	Location	$\bar{X}$ % Weight Loss	$\bar{X}$ g/cc Density	Significant Diff. Test	P-Value Weight Loss	P-Value Density
A	0.495	3.219	A1*	0.50	3.22	A1 - A2	0.681	0.461
B	0.711	3.227	A2	0.486	3.21	A1 - A3	0.681	0.793
C	0.844	3.227	A3	0.514	3.22	A2 - A3	0.563	0.448
D	0.747	3.216	B1	0.70	3.237	B1 - B2	0.10	0.184
E	0.747	3.219	B2	0.70	3.216	B1 - B3	0.851	0.467
			B3	0.733	3.227	B2 - B3	0.851	0.467
Center*	0.495	3.219	C1	0.667	3.230	C1 - C2	0.219	0.767
Circumf.*	0.745	3.215	C2	0.867	3.223	C1 - C3	0.202	0.877
			C3	1.00	3.226	C2 - C3	0.609	0.874
Significant Difference Test of the Mean Groups	P-Value Weight Loss	P-Value Density	D1	0.60	3.214	D1 - D2	0.0039	0.840
			D2	0.76	3.216	D1 - D3	0.0004	0.619
			D3	0.88	3.218	D2 - D3	0.0278	0.803
A - B	0.000	0.323	E1	0.620	3.230	E1 - E2	0.241	0.346
A - C	0.000	0.368	E2	0.660	3.212	E1 - E3	0.053	0.407
A - D	0.000	0.531	E3	0.820	3.216	E2 - E3	0.111	0.666
A - E	0.000	0.981						
B - C	0.216	1.00	Circumf. 1	0.637	3.210	Circumf. 1 - Circumf. 2	0.0196	0.577
B - D	0.576	0.079						
B - E	0.576	0.411	Circumf. 2	0.737	3.216	Circumf. 1 - Circumf. 3	0.0007	0.329
C - D	0.237	0.138						
C - E	0.237	0.451	Circumf. 3	0.856	3.221	Circumf. 2 - Circumf. 3	0.064	0.413
D - E	1.00	0.626						
Center - Circumf.	0.000	0.553						

*Center location is the location A. Circumferential location is B + C + D + E
*Number 1, 2, 3, is layer 1, 2, 3
*P Value is the probability the two groups to be equal

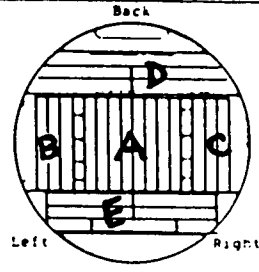

TABLE XIII.--SINTERING DATA: BASELINE MATERIAL TASK I, LOAD 4

All Layer			Separated Layer					
Location	$\bar{X}$ % Weight Loss	$\bar{X}$ g/cc Density	Location	$\bar{X}$ % Weight Loss	$\bar{X}$ g/cc Density	Significant Diff. Test	P-Value Weight Loss	P-Value Density
A	0.636	3.225	A1*	0.462	3.222	A1 - A2	0.097	0.783
B	1.067	3.233	A2	0.557	3.224	A1 - A3	0.000	0.365
C	1.244	3.229	A3	0.914	3.228	A2 - A3	0.000	0.218
D	1.080	3.228	B1	0.867	3.227	B1 - B2	0.896	0.250
E	0.993	3.225	B2	0.90	3.237	B1 - B3	0.151	0.417
			B3	1.433	3.237	B2 - B3	0.21	1.00
Center*	0.636	3.225	C1	1.10	3.227	C1 - C2	1.0	0.518
Circumf.*	1.0813	3.228	C2	1.10	3.223	C1 - C3	0.217	0.101
			C3	1.533	3.237	C2 - C3	0.245	0.047
Significant Difference Test of the Mean Groups	P-Value Weight Loss	P-Value Density	D1	0.840	3.218	D1 - D2	0.0486	0.241
			D2	1.020	3.226	D1 - D3	0.0002	0.025
			D3	1.380	3.240	D2 - D3	0.006	0.147
A - B	0.0008	0.059	E1	0.720	3.218	E1 - E2	0.0415	0.291
A - C	0.000	0.328	E2	0.920	3.226	E1 - E3	0.0002	0.078
A - D	0.000	0.475	E3	1.340	3.232	E2 - E3	0.0003	0.494
A - E	0.0001	0.931						
B - C	0.380	0.343	Circumf. 1	0.856	3.221	Circumf. 1 - Circumf. 2	0.113	0.081
B - D	0.926	0.361						
B - E	0.624	0.128	Circumf. 2	0.981	3.227	Circumf. 1 - Circumf. 3	0.000	0.0005
C - D	0.22	0.869						
C - E	0.08	0.451	Circumf. 3	1.406	3.236	Circumf. 2 - Circumf. 3	0.000	0.000
D - E	0.403	0.597						
Center - Circumf.	0.000	0.275						

*Center location is the location A. Circumferential location is B + C + D + E

*Number 1, 2, 3, is layer 1, 2, 3

*P Value is the probability the two groups to be equal

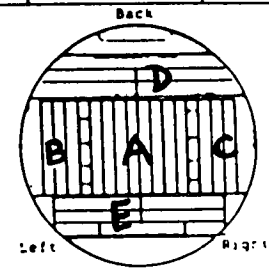

TABLE XIV.--COMPARISON OF DATA FROM LOAD TO LOAD

Load	$\bar{X}$ Weight loss	$\bar{X}$ Density	Significant difference test of the mean groups	P-value, weight loss	P-value, density
1 (Rerun)	1.63	3.227	1-2	0.000	0.000
2	0.48	3.197	1-3	0.000	0.060
3	0.70	3.221	1-4	0.002	0.856
4	1.00	3.228	2-3	0.007	0.000
			2-4	0.001	0.000
			3-4	0.035	0.046

TABLE XV.--SINTERING DATA: FOUR MATERIALS, MATRIX 1, AND TASK VII

1850C					1900C				
	Layer 2		Layer 3			Layer 2		Layer 3	
Material	Weight Loss	Density	Weight Loss	Density	Material	Weight Loss	Density	Weight Loss	Density
1*	-0.825	3.187	0.78	3.160	1	-0.225	3.205	0.350	3.20
3	+1.486	3.062	1.517	3.067	3	+2.52	3.006	2.433	2.975
4	+1.072	2.998	1.120	3.160	4	+1.871	3.205	1.90	3.055
7	-1.025	3.17	0.880	2.986	7	-0.20	3.05	0.375	3.207

Comparison Within Layer					Comparison Within Layer				
	Layer 2		Layer 3			Layer 2		Layer 3	
Group	P_{Weight}	$P_{Density}$	P_{Weight}	$P_{Density}$	Group	P_{Weight}	$P_{Density}$	P_{Weight}	$P_{Density}$
1 - 3	0.0001	0.0002	0.000	0.0005	1 - 3	0.000	0.000	0.000	0.000
1 - 4	0.1097	0.000	0.0140	0.000	1 - 4	0.000	0.000	0.000	0.000
1 - 7	0.0656	0.189	0.364	0.0137	1 - 7	0.571	0.878	0.537	0.537
3 - 4	0.0026	0.0044	0.0016	0.0012	3 - 4	0.000	0.0041	0.0003	0.000
3 - 7	0.0003	0.0007	0.000	0.000	3 - 7	0.000	0.000	0.000	0.000
4 - 7	0.734	0.000	0.0416	0.000	4 - 7	0.256	0.000	0.000	0.000

Comparison Between Layer			Comparison Between Layer		
Group	P_{Weight}	$P_{Density}$	Group	P_{Weight}	$P_{Density}$
(Material 1 Layer 2) - (Material 1 Layer 3)	0.70	0.083	(Material 1 Layer 2) - (Material 1 Layer 3)	0.0170	0.134
(Material 3 Layer 2) - (Material 3 Layer 3)	0.6995	0.804	(Material 3 Layer 2) - (Material 3 Layer 3)	0.1664	0.0676
(Material 4 Layer 2) - (Material 4 Layer 3)	0.713	0.401	(Material 4 Layer 2) - (Material 4 Layer 3)	0.774	0.465
(Material 7 Layer 2) - (Material 7 Layer 3)	0.136	0.0369	(Material 7 Layer 2) - (Material 7 Layer 3)	0.0042	0.000

*MATERIAL 1 - M_1 SIGMA

*MATERIAL 3 - M_2 SIGMA

*MATERIAL 4 - M_4 SIGMA

*MATERIAL 7 - M_1 HAAKE

Materials tested: The specimens analyzed in this subtask are those that were sintered in the four sintering runs described in Subtask 3.

Test apparatus: Strength data were generated at GTEC on an Instron model 1125. X-ray radiography was conducted at GTEC using microfocus X-ray techniques. Zyglo dye penetrant inspection was done at GTEC using white and/or black light at magnifications up to 40 times. Fractography was conducted at GTEC using light microscopy and an ETEC autoscan SEM.

Test procedures: Strength data were generated at GTEC at a strain rate of 0.5 mm (0.020 in.) per minute. All test data and inspection observations were compiled using techniques and practices developed primarily at GTEC over a 10-year period on a number of ceramic development programs.

Prior to MOR testing, all specimens were visually inspected at 40 times magnification and then examined using X-ray and Zyglo dye penetrant. Each test bar was assigned two grades of 0 to 5, one based on the microfocus X-ray results in accordance with the definitions of these grades in table XVI, the other based on visual inspection of surface quality.

Test results: The Task I block diagram of figure 20 indicates that 210 baseline bars and 74 experimental bars (including 68 that were resintered after an interruption in the programmed sintering cycle) were available for baseline characterization. This characterization included determination of room temperature strength, strength at each of three elevated temperatures, strength after oxidation, and stress rupture.

Every sintered bar was inspected with an optical microscope up to 40 times magnification, and a surface quality grade was assigned on a scale of 0 to 5, indicating decreasing surface quality. Figure 31 is a histogram showing the distribution of the number of sintered test bars as a function of the surface quality grade.

Three groups of 20 bars were selected from the randomized listing along with 6 experimental bars, which included bars from both the resintered lot and the periphery of the sintering furnace. These were tested to measure flexural strength (MOR) at room temperature.

Figure 32 is a Weibull plot (two-parameter model) of the 66 bars with bar number and visual quality grade marked at each datum point. The average MOR, 540 MPa (79.3 ksi), and Weibull modulus (m) of 7.9 are consistent with the properties of the baseline material at the time the proposal was prepared. This group of test bars included some bars from the resintered group as well as some sintered in locations different from the controlled arrangement specifically designed for this program. These variations in sintering were typical of the practices prior to the start of this program at ACC.

TABLE XVI.--VISUAL AND X-RAY GRADE DEFINITIONS

Grade	Description
0	Best
1	Minor flaw(s) outside test zone
2	Major flaw(s) outside test zone
3	Minor flaw(s) in test zone, probably not strength limiting*
4	Moderate flaw(s) in test zone, probably strength limiting
5	Serious flaw(s) in test zone, significantly strength limiting

*Does not exclude the possibility of major flaws outside the test zone.

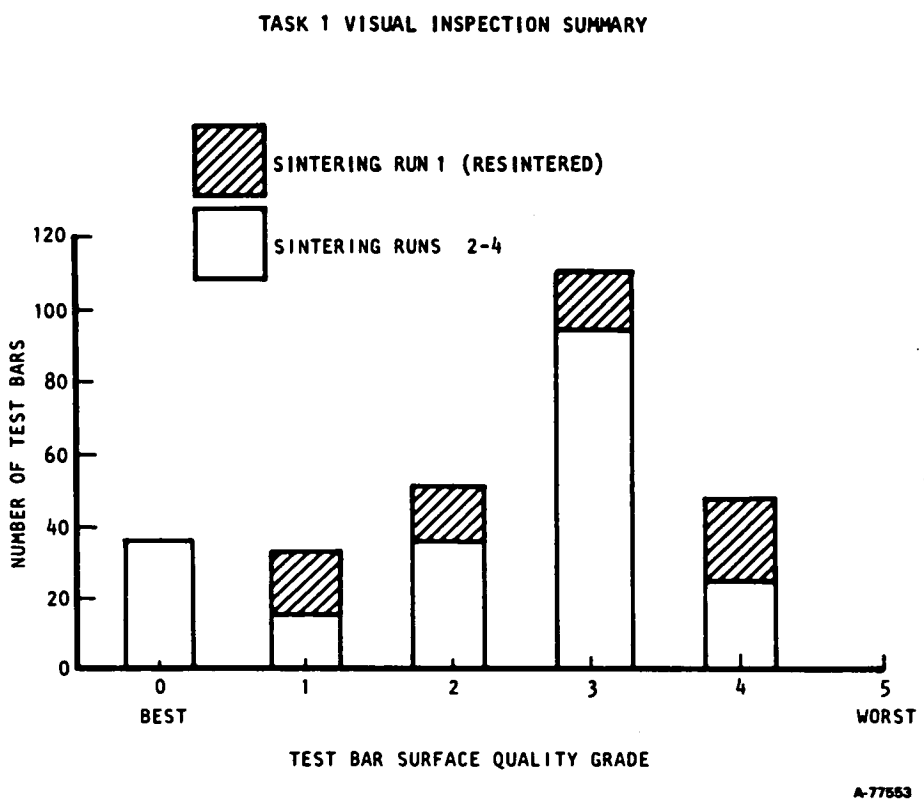

Figure 31.--Distribution of sintered test bars as a function of surface quality.

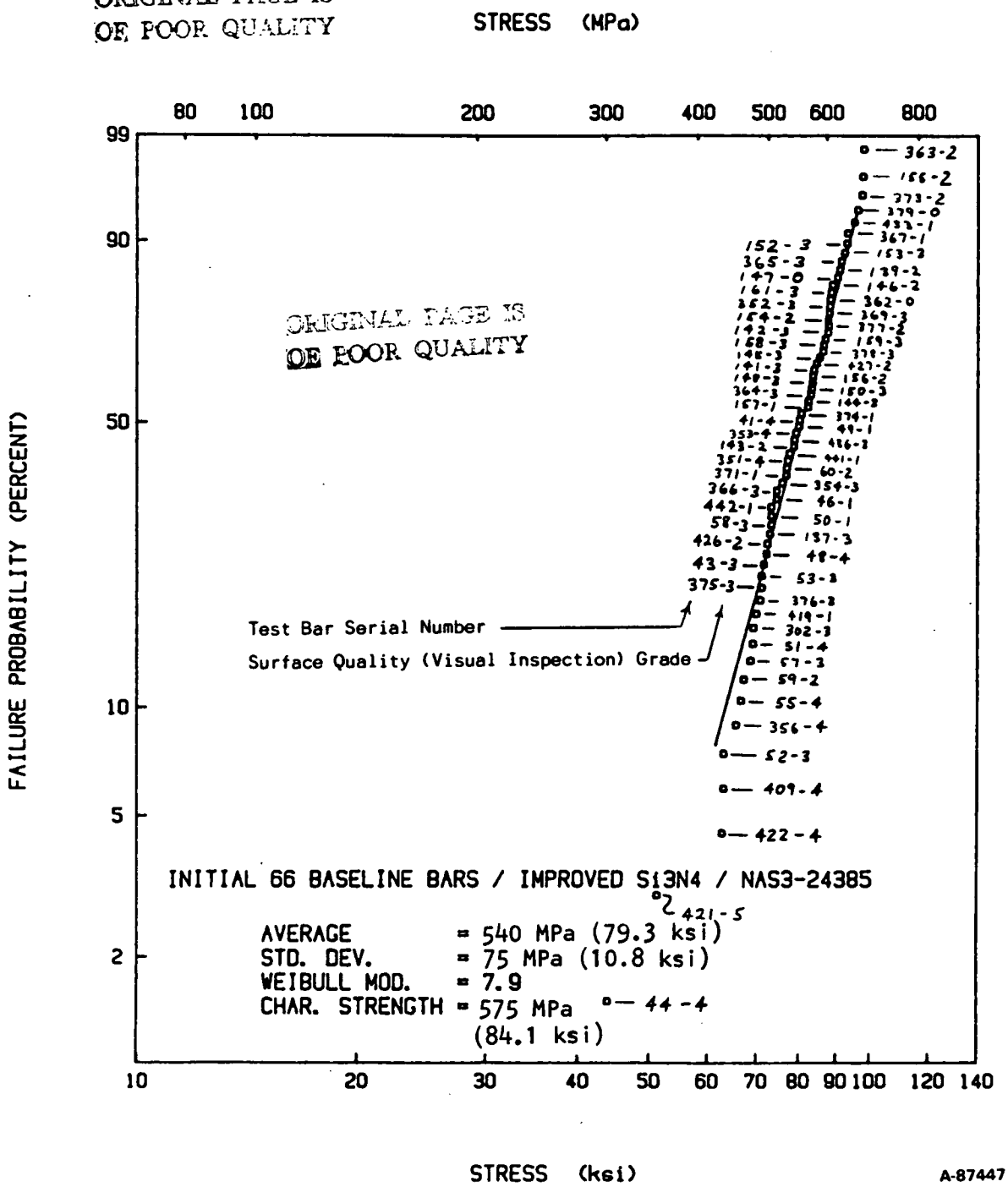

Figure 32.--Weibull plot preliminary testing on baseline bars.

After establishing the initial baseline room temperature strength and Weibull modulus, additional test bars were flexure tested at room temperature. This testing increased the Task I data base to 116 bars, 26 of which were resintered. This additional room temperature data was necessary to enable a more conclusive statistical analysis of Task I variables (i.e., dewax weight loss, sintering position, sintering weight loss, density, etc.).

The mean and standard deviation for the 90 sintered specimens that were tested was 560 +53 MPa (81.8 +7.9 ksi) (normal distribution). This includes eight Task VII specimens that were processed using baseline procedures. The mean and standard deviation for the 26 Task I resintered specimens tested was 475 $\pm$46 MPa (70.2 $\pm$6.7 ksi).

All fracture surfaces of the tested specimens were examined using a 40 times magnification binocular microscope. Some of the failures originated from inclusions, which were either metallic or rust-colored in appearance. SEM and EDX analyses were performed on selected baseline specimens flexure tested at room and elevated temperatures to determine the nature of these inclusions. Inclusions were seen on the fracture surfaces of several specimens. An example is shown in figure 33. The EDX analysis of this inclusion, shown in figure 34, revealed iron as the major constituent in most cases. Traces of chromium and nickel were present along with the iron, suggesting a stainless steel as the contaminant source. Some specimens exhibited spherical inclusions which contained, in addition to iron, a significant amount of molybdenum (fig. 35 and 36). Molybdenum was detected only in these spherical inclusions. Many of the fracture surfaces of the 1399°C (2550°F) test specimens exhibited bright areas near the tensile face. An example is shown in figure 37. An EDX spectrum of this area (fig. 38) showed that the bright area consisted mostly of titanium and chromium along with several other elements.

A closer examination of selected specimens found that there was a skin effect on the fracture surface. EDX analysis of the different shaded areas gave the same energy spectrum showing silicon peaks only. BSE imaging with an SEM is sensitive to the density of the material and was used to highlight this effect. An example is shown in figure 39. The brighter areas of the micrograph may be the denser regions. Polished sections will be prepared to examine the skin effect in more detail.

Large flaws (of about 2 mm) were detected in specimens by X-radiography. Figures 40 and 41 show internal and subsurface flaws. Laminar flaws, revealed by SEM on a fractured surface as shown in figure 40, are generally clear in X-radiography. The effect these flaws have on the strength is entirely dependent on their location. They may not influence the reported strength of a specific bar.

In order to compare the elevated temperature strength of normally sintered bars with that of resintered test bars, 38 specimens were flexure tested at elevated temperatures; 30 were sintered specimens, and 8 were resintered. The flexure strength is plotted as a function of

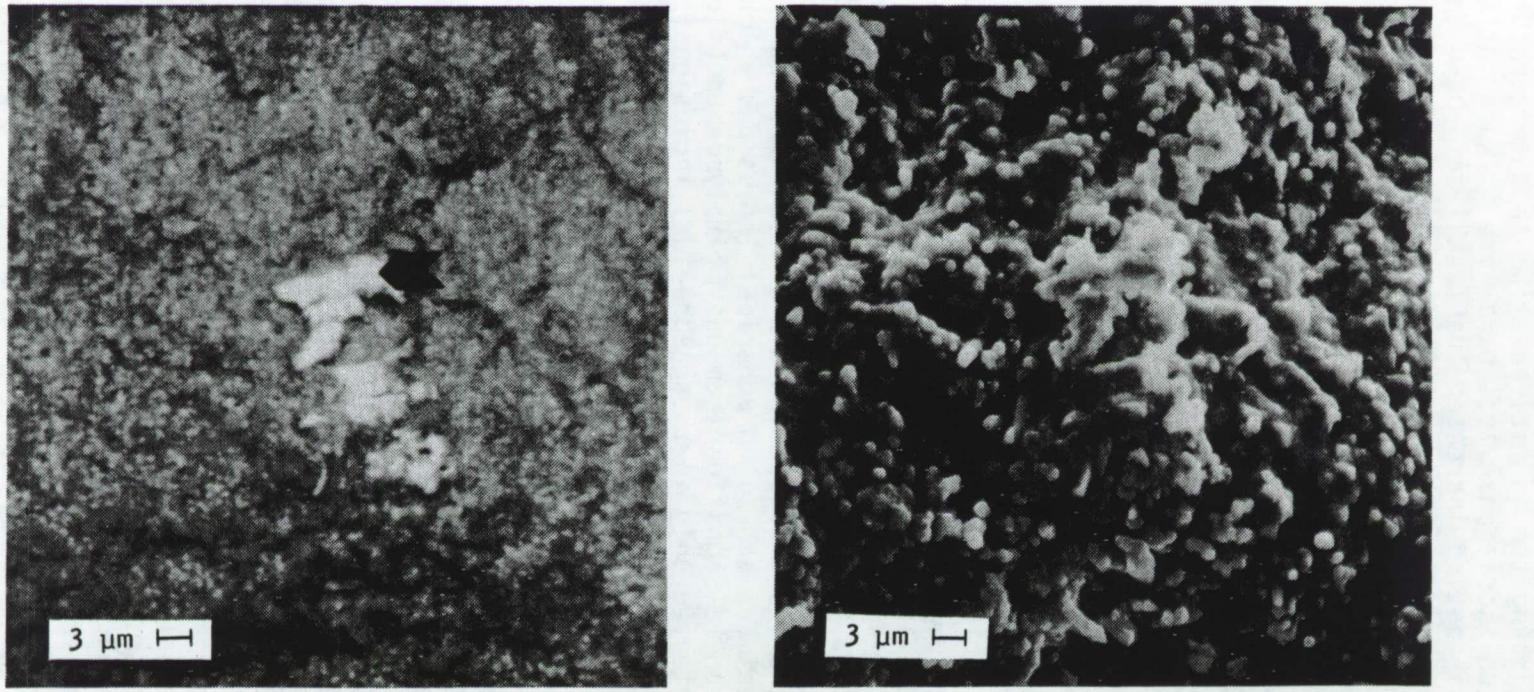

BSE Image

Secondary Emission Image

91689-4

F-47919

Figure 33.--SEM micrographs of fractured surface (test bar no. 202, fractured at room temperature) showing a metallic, irregularly shaped inclusion.

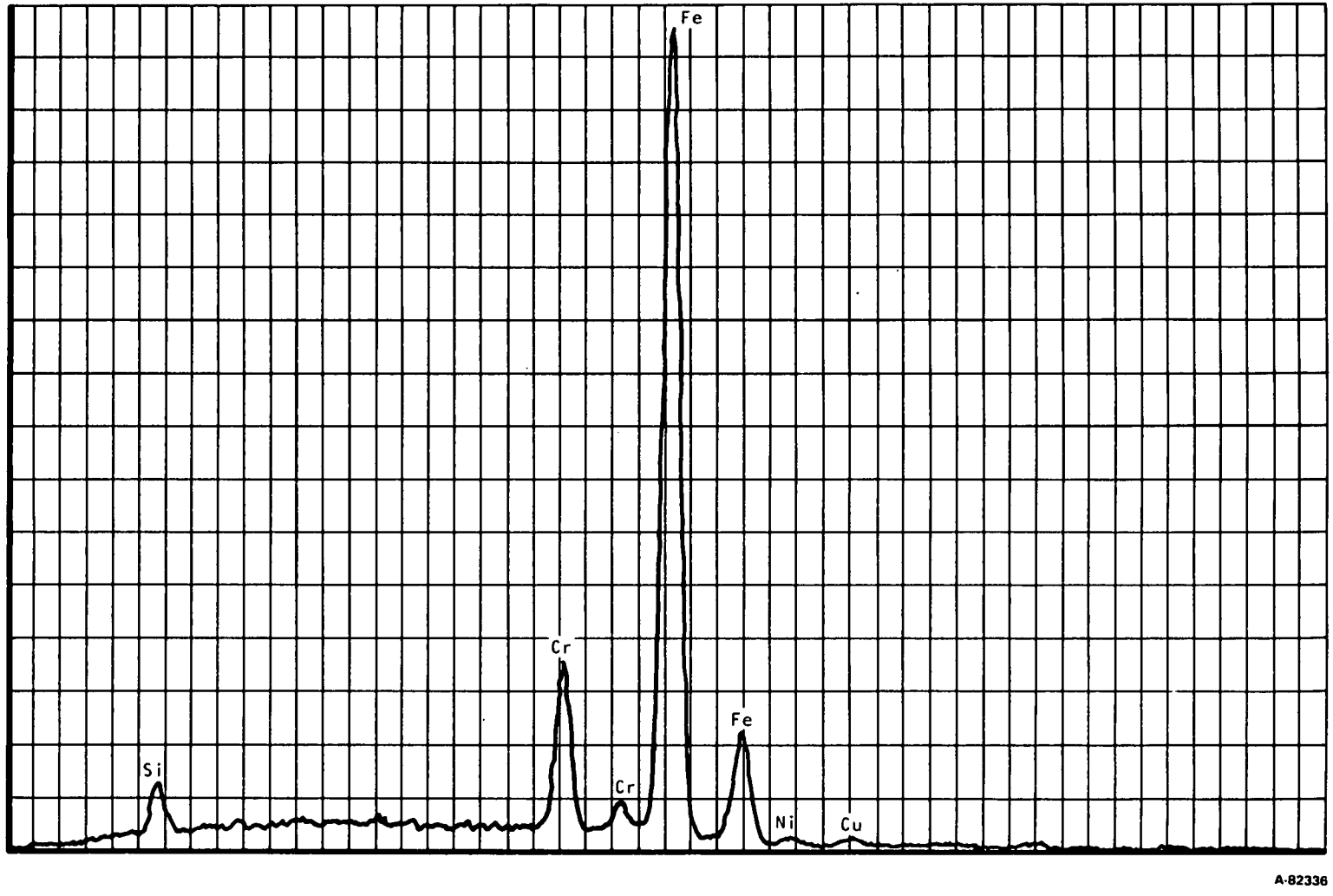

Figure 34.--EDX spectrum of bright area in BSE image of test bar no. 202 (fig. 33), showing inclusion to consist of iron, chromium, and nickel.

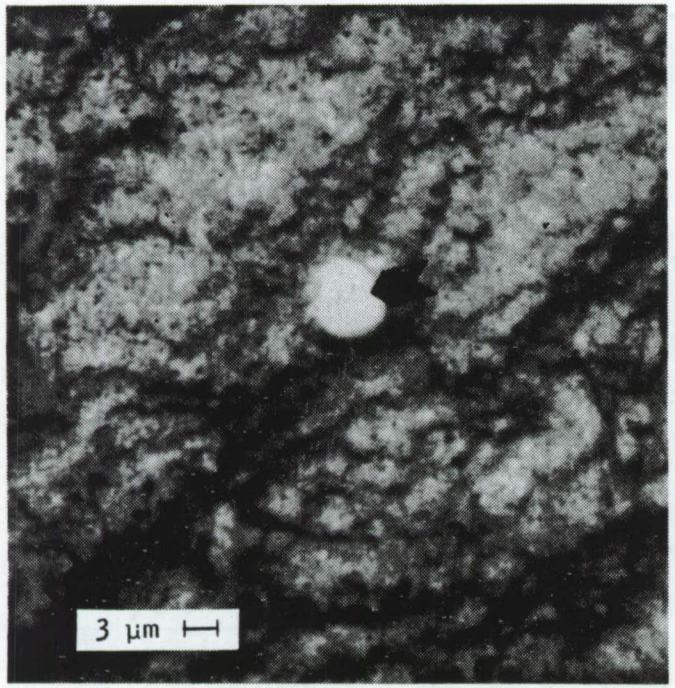

BSE Image

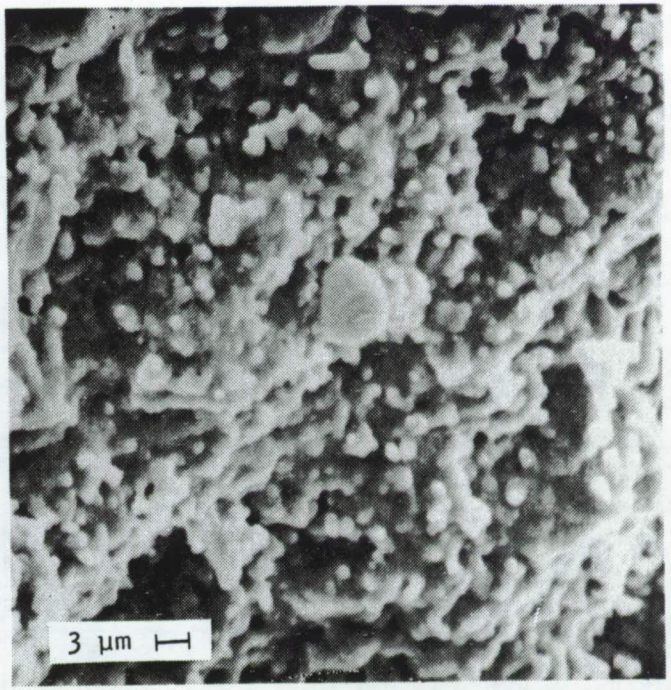

Secondary Emission Image

91689-5

F-47920

Figure 35.--SEM micrographs of fractured surface of test bar no. 202, showing a spherical metallic inclusion.

Figure 36.--EDX spectrum of the spherical inclusion in figure 35, showing inclusion to consist of iron, molybdenum, nickel, and copper.

Figure 37.--SEM micrographs of the fracture surface of test bar no. 255 (flexure tested at 1399°C).

Figure 38.--EDX spectrum of the bright area near tensile face of test bar no. 255 (fig. 37), showing mostly titanium and chromium with other minor constituents.

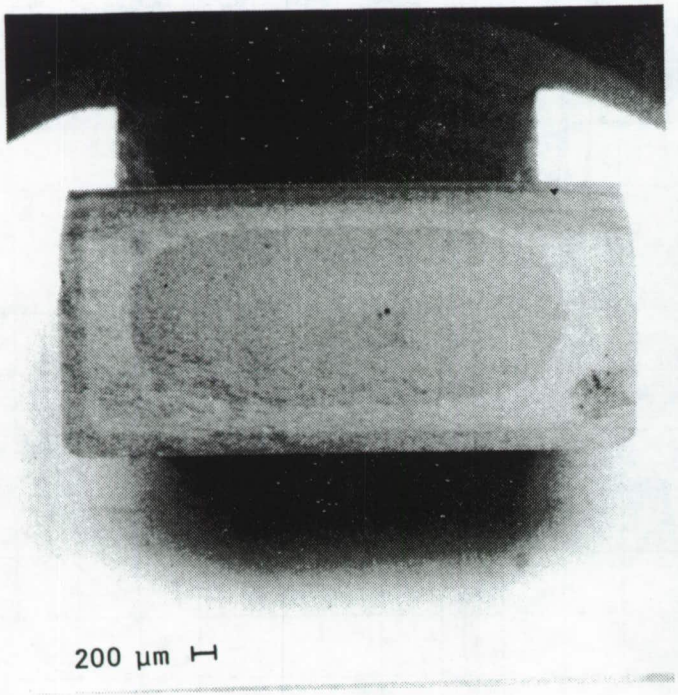

BSE Image

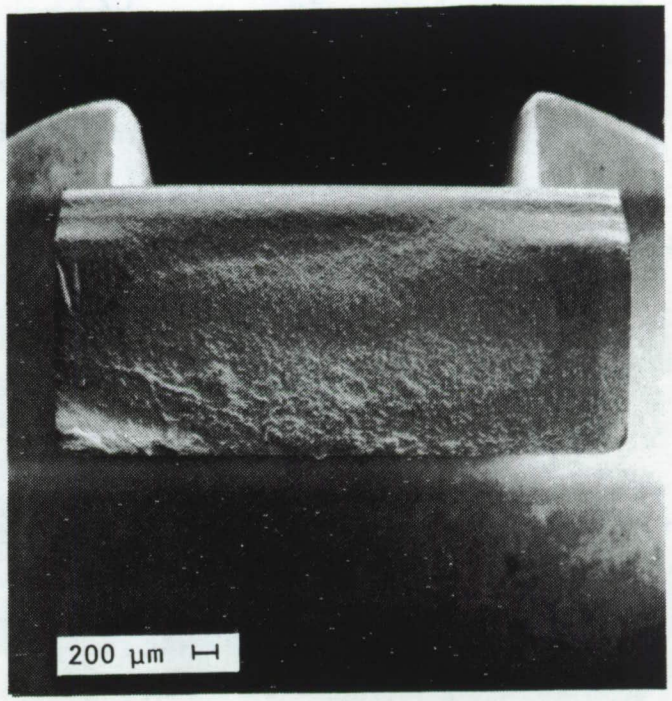

91689-3

Secondary Emission Image

F-47922

Figure 39.--Skin effect observed on the fractured surface of test bars tested at high temperature (test bar no. 250, tested at 1232°F).

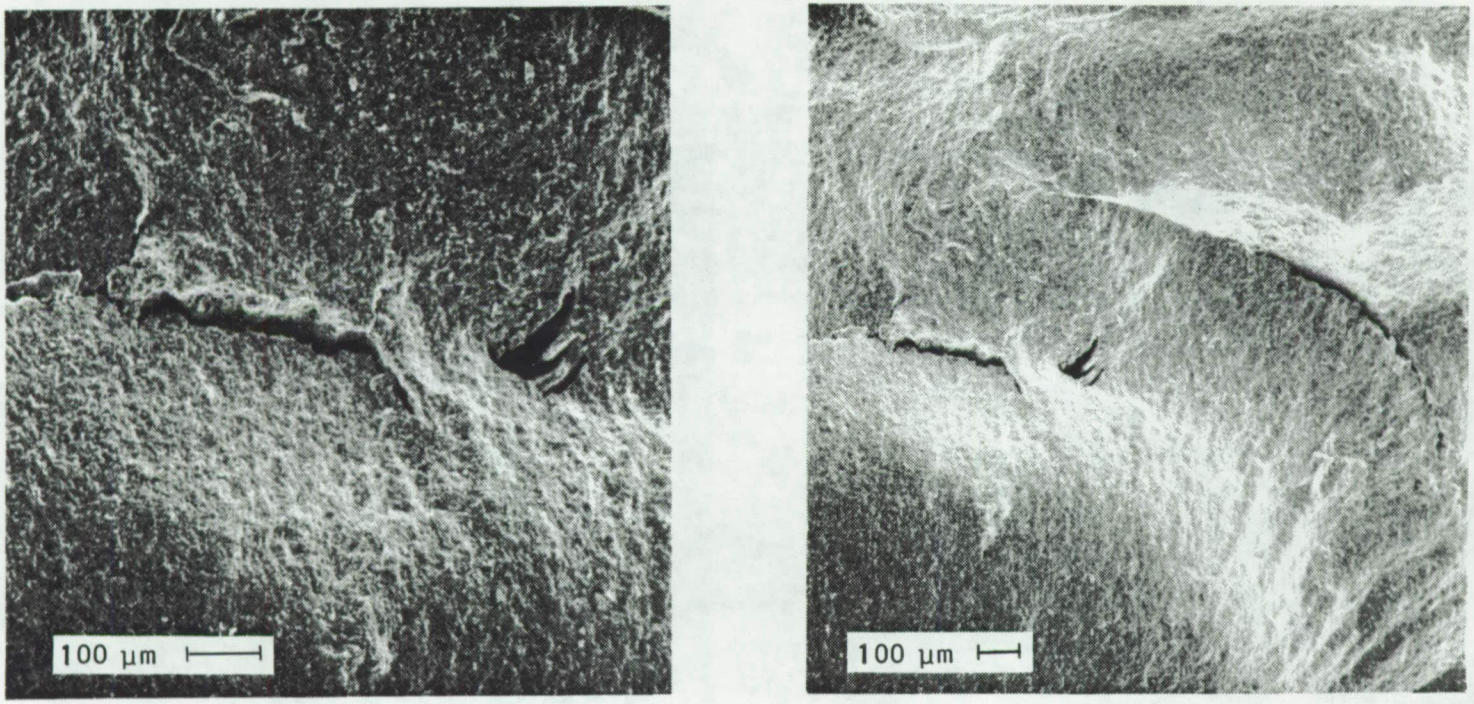

91644-5

F-47923

Figure 40.--SEM micrographs showing internal laminar flaw observed on fractured surface (test bar no. 321).

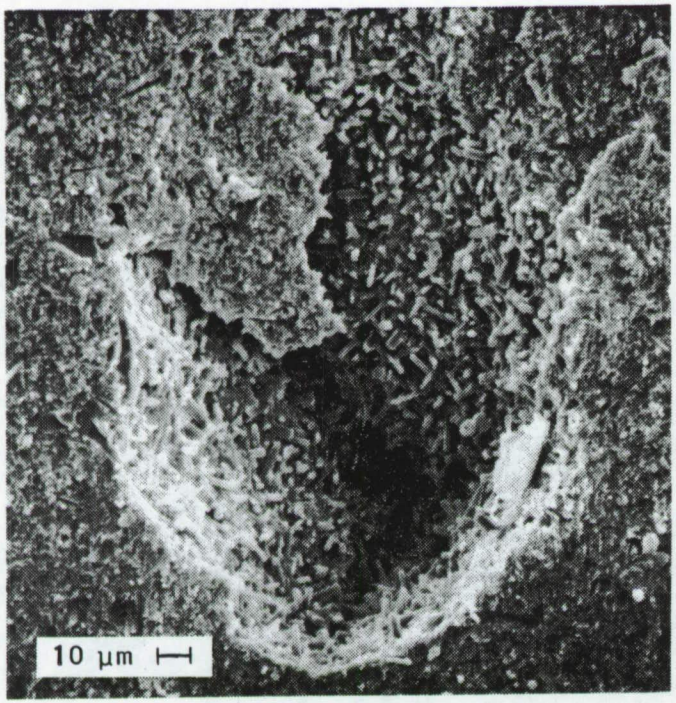

TEST BAR NO. 302

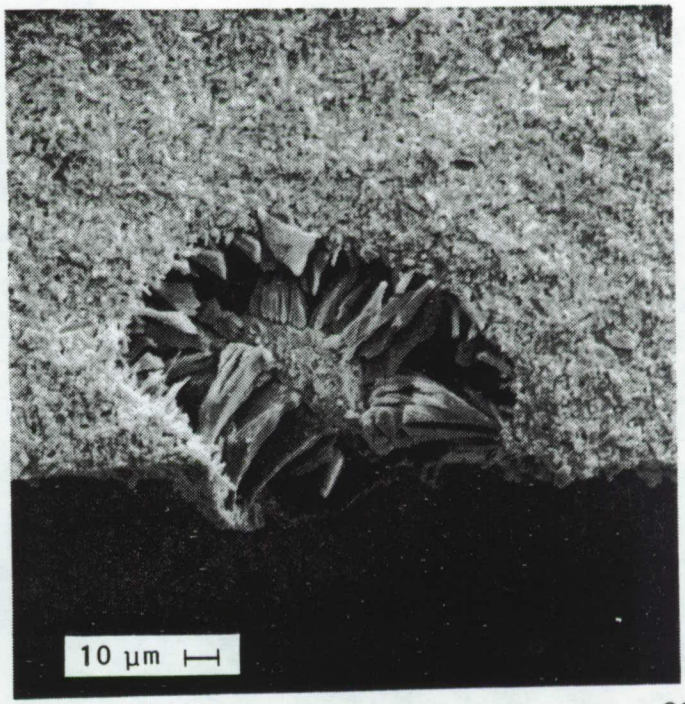

TEST BAR NO. 356

91644-11

F-47924

Figure 41.--SEM micrographs showing internal and subsurface flaws on fractured surfaces (test bars no. 302 and 356).

temperature for sintered and resintered specimens in figures 42 and 43, respectively, and is tabulated as follows.

Temperature, °C (°F)	Flexure strength, sintered, MPa (ksi)	Number of samples	Flexure strength, resintered, MPa (ksi)	Number of samples
Room temp.	560 ± 53 81.8 ± 7.9	90	475 ± 46 (70.2 ± 6.7)	26
1066 (1950)	420 ± 48 61.1 ± 7.2	10	350 ± 21 (50.1 ± 3.2)	3
1232 (2250)	320 ± 38 (47.1 ± 5.7)	10	320 ± 18 (47.1 ± 2.6)	3
1399 (2550)	140 ± 43 (21.7 ± 6.3)	10	125 ± 1.4 (18.0 ± 0.2)	2

A drop-off in strength is seen for both the sintered and resintered specimens at 1066°C. Because 1066°C was the lowest elevated test temperature, the threshold temperature for strength degradation is not evident. At 1399°C, the highest elevated test temperature, both the sintered and resintered specimens exhibited slow crack growth during fast fracture tests. Most of the 1399°C specimens exhibited rust-colored inclusions on the fracture surfaces as well as on the test bar surfaces. Also, some large green areas were visible on the fracture surfaces of some specimens. (SEM and EDX analyses were discussed with the room temperature data.)

In the high-temperature tests described above, an oversize test fixture was required to accommodate the widest bars and some warped bars. In order to eliminate potential errors due to fixturing or bar geometry, 20 Task I sintered specimens were machined on 3 sides. The flexure test tensile surface was left as-processed.

A test temperature of 1399°C was selected to flexure test 15 bars in addition to the first 12 to 13 that were broken at each of 3 temperatures (1066°, 1232°, and 1399°C). The 15 bars has been machined on 3 sides to eliminate any effects of warped or oversized bars. The tensile surface remained in the as-sintered condition.

The average strength of the 15 machined specimens was 340 ± 31 MPa (48.7 ±4.5 ksi) at 1232°C. This is statistically equivalent to the value of 320 ± 38 MPa (47.1 ±5.7 ksi) obtained on unmatched specimens. Therefore, slight warp of some specimens and the use of a modified fixture in earlier high-temperature testing did not have a significant effect on the data.

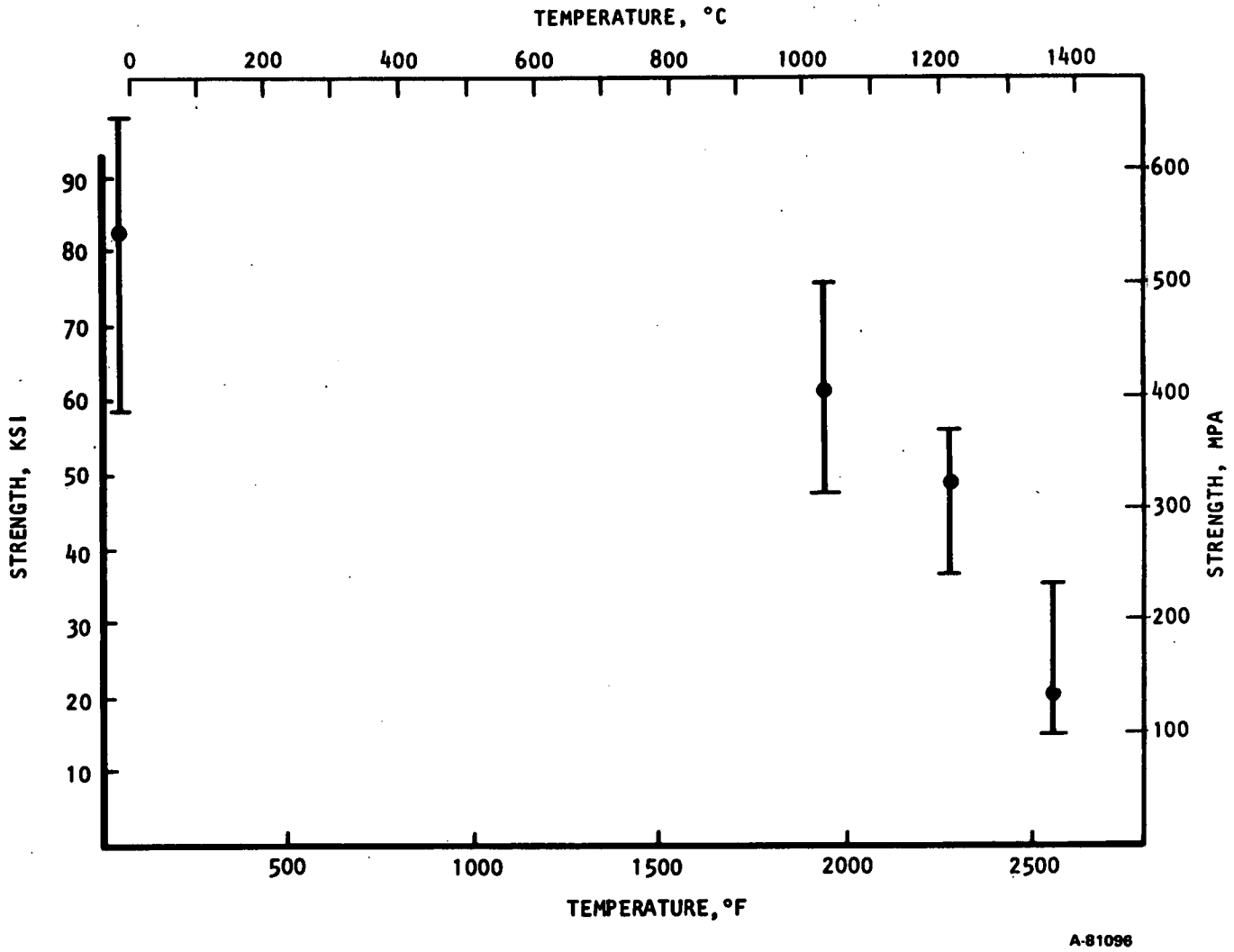

Figure 42.--Task I sintered test bars--strength vs temperature.

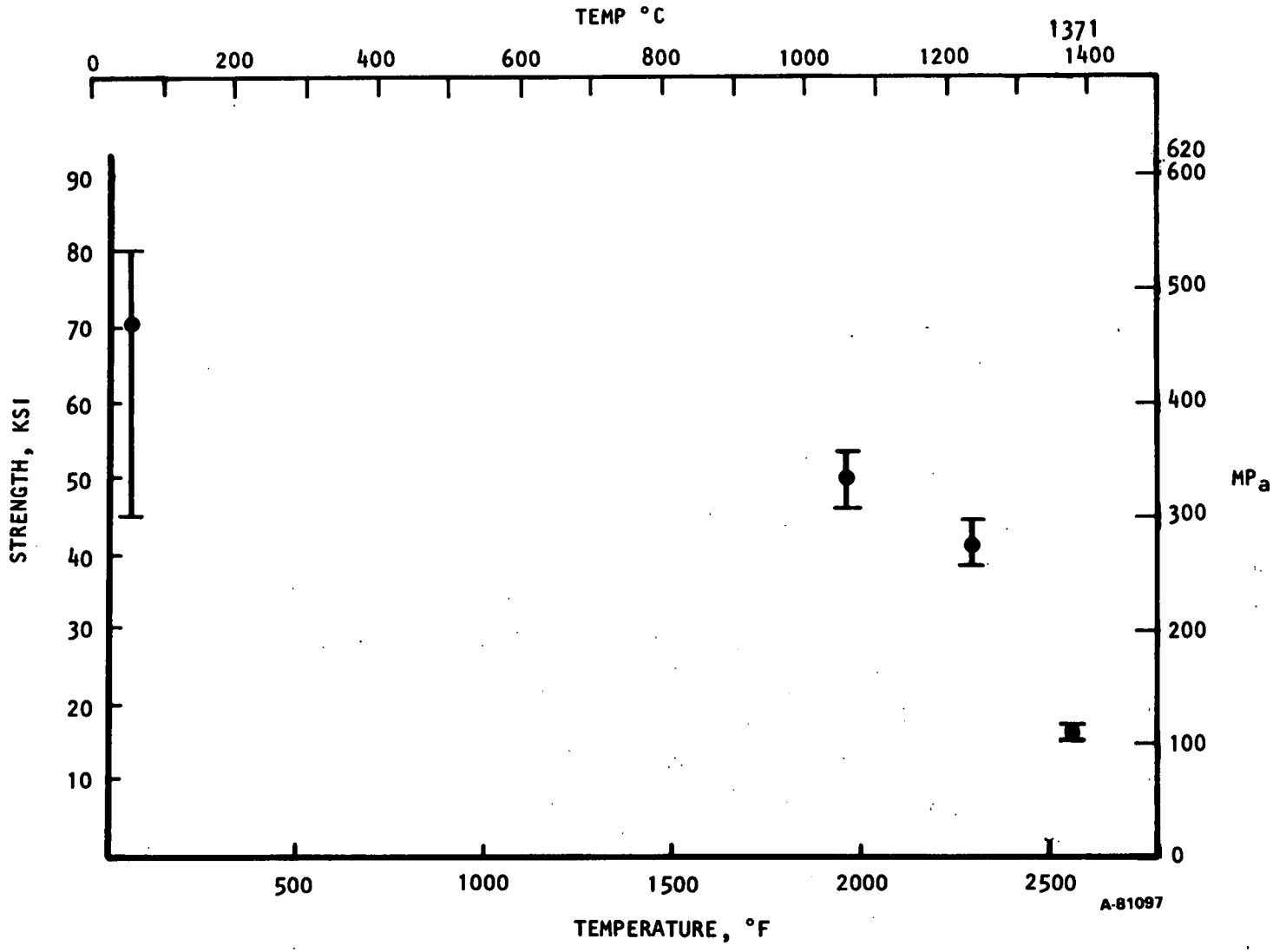

Figure 43.--Task I resintered test bars--strength vs temperature.

Figure 44 shows Weibull statistical analysis of high-temperature strength data for all baseline bars. Values presented are based on 13 bars tested at 1066°C, 28 bars tested at 1232°C, and 12 bars tested at 1399°C.

Oxidation durability tests were conducted in a gradient furnace with a static air atmosphere. Analysis of the bend-strength test (MOR) data of oxidized samples was completed. Twenty bars had been exposed to air for 200 hr in a temperature gradient furnace over a temperature range of 388° to 1296°C (730° to 2365°F). The bars were visually inspected after heat treatment. The only specimens that changed significantly during heat treatment were those exposed to temperatures above 1260°C (2300°F). These specimens changed from light gray (as-processed) to pale yellow speckled with brown. Figure 45 shows the room-temperature MOR as measured on individual specimens. Fractography on the specimens was compared to previous nondestructive evaluations (NDE) and showed that the two lowest strength values resulted from flaws existing before heat treatment. All other data are within the normal distribution for the baseline material room temperature strength. It appears that a slight strength decrease occurs as a result of increasing oxidation temperatures.

Ten baseline specimens were stress rupture tested to establish a baseline from which to judge subsequent material improvements. Initially, a one-stepped stress rupture test was conducted at each test temperature (982°, 1204°, and 1371°C, 3500 hr durability). The tests were started at 65 MPa and increased by 65 MPa every 24 hr until the specimen failed. The results are listed below.

982°C	1204°C	1371°C
65 MPa - 24 hr	65 MPa - 24 hr	65 MPa - 9 hr, 42 min
130 MPa - 24 hr	130 MPa - 24 hr	
195 MPa - 24 hr	195 MPa - 24 hr	
260 MPa - 1 min	260 MPa - 24 hr	
	235 MPa - 0	

These results furnished information for choosing test conditions for controlled tests (fixed stress and temperature). The results of the stress rupture tests on the remaining seven specimens are listed below.

982°C	1204°C
260 MPa - 7 hr, 22 min	260 MPa - 0
260 MPa - 17 hr, 19 min	195 MPa - 1 min
	195 MPa - 4 hr, 55 min
195 MPa - 100 hr (survived)	195 MPa - 3 hr, 38 min

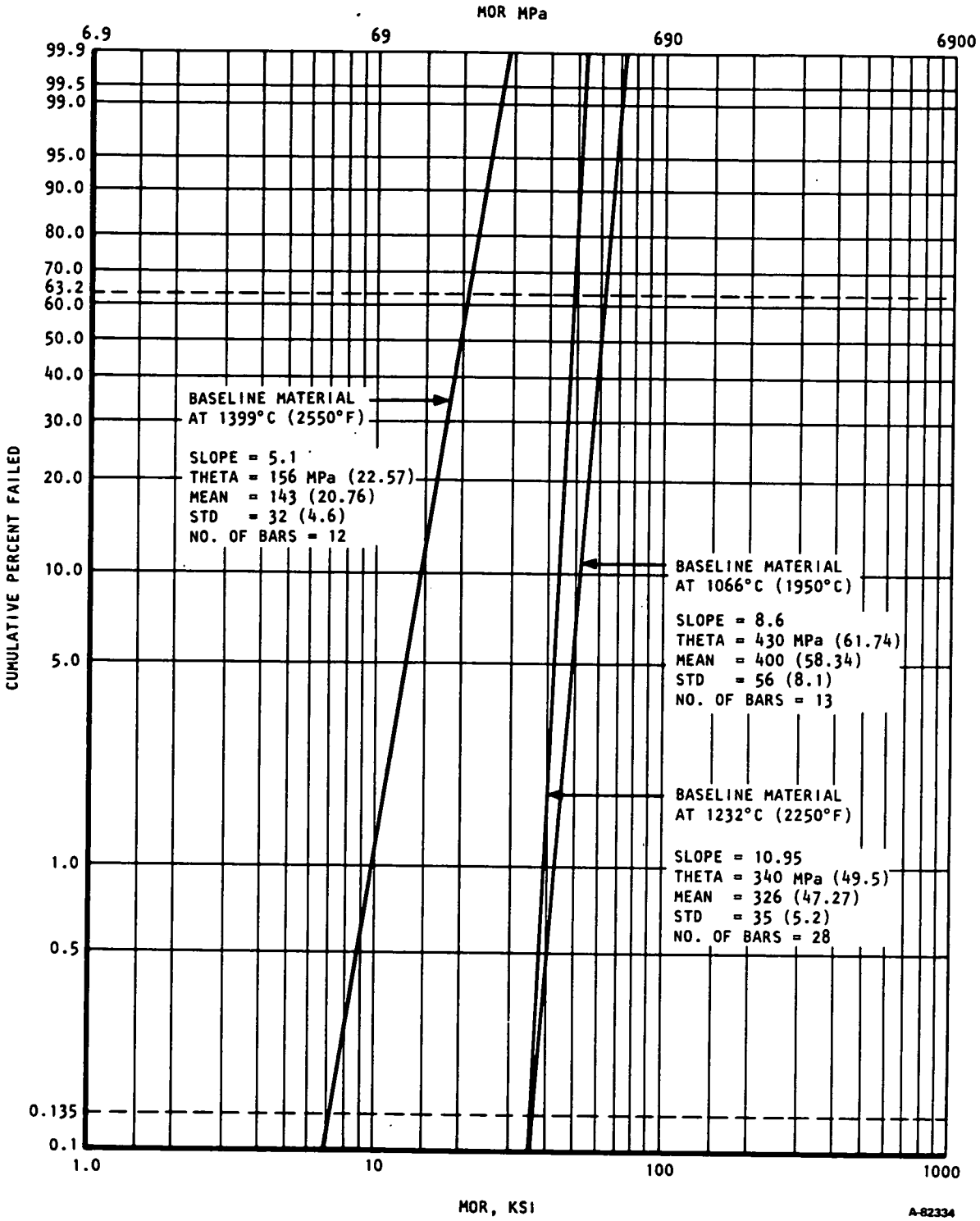

Figure 44.--Weibull statistical plots of high-temperature MOR tests.

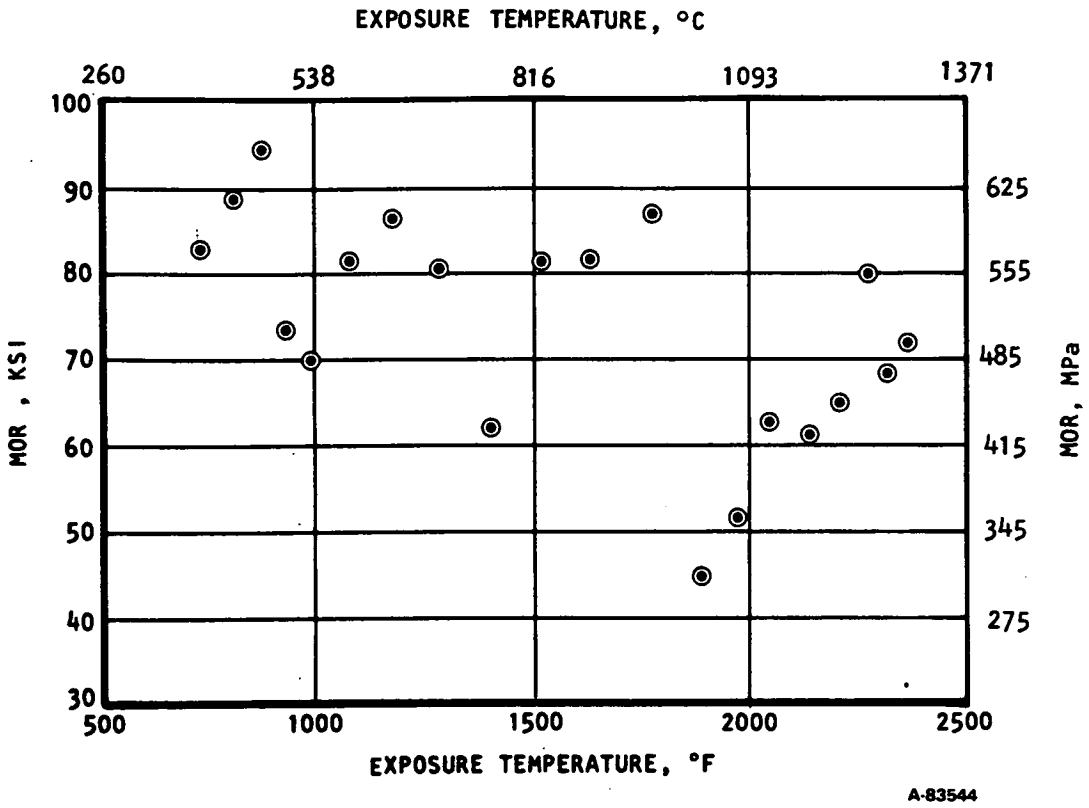

Figure 45.--Room temperature strength after 200 hours at temperature in air.

X-ray diffraction analysis was conducted on the surfaces of selected test bars. Preliminary evaluation of the patterns indicate the following.

- Resintering did not affect phase composition under the conditions used.
- High-temperature testing (at 2550°F) significantly affected phase composition.
- The major phase in all samples is β-Si_3N_4; several unidentified minor phases are also present.

The computerized data base for test bars has been updated to include room- and high-temperature MOR data. Table XVII presents the information currently included in the data base. Relationships of the variables in this data base are analyzed for the sintered material.

TABLE XVII.--SAMPLE DATA BASE--RESINTERED BARS

BAR#	MOLD LOC	MOLD DMT	SINTER LOC	SINTER SHT	DENSITY	MATERIAL	DEMAX RUN	SINTER TEMP	SINTER RUN	MOR	TEST TEMP.	INSPEC. GRADE VIS.	X-RAY
22	2	15.5				1 SIGMA	58	1850					
23	3	15.2	A	-0.8	3.23	1 SIGMA	58	1850	U482-99			2*	3
24	4	15.7	B	-2.1	3.23	1 SIGMA	58	1850	U482-99			4	3
25	1	15.9	D	-2.5	3.24	1 SIGMA	58	1850	U482-99	72.8	R	4	0
27	3	15.3	C	-1.3	3.23	1 SIGMA	58	1850	U482-99			3	2
28	4	15.4	E	-1.5	3.22	1 SIGMA	58	1850	U482-99			2	1
29	1	15.5	E	-2.3	3.23	1 SIGMA	58	1850	U482-99			4	0
30	2	15.5	C	-1.6	3.23	1 SIGMA	58	1850	U482-99	72.3	R	4	0
32	4	15.6	D	-1.3	3.22	1 SIGMA	58	1850	U482-99			3	3
33	1	15.7				1 SIGMA	58	1850					
34	2	15.5	B	-2.3	3.24	1 SIGMA	58	1850	U482-99			4	0
35	3	15.5	B	-1.5	3.23	1 SIGMA	58	1850	U482-99			3*	2
41	1	15.7				1 SIGMA	58	1850	U491	79.9	R	4	1
42	2	15.7				1 SIGMA	58	1850					
43	3	15.7	A	-1.9	3.25	1 SIGMA	58	1850	U482-99	71.5	R	3*	4
44	4	15.7				1 SIGMA	58	1850	U491	43.9	R	4*	4
46	2	15.2	C	-1.4	3.22	1 SIGMA	58	1850	U482-99	74.4	R	1	3
47	3	15.5				1 SIGMA	58	1850					
48	4	15.0	B	-2.1	3.25	1 SIGMA	58	1850	U482-99	72.1	R	4*	4
49	1	15.3	A	-1.0	3.21	1 SIGMA	58	1850	U482-99	79.7	R	1	0
50	2	15.2	E	-1.3	3.23	1 SIGMA	58	1850	U482-99	73.2	R	1	0
51	3	15.0	C	-2.7	3.24	1 SIGMA	58	1850	U482-99	69.1	R	4	1
52	4	15.2	E	-2.3	3.23	1 SIGMA	58	1850	U482-99	63.1	R	3	3
53	1	15.3	D	-1.3	3.22	1 SIGMA	58	1850	U482-99	71.0	R	3*	0
55	3	15.2	D	-2.4	3.23	1 SIGMA	58	1850	U482-99	66.6	R	4	1
56	4	15.2				1 SIGMA	58	1850					
57	1	15.3	A	-1.1	3.21	1 SIGMA	58	1850	U482-91	68.6	R	3	0
58	2	15.5	A	-1.1	3.22	1 SIGMA	58	1850	U482-99	73.2	R	3	1
59	3	15.1	D	-1.5	3.23	1 SIGMA	58	1850	U482-91	67.2	R	2	0
60	4	15.5	D	-1.2	3.22	1 SIGMA	58	1850	U482-99	76.8	R	2*	2
61	1	15.2	B	-1.9	3.24	1 SIGMA	58	1850	U482-99			2	3
62	2	15.2	E	-2.2	3.22	1 SIGMA	58	1850	U482-99	69.8	R	2	0
64	4	15.0	A	-1.0	3.22	1 SIGMA	58	1850	U482-99	46.4	1950	1	0
65	1	15.3				1 SIGMA	58	1850					
66	2	15.5	D	-1.3	3.22	1 SIGMA	58	1850	U482-99			2	0
67	3	15.1	B	-2.8	3.25	1 SIGMA	58	1850	U482-99	73.0	R	4	3
68	4	15.3	C	-1.0	3.22	1 SIGMA	58	1850	U482-99	41.5	2250	3	3
69	1	15.2	C	-1.8	3.23	1 SIGMA	58	1850	U482-99	71.6	R	3	0
70	2	15.3	D	-2.3	3.23	1 SIGMA	58	1850	U482-99	69.5	R	2	0
71	3	15.3	D	-1.3	3.22	1 SIGMA	58	1850	U482-99			1	0
73	1	15.7	E	-1.3	3.24	1 SIGMA	58	1850	U482-99			1	0
74	2	15.2				1 SIGMA	58	1850					
75	3	15.1	E	-2.1	3.23	1 SIGMA	58	1850	U482-99			1*	3
76	4	15.2	D	-1.5	3.23	1 SIGMA	58	1850	U482-99			4*	0
81	1	15.4	E	-2.1	3.24	1 SIGMA	58	1850	U482-99			4	0
82	2	15.5	A	-1.9	3.27	1 SIGMA	58	1850	U482-99			4	3
83	3	15.3	A	-1.0	3.23	1 SIGMA	58	1850	U482-99	17.8	2550	1*	0
84	4	15.2	A	-1.1	3.21	1 SIGMA	58	1850	U482-99			1*	3
86	2	15.5	C	-2.1	3.25	1 SIGMA	58	1850	U482-99			4	3
87	3	15.4				1 SIGMA	58	1850					
88	4	15.5	A	-1.4	3.21	1 SIGMA	58	1850	U482-99	52.1	1950	1	3
89	1	15.5	B	-1.3	3.21	1 SIGMA	58	1850	U482-99	51.8	1950	2	3

BAR #1-416 ARE BASELINE TASK1
BAR #417-534 ARE MATRIX 1 TASK 7
BAR #745-1088 ARE MATRIX 3 TASK 7. MILLING TIME (OR PSD) OF THESE BARS CAN BE IDENTIFIED UNDER COLUMN "MATERIAL".
SINTERING TEMPERATURES OF BAR #745-1088 ARE MOLDING TEMPERATURES
* IS THE INSPECTION GRADE FROM GTEC, 0-5 IS FROM ACC
GRADE 0 TYPICAL. ACCEPTABLE QUALITY.
1 MINOR FLAW(S) OUTSIDE TEST ZONE
2 MAJOR FLAW(S) OUTSIDE TEST ZONE
3 MINOR FLAW(S) IN TEST ZONE, PROBABLY NOT STRENGTH LIMITING
4 MODERATE FLAW(S) IN TEST ZONE, PROBABLY STRENGTH LIMITING
5 SERIOUS FLAW(S) IN TEST ZONE; WILL SIGNIFICANTLY EFFECT MEASUREMENT

Two-variable relationships of the sintered material and process were analyzed using the computerized data base. Figures 46 and 47 and table XVIII show some of the results of these relationships. From these results, it can be concluded that:

(1) There is no relationship between dewax weight loss and sintering weight loss (fig. 46b) or between dewax weight loss and density (fig. 46c). The relationship between sintering weight loss and density, however, can not be conclusively determined from the results (fig. 46a).

(2) The relationship of MOR with density or dewax weight loss is insignificant (random) either at room temperature (fig. 47b and 47c) or at high temperature (not shown). However, the relationship of MOR with sintering weight loss appears significant both at room temperature (fig. 47a) and high temperature (not shown). With these samples, there is a tendency toward low strengths associated with high weight loss. Therefore, the variables which related to sintering weight loss should be investigated more carefully.

(3) Table XVIII indicates that there is no relationship between molding cavity and surface visual inspection grade.

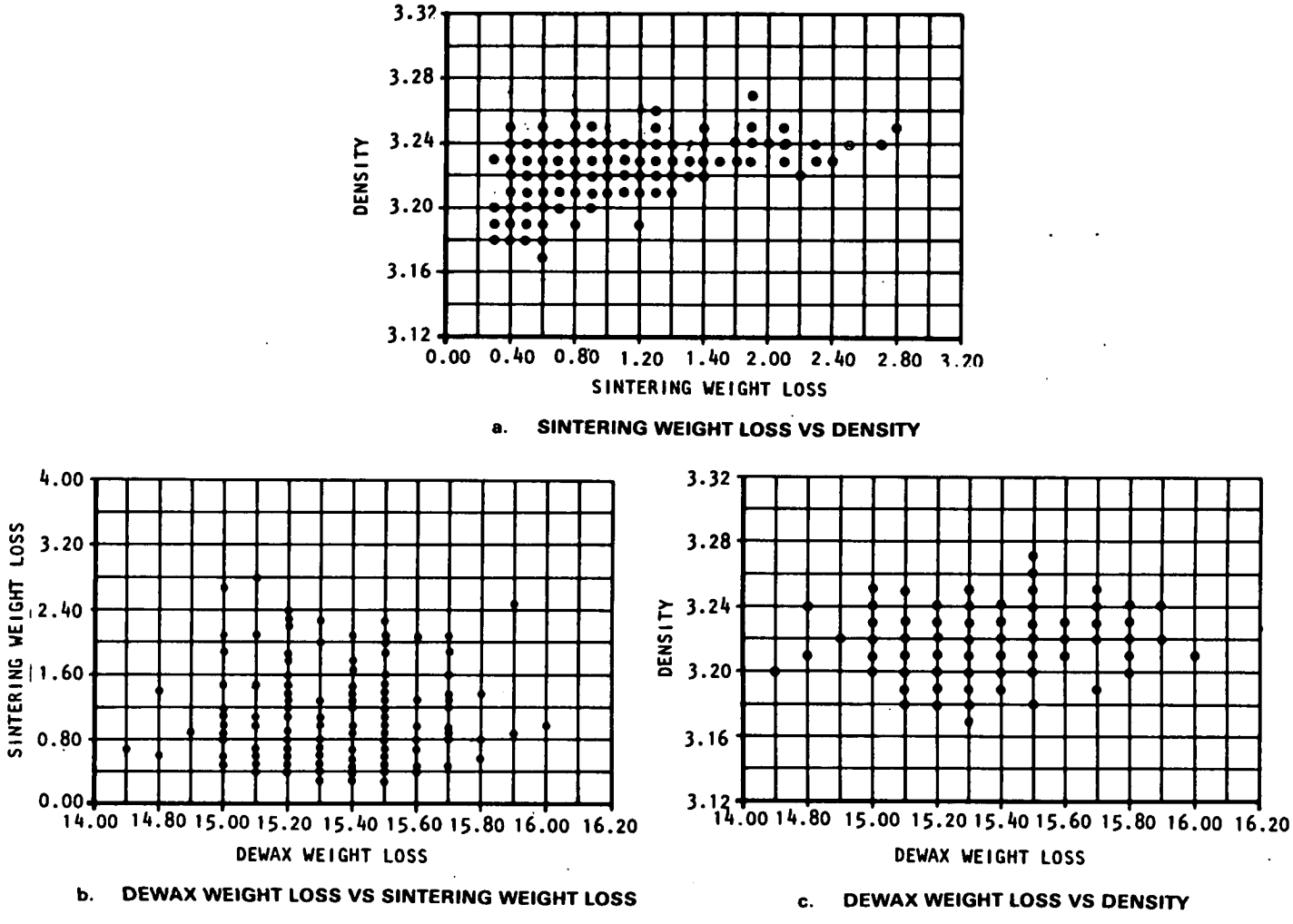

Figure 46.--Room temperature data, relationship of the variables--set I.

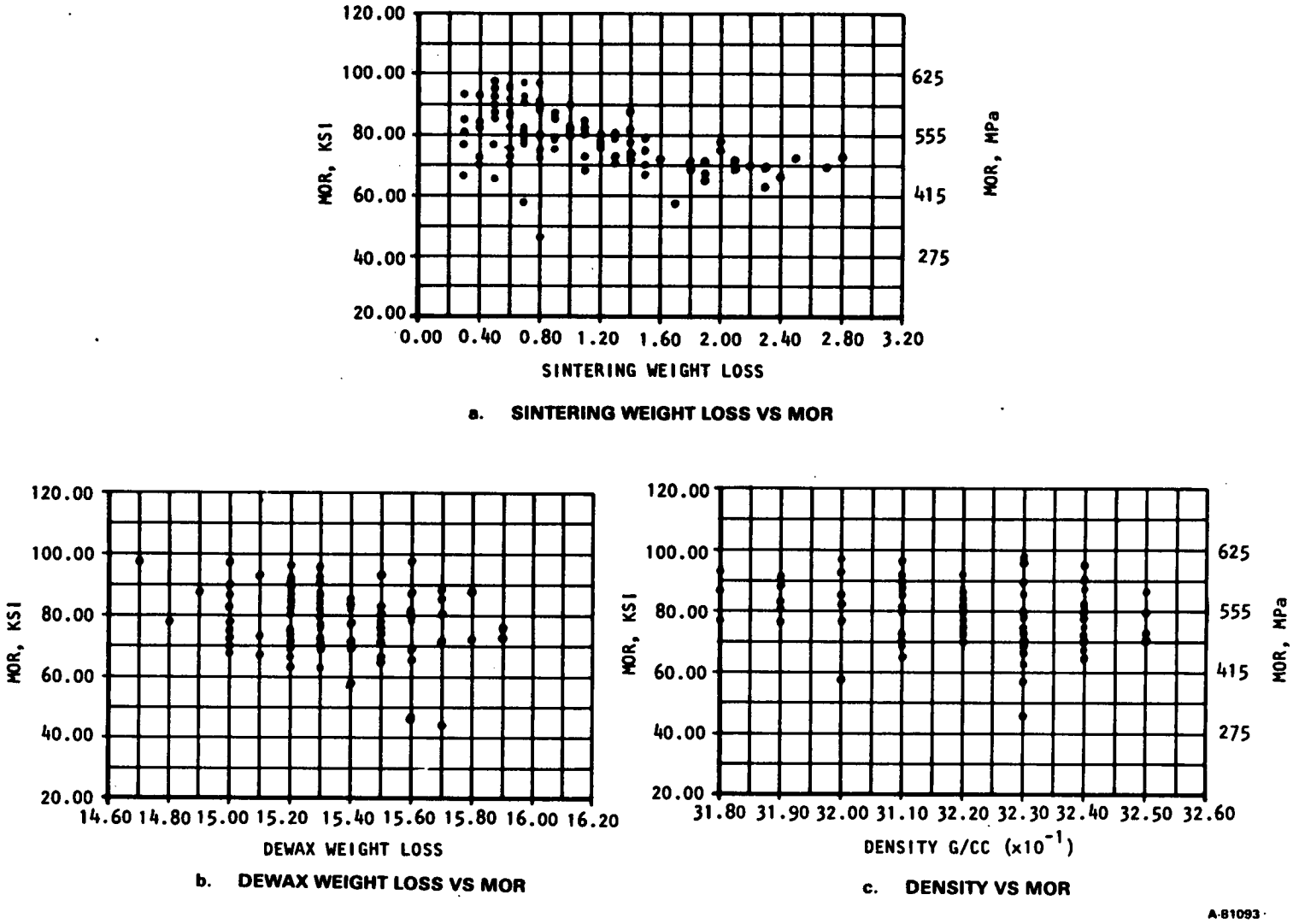

Figure 47.--Room temperature data, relationship of the variables--set II.

TABLE XVIII.--MOLDING CAVITY LOCATION AND VISUAL INSPECTION GRADE RELATIONSHIP

Molding cavity	Number of bars				
	Visual inspection grade				
	0	1	2	3	4
1	9	7	14	30	14
2	9	7	10	34	10
3	14	10	14	22	10
4	4	10	14	28	15

Molding cavity location: $i = 1, 2, 3, 4$

Visual inspection guide: $j = 0, 1, 2, 3, 4$

Task II - MOR Bar Matrix Study

The results of Task I, the first years results of Task VII, and information and experience from previous programs, were all used to develop a test plan. This test plan was designed to establish the optimum materials and processing parameters to achieve the initial program goals of improving test bar properties and reliability. This plan, originally submitted in June 1985 and modified after suggestions from the NASA project manager, allowed the experimental work on Task II to begin on a limited basis in July 1985. The revised plan is reproduced in Appendix B of this report. The following is a report of progress made during the first 10 weeks of the 18-month program.

Matrix II-1.--As described in detail in Appendix B, the lot-to-lot variations in GTE SN-502 powder identified in Task VII along with the uncertainty in future commercial availability of the powder suggested that alternates to the powder used in the Task I baseline characterization be considered. Accordingly, Starck H-1 silicon nitride was selected as the powder to be used in Matrix II-1 (Task II, Matrix 1). The process flowchart, shown in figure 48, outlines the steps required to complete Matrix II-1.

Materials tested: The materials tested in Matrix II-1 were the same as those tested in Task I, with the exception of the Si_3N_4 powder, which was Starck H-1 rather than GTE SN-502.

Apparatus and procedures: The same processing apparatus used in Task I was used in producing the test bars for Matrix II-1. In addition, a Haake torque rheometer was used to characterize the molding mixes and, with the aid of a high-shear, twin-screw extension adaptor, to vary mixing procedure. The test plan variations described in Appendix B were followed.

Results and discussion: Milling and mixing of the eight molding batches were completed in accordance with the test plan. Characterization torque data are presented in table XIX (for all eight mixes) and in figure 49 (for the mixes prior to extrusion). Torque data in table XIX were obtained from a cycle that was introduced for the purpose of characterizing premixed powder and binder. The cooling rate of this cycle was changed to 1°C (1.8°F) per minute. Another cycle, with a cooling rate of 2°C (3.6°F) per minute, had been used for mixing in most of the previous experiments of Task VII. The new cycle provides for better temperature control.

The data in Table XIX are consistent in showing that by reducing the binder content the torque is increased. The data also indicate that passing the mix through a high-shear, twin-screw extruder reduces the torque.

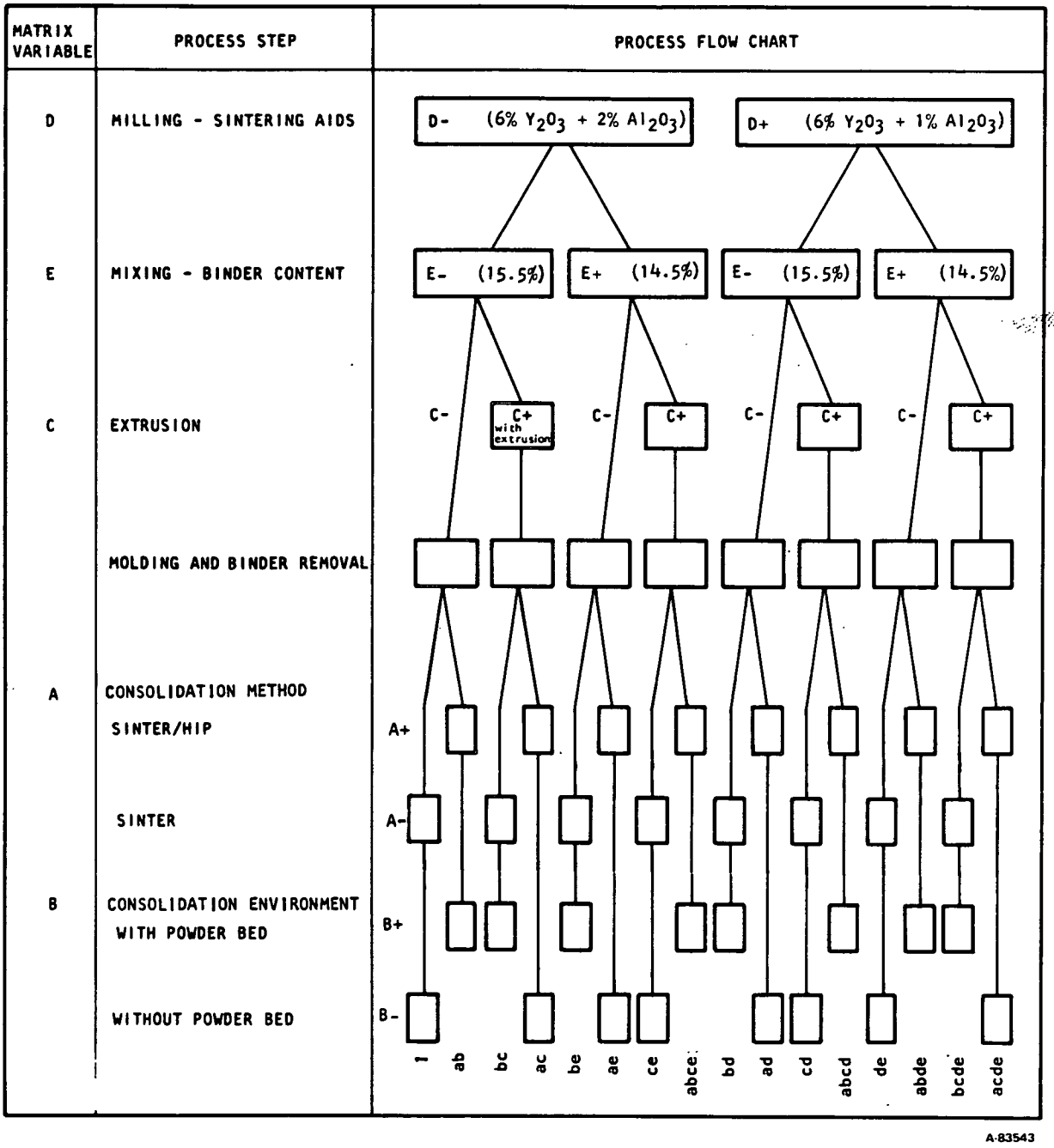

Figure 48.--Process flowchart for Task II, Matrixes 1 and 2.

TABLE XIX.--TORQUE AT 65°C (150°F) FOR MATRIX II-1 INJECTION MOLDING BATCHES

	Torque, m·g			
	D- (6% Y_2O_3 + 2% Al_2O_3)		D+ (6% Y_2O_3 + 1% Al_2O_3)	
	E- (15.5% Binder)	E+ (14.5% Binder)	E- (15/5% Binder)	E+ (14.5% Binder)
C-	1450	1500	1386	1544
C+ (extruded)	1100	1452	762	1290

Notes:

1. Values are from single mixer runs.
2. Mixer cooling rate was 1°C (1.8°F) per minute.
3. m·g = meter·gram

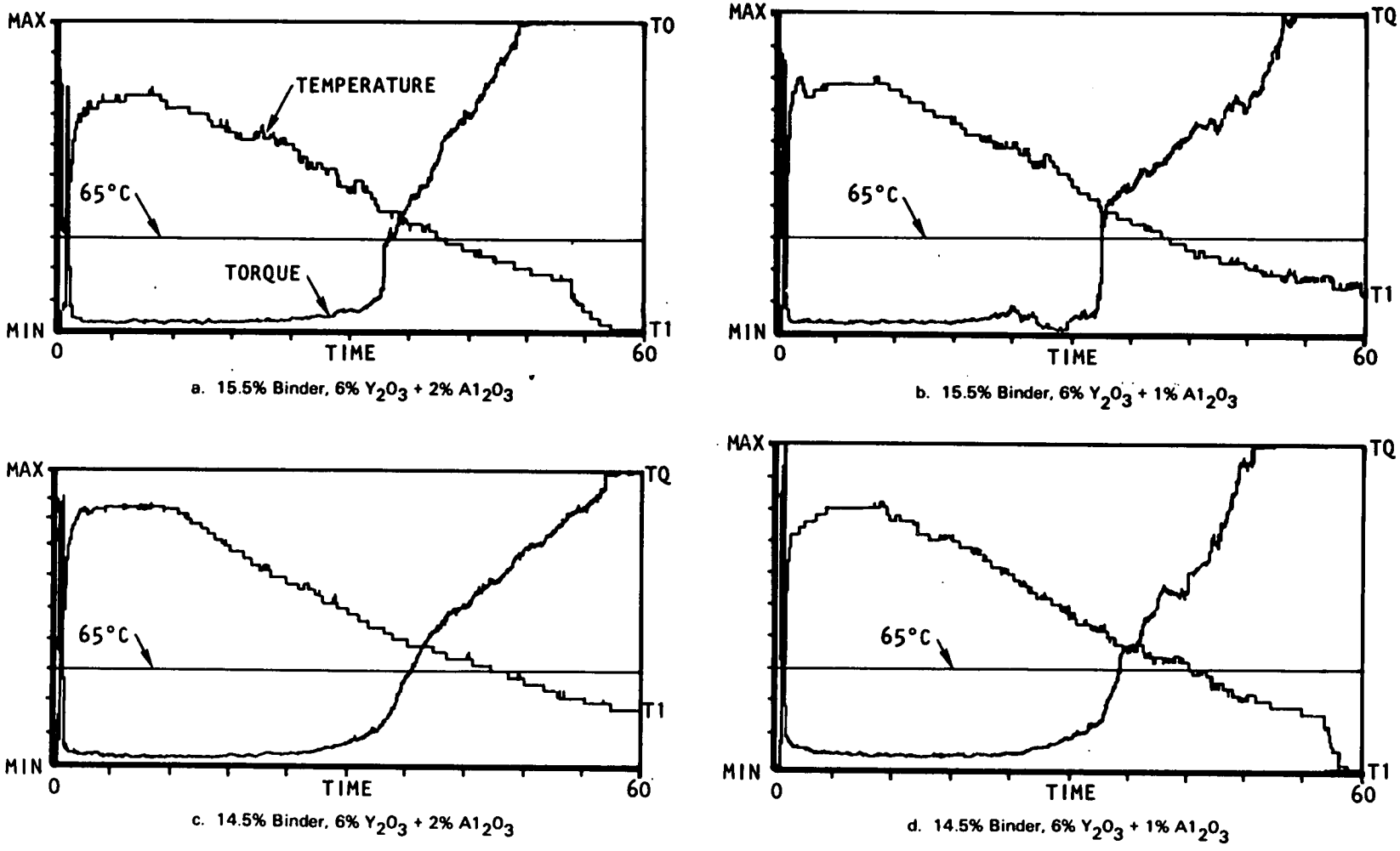

Figure 49.--Torque characterization curves, Matrix II-1, not extruded; torque and temperature are plotted as a function of time with scale minimum values of 0 m·g and 50°C (122°F) and maximum values of 2500 m·g and 100°C (212°F).

For the powders milled in Matrix II-1, figure 49 illustrates that there is a significant difference in torque behavior between those with 15.5 percent and those with 14.5 percent binder content. Figure 49a and 49b show the two powder compositions that were mixed with 15.5 percent binder. Both torque curves show a sudden increase at about 68°C (154°F). The same material, mixed with 14.5 percent binder, show a more uniform torque increase.

The probable mechanism that causes the sudden torque increase is a phase separation between the low-viscosity binder and the solid particles. Excess binder separates and provides a slip plane between the higher-viscosity material at the cooled mixer wall and the lower-viscosity material near the warmer, uncooled rotor. As the temperature continues to drop, the binder itself becomes sufficiently viscous to prevent slipping. The entire mix is then suddenly brought into a high-torque mixing mode. Torque curves for the four materials after extrusion (not shown) exhibit the same trend, but indicate less tendency toward phase separation.

Injection molding of 1592 bars in a four-cavity die was accomplished, thereby completing the molding requirements for Matrix II-1. A summary of the injected bars is provided in table XX. The process code, listed in the summary, indicates the values chosen for the variables being studied. Each of the 8 groups of bars will be subjected to 2 different densification (consolidation) conditions to provide the 16 treatments identified for this matrix. Injection molding temperature (material temperature prior to injection into the die cavity) was first estimated by rheometer data and then established by visual inspection of the injected bars. Bars that were determined by visual inspection to be of good quality were obtained at 82°C(180°F) for all mixes containing 15.5 percent binder. A higher temperature, 88°C (190°F), was required to obtain good quality bars for mixes with 14.5 percent binder.

A total of 640 of the 1592 test bars were completed through dewax, with no degradation observed in any of the samples. Further results will be reported in subsequent monthly progress reports.

Matrix II-2.--Matrix II-2 is a parameter evaluation program parallel to Matrix II-1 in which Denka 9FW powder is substituted for Starck H-1.

Materials tested: The materials tested in Matrix II-2 were the same as those tested in Matrix II-1, except that Denka 9FW powder was substituted for Starck H-1 powder.

Apparatus and procedures: The same apparatus and procedures used in Matrix II-1 are being used in Matrix II-2.

TABLE XX.--MATRIX II-1 TEST BAR INJECTION SUMMARY

Bar serial numbers	Process code[1]	Molding temperature, °C (°F)
1541-1744	1 ab	82 (180)
1957-2132	bc ac	82 (180)
1753-1956	be ae	88 (190)
2343-2542	ce abce	88 (190)
2543-2742	bd ad	82 (180)
2743-2942	cd abcd	82 (180)
2133-2342[2]	de abde	88 (190)
2943-3142	bcde acde	88 (190)

Notes:

1. Statistical design treatment codes defined in Appendix B.

2. Serial numbers 2325-2334 were not used.

Results and discussions: All materials were received and milling and mixing of the eight molding batches were completed. Torque rheometer data are presented in Table XXI. Results are consistent with Matrix II-1 data and will be coordinated with subsequent processing. Injection molding was initiated with a high X-ray yield (96 percent) and good visual inspection results on the first two groups. Further results will be reported in subsequent monthly progress reports.

TABLE XXI.--TASK II MATRIX II-2 RHEOLOGY DENKA 9FW

	Temp., °C	D- 6% Y_2O_3 + 2% Al_2O_3		D+ 6% Y_2O_3 + 1% Al_2O_3	
		E- (15.5% Binder) IM94-112	E+ (14.5% Binder) IM94-112A	E- (15.5 Binder) IM94-112B	E+ (14.5% Binder) IM94-113
C-	60	1657	1843	1770	1968
	65	876	1304	948	1175
	80	120	141	127	140
C+ extruded	60	1100	1831	1700	2000
	65	439	796	500	748
	80	98	153	143	156

Task VII - Advanced Materials and Processing

The purpose of this task is to explore new concepts in processing, to investigate the impact of major processing parameters on material properties, and to study the interactions between major processing parameters. This task is cost shared by ACC. In the first year, following eight major parameters were selected for evaluation:

(1) Alternate raw materials (Si_3N_4)

(2) Alternate binder system

(3) Binder extraction cycle (dewax)

(4) Injection molding parameters

(5) Alternate powder preparation (PSD)

(6) Additive composition (sintering aids)

(7) Sintering cycles

The evaluations were conducted iteratively. Two or more processing parameters were investigated in a statistically designed experimental matrix to determine possible interactions between those parameters. Prior experience and efficiency of experimental work were used to guide the selections of parameters included in a particular matrix.

Table XXII shows the parameters chosen for evaluation and the combinations of these parameters in Matrixes 1 through 6. The design and rationale of each matrix will be explained in the subsequent sections.

Matrix 1 - raw materials/sintering temperatures.--As the first iteration, four commercial Si_3N_4 powders were selected for comparison. These four materials were processed through the dewax cycle using baseline processing. The last step, sintering, was carried out at two different peak temperatures to assess the interaction between raw materials and peak sintering temperature. Figure 50 shows the experimental matrix design.

Experimental procedures: Figure 51 is a flowchart showing the major processing procedures and guidelines. The silicon nitride powders chosen for study were GTE SN-502 (baseline), Denka 9S, UBE SN-EN, and Starck H-1. The powders were prepared by baseline milling procedures described in Task I. Each milled powder was blended with a 15.5 percent ACC standard binder (identified as B_1) using a HAAKE Rheomix model 600 mixer. This unit was used instead of the baseline mixer (double-arm, sigma-bladed) which requires a minimum of 4000 g of materials to achieve an adequate mixing action. The HAAKE Rheomix 600 requires only 107 g of material, and the mixing parameters are more readily controlled and monitored.

TABLE XXII.--RELATIONSHIP BETWEEN PROCESS SUBTASKS AND EXPERIMENTAL MATRIXES

	Experimental matrix number						
	1	2	3	4	5	6	7
Subtask 1 Raw material	X				X	X	
Subtask 2 Binder		X			X	X	X
Subtask 3 Binder extraction			X			X	X
Subtask 4 Injection molding			X			X	
Subtask 5 Powder preparation (milling)			X		X		
Subtask 6 Composition				X			
Subtask 7 Sintering cycle	X			X		X	

	M_1	M_2	M_3	M_4
S_1	10 MOR	10 MOR	10 MOR	10 MOR
S_2	10 MOR	10 MOR	10 MOR	10 MOR

M_1 = GTE SN-502 Si_3N_4 powder + 6% Y_2O_3 + 2% Al_2O_3

M_2 = DENKA 9S Si_3N_4 powder + 6% Y_2O_3 + 2% Al_2O_3

M_3 = UBE SN-EN Si_3N_4 powder + 6% Y_2O_3 + 2% Al_2O_3

M_4 = STARCK H-1 Si_3N_4 powder + 6% Y_2O_3 + 2% Al_2O_3

S_1 = Baseline sintering temperature and conditions

S_2 = Baseline plus 50°C

Figure 50.--Experiments designed to investigate the interaction between raw materials and sintering cycles.

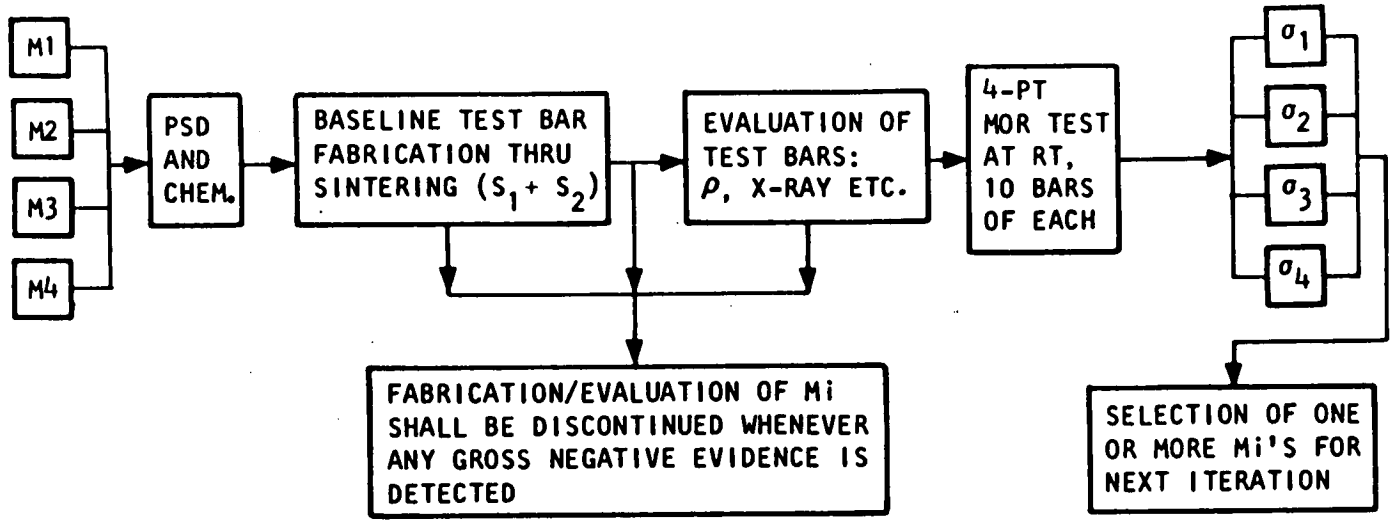

NOTE:

M1 = BASELINE Si_3N_4
(SN 502 + 6% Y_2O_3 + 2% Al_2O_3)

Mi = ALTERNATE Si_3N_4,
where i = 2, 3 AND 4

B_1 = BASELINE BINDER

B_i = ALTERNATE BINDER SYSTEMS

DC_i = DEWAX CYCLES

S_i = SINTERING CYCLES

σ_i = STRENGTHS

A-70733

Figure 51.--Flowchart showing the experimental approach of Matrix I alternate new materials/sintering temperature).

A new set of mixing parameters, "HAAKE baseline", was chosen for blending powder and binder for this matrix. Any subsequent experiments in Task VII that require only a small amount of blended injections mix also will be processed in this manner.

Results and discussion: All above-mentioned powders, except UBE SN-EN, were blended successfully using the new baseline blending procedures. Slow wetting of the UBE powder by the binder and the very high mixing torques required indicated that this powder, milled by the "HAAKE baseline" process, was not suitable for injection molding. Therefore, processing of UBE SN-EN beyond blending was discontinued.

The three successfully blended materials were injection molded by baseline injection molding procedures (see Task I) after the materials were pelletized. No difficulty was encountered during injection molding, and all test bars appeared acceptable by visual inspection.

Binder was removed from 84 bars using the baseline cycle. Bars of baseline material, M_1, appear to be in good condition; however, the other two materials, M_2 and M_4, exhibited cracking.

The test bars subsequently were sintered in two sintering runs, 1850°C (3360°F) and 1900°C (3450°F) at 0.68 MPa (95 psig) nitrogen. Sintered densities are reported in table XXIII. A small density increase was observed at the increased sintering temperature for M_1 and M_4 powders, but a slight decrease occurred for M_2. Blistering was observed on M_2 bars sintered at the higher temperature but not on the other bars.

Sintering shrinkage was measured on each bar. M_3 and M_4 bars showed isotropic shrinkage, but baseline M_1 bars demonstrated higher shrinkage in thickness than in length, 16.3 percent compared with 13.9 percent.

This anisotropic shrinkage was probably due to a small amount of needle-like materials, that remained in the milled GTE SN-502 Si_3N_4 powder.

Visual and X-ray radiography inspection of the sintered bars showed that the quality of M_1 bars was comparable to that of the Task 1 bars; however, the M_2 and M_4 bars had a high rejection rate, 96 and 75 percent, respectively.

Room temperature MOR measurement data correlated well with the quality of test bars. The MOR values for M_1 bars ranged from 515 to 570 MPa (75 to 83 ksi), while the values for M_2 and M_4 were mostly below 345 MPa (50 ksi). The low MOR's for M_2 and M_4 are clearly due to lower sintered densities and the presence of defects.

The M_2 material exhibited large internal voids on the fracture surfaces, often associated with large blisters. The M_4 material exhibited some large internal porosity on the fracture surface, but the porosity was less common and smaller than that of the M_2 material. Some specimens also exhibited internal cracking.

TABLE XXIII.--SINTERED DENSITIES USING DIFFERENT Si_3N_4 STARTING POWDERS

	Density and standard deviation, g/cc			
	1850°C (3360°F)		1900°C (3450°F)	
Starting powder	ρ	Δ	ρ	Δ
M_1	3.18	0.03	3.21	0.01
M_2	3.06	0.04	2.99	0.03
M_4	2.99	0.02	3.05	0.01

ρ: average density
Δ: standard deviation

The low strength and excessive defects observed in the M_2 and M_4 test bars suggest either that these two material are intrinsically poor or that they require a set of processing parameters significantly different from the baseline processing parameters that were used.

Matrix 2 - binder/wetting agent/mixing.--The degree and homogeneity of ceramic powder dispersion in the binder are believed to be very important to the quality of injection-molded ceramic parts. Figure 52 shows the design of a matrix which combines binder system, wetting agents, and mixing conditions.

Experimental procedures: The baseline binder, B_1, and an alternate binder, B_2, in conjunction with several wetting agents, and different ways of mixing the wetting agents with the powder/binder are being investigated. Baseline powder was used throughout the matrix.

All mixing was carried out on the Rheomix 600 using the "HAAKE baseline" procedures. The mixer chamber was heated (80°C/175°F) to melt the binder, then the powder was added to the mixer. A wetting agent was added 5 minutes after the onset of each mixing run. The twin mixing rotors were run at 60 and 15 rpm at the end of the mixing cycle in order to evaluate the rheology dependency on shear rate of the mixed material.

An initial mixing process study was completed using binders B_1 and B_2 with wetting agents WA_1, WA_2, WA_3, and WA_4, all of which are proprietary.

Figures 53 and 54 show examples of torque and temperature curves plotted by the HAAKE Rheomix mixer.

	TB_1	TB_2	TB_3
WA_1	B_{11}	B_{22}	B_{21}
WA_2	B_{12}	B_{21}	B_{22}
WA_3	B_{21}	B_{11}	B_{12}
WA_4	B_{22}	B_{12}	B_{11}

TB_i = Blending temperature, where i = 1, 2, and 3

WA_i = Wetting agent, where i = 1, 2, and 3

B_{11} = Binder system 1 at level 1

B_{12} = Binder system 1 at level 2

B_{21} = Binder system 2 at level 1

B_{22} = Binder system 2 at level 2

Figure 52.--Matrix 2 design.

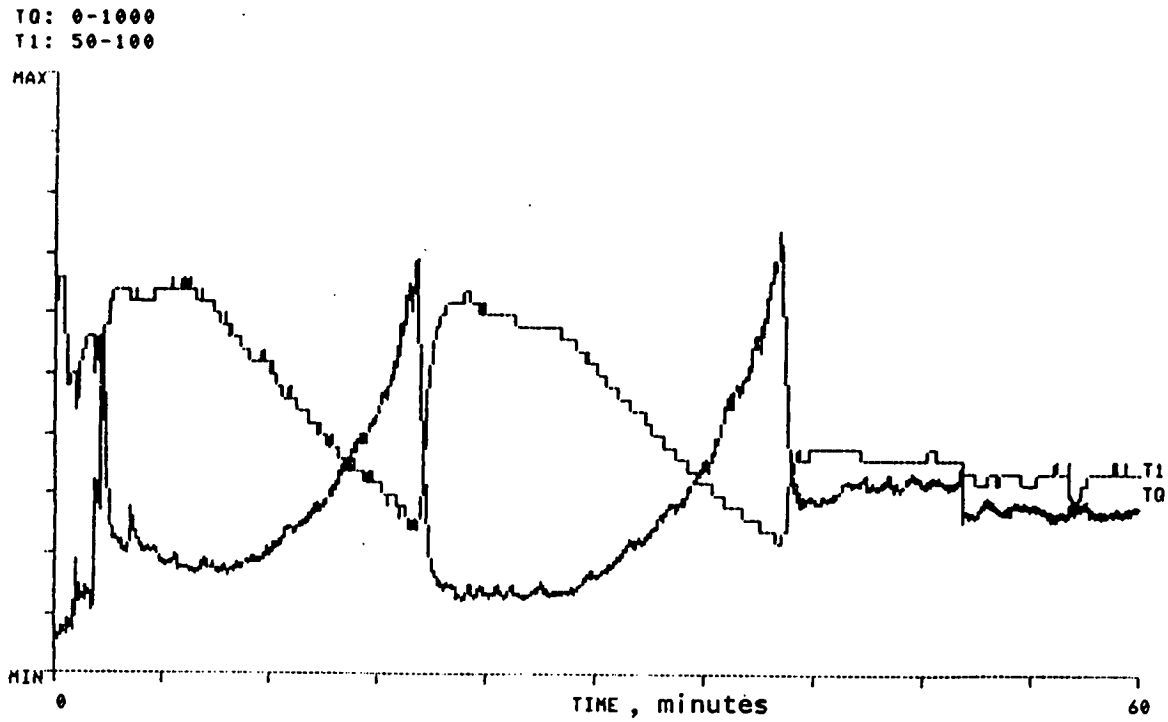

Figure 53.--Mixing torque and temperature curves for baseline powder and B_1 binder.

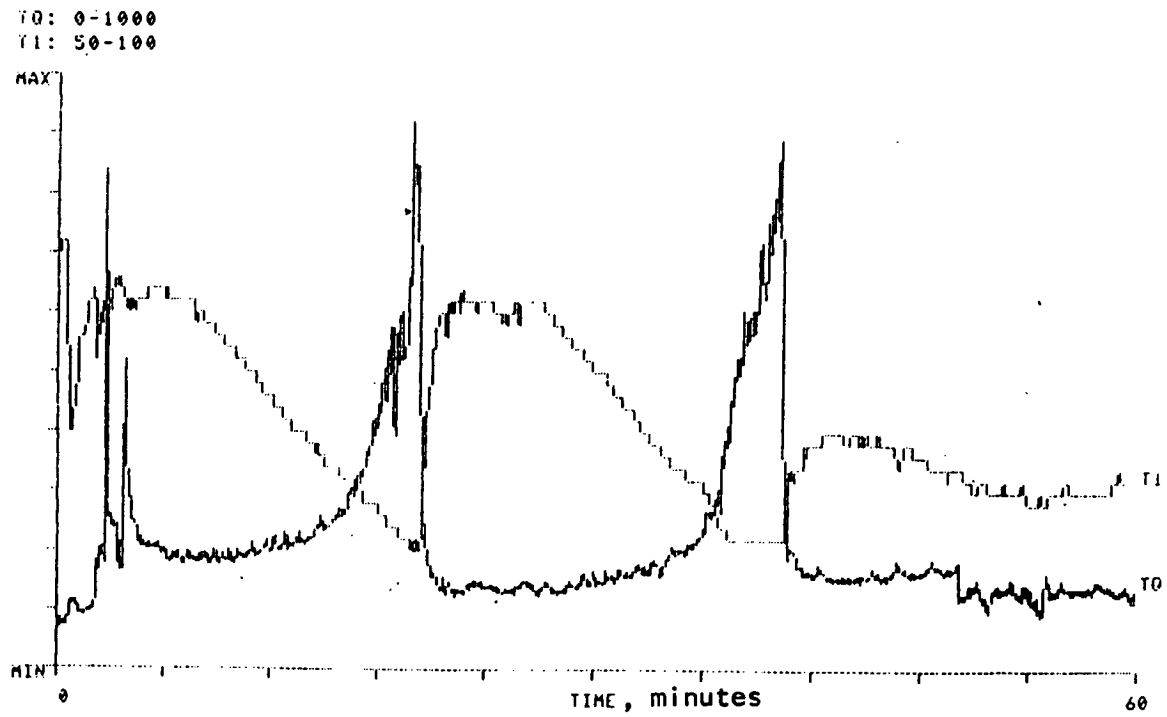

Figure 54.--Mixing torque and temperature curves for baseline powder and B_2 binder.

Results and discussion: The results of the experiments are shown in the matrix blocks in table XXIV. The response of each treatment is the measured torque at high and low shear rates and their ratio. A detailed analysis of Matrix 2 was conducted and only the highlights are summarized here.

The results of the data analyses indicated that interaction may exist among the variables included in this matrix.

(1) Judging from the data in the matrix, the calculated values of the variances (S^2) are significantly high thereby making the numbers of critical statistics (w) unreasonably higher than the differences of the main effects.

(2) From figures 55, 56, and 57, the combined effects of mixing temperature, wetting agent, and binder (B_{xy}) to torque exhibited the same pattern of effect. These figures illustrate a significant interaction between the binder (B_{xy}) and the wetting agent.

When interaction exists, the nature of the main effect being unknown (it depends on the level of other variables), and the significant test to estimate the difference of any effect will draw a misleading result.

The identified interaction probably results from specific, proprietary binder (B_{xy}) components and wetting agents. Significance of this behavior, with regard to test bar fabrication, will be determined in separate experiments.

Matrix 3 - binder extraction/injection molding/powder preparation.-- This matrix was designed to study the relationship between dewax cycle, molding material temperature, and milling time (i.e., PSD). Figure 58 illustrates the matrix design which is known as the Youden square design. Due to experimental difficulties, certain treatments in the matrix could not be carried to injection molding, and therefore, the intended statistical analysis of variance could not be conducted. However, even though the originally planned statistical analysis could not be conducted, several simpler analyses and observations could be performed and meaningful conclusions were obtained.

Experimental procedures: The baseline material (GTE SN 502 + 6% Y_2O_3 + 2% Al_2O_3) was used throughout the matrix. The processing procedures, milling through sintering, were part of the matrix evaluation and are more conveniently described along with results relating to the evaluation of the particular processing parameters to be followed. The baseline process was used as one of the experimental variations in this experiment.

TABLE XXIV.--MATRIX 2 EXPERIMENTS BINDER/WETTING AGENT/MIXING TEMPERATURE

WETTING AGENT	Blending Temperature			Total
	TB_1	TB_2	TB_3	
WA_1	B_{11} $\frac{305}{300} = 1.107$	B_{22} $\frac{170}{110} = 1.545$	B_{21} $\frac{130}{115} = 1.130$	Ratio R_1 = 3.692 H Shear R_1 = 605 L Shear R_1 = 525
WA_2	B_{12} $\frac{340}{350} = 0.97$	B_{21} $\frac{220}{150} = 1.47$	B_{22} $\frac{120}{100} = 1.20$	Ratio R_2 = 3.64 H Shear R_2 = 680 L Shear R_2 = 600
WA_3	B_{21} $\frac{160}{125} = 1.29$	B_{11} $\frac{640}{750} = 0.853$	B_{12} $\frac{295}{240} = 1.23$	Ratio R_3 = 3.363 H Shear R_3 = 1095 L Shear R_3 = 1115
WA_4	B_{22} $\frac{280}{240} = 1.167$	B_{12} $\frac{700}{800} = 0.875$	B_{11} $\frac{380}{350} = 1.086$	Ratio R_4 = 3.128 H. Shear R_4 = 1360 L. Shear R_4 = 1390
Total	Ratio C_1 = 4.434 H Shear C_1 = 1085 L Shear C_1 = 1015	Ratio C_2 = 4.743 H Shear C_2 = 1730 L Shear C_2 = 1810	Ratio C_3 = 4.646 H Shear C_3 = 925 L Shear C_3 = 805	Ratio G = 13.823 H Shear G = 3740 L Shear G = 3630

B_{xy} = Binder Type x at y level

Response is torque ratio of high shear rate (at 60 rpm) and low shear rate (at 15 rpm)

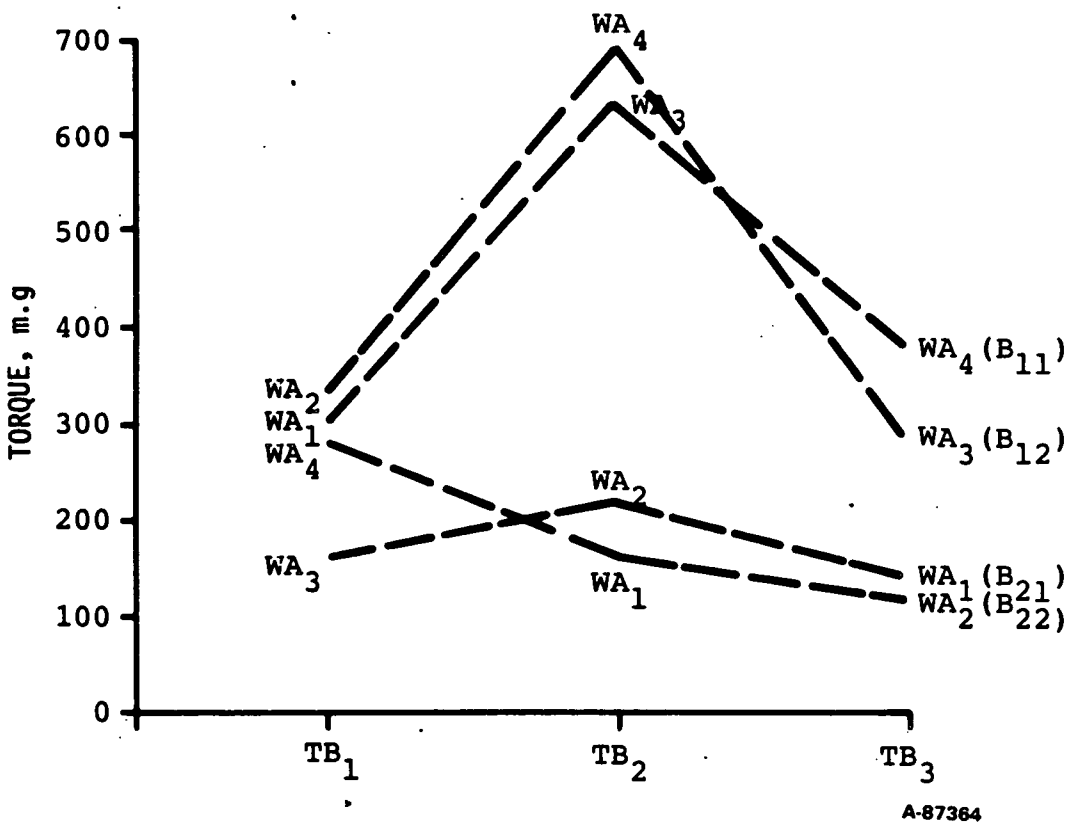

Figure 55.--Mixing torque at high shear rate (60 rpm).

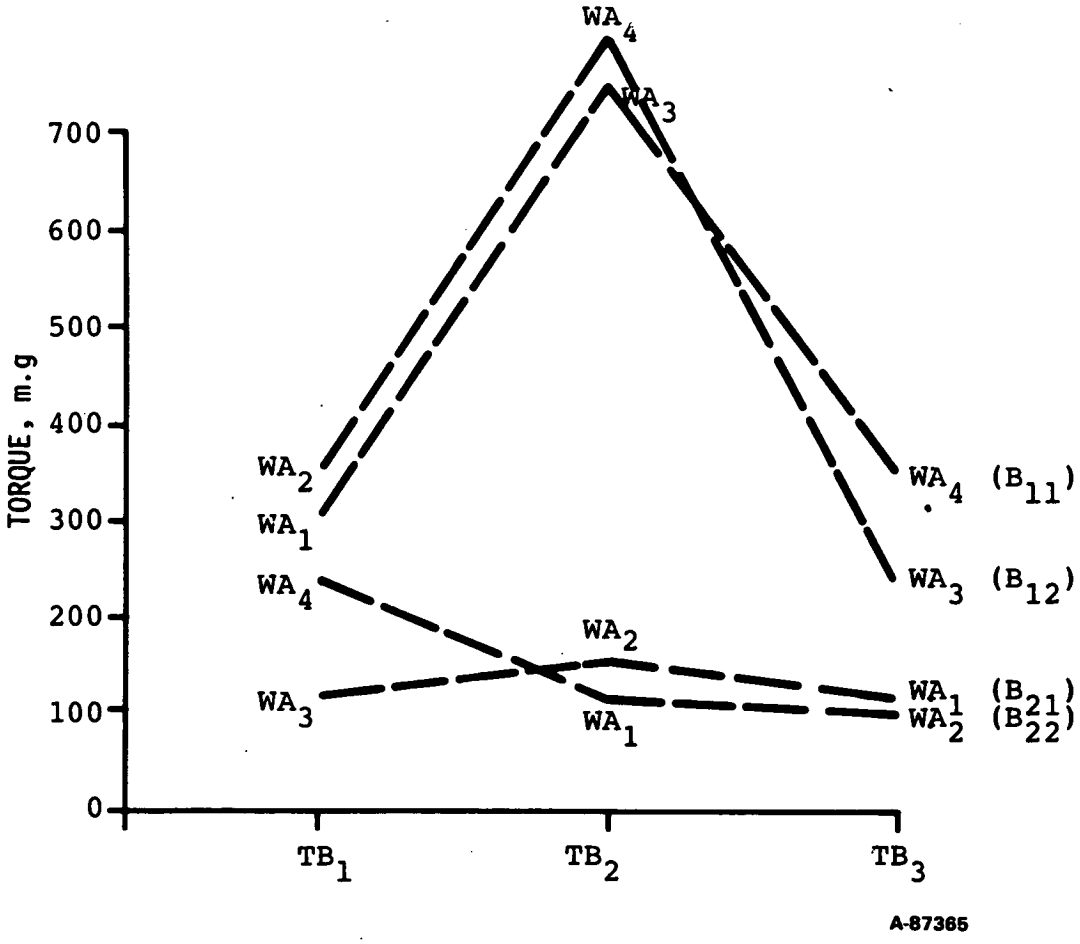

Figure 56.--Mixing torque at low shear rate (15 rpm).

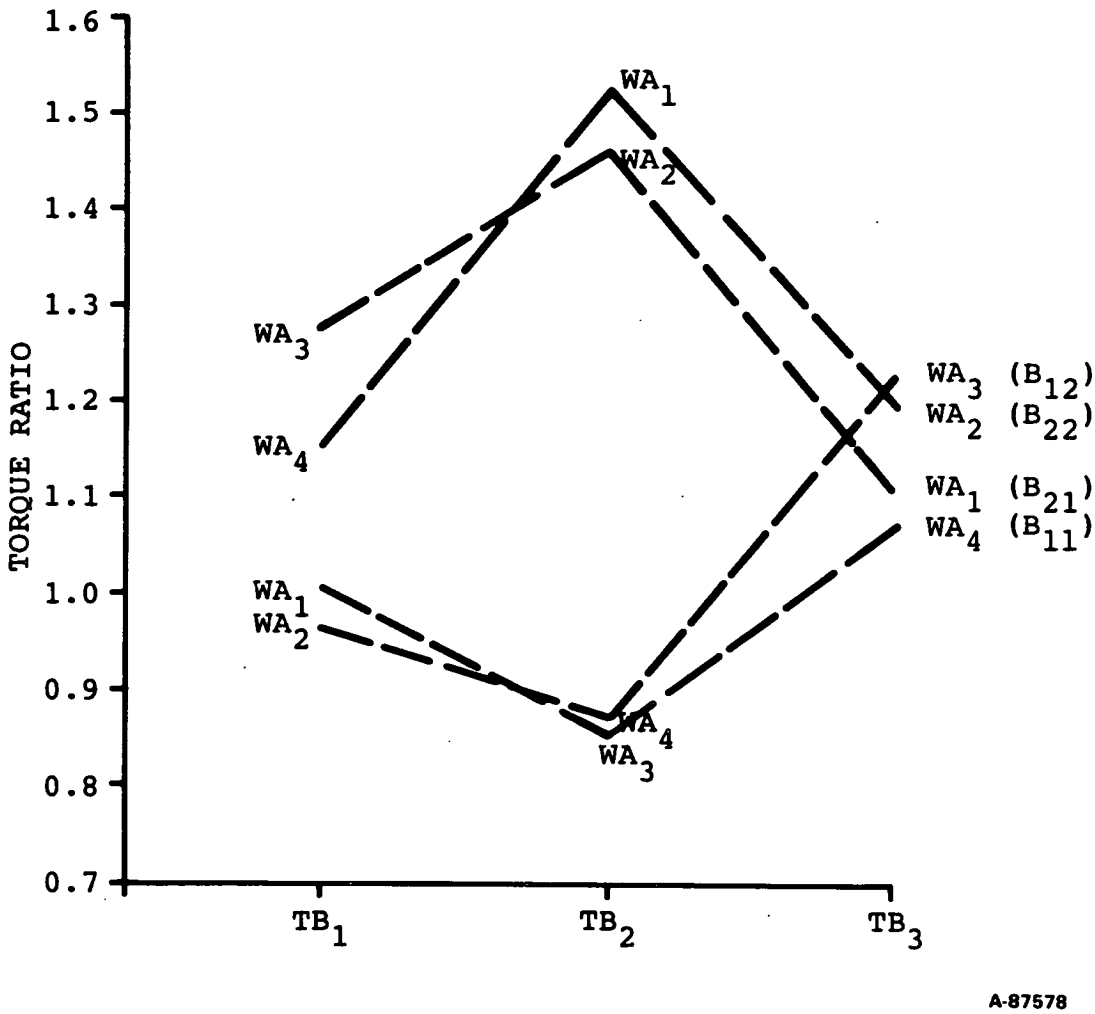

Figure 57.--Mixing torque ratio (high shear rate/low shear rate).

	DC_1	DC_2	DC_3	DC_4
T_1	PSD_1	PSD_2	PSD_3	PSD_4
T_2	PSD_2	PSD_3	PSD_4	PSD_1
T_3	PSD_3	PSD_4	PSD_1	PSD_2
T_4	PSD_4	PSD_1	PSD_2	PSD_3

DC_i = Binder extraction at different thermal cycles, where i = 1, 2, ...

PSD_i = Particle size distribution

T_i = Injection molding temperature

Figure 58.--Matrix 3 design.

Results and discussion:

(1) Powder milling (PSD) effect on mixing.--In order to evaluate the effect of powder particle size distribution on mixing (with a binder) and injection molding of the mix, the baseline powder was milled for 8, 24, 48, and 96 hours. These milled powders subsequently were mixed with a fixed quantity of the baseline binder (B_1) in a HAAKE Rheomix under a programmed temperature profile (fig. 59a) at 60 rpm rotor rotation speed. The temperature profile and rotor speed were selected to provide good mixing and an appropriate torque output for rheological evaluation. It is demonstrated (see figure 59b) that throughout the 40-minute mixing period, the torque output level systematically varied inversely with milling time. Also, it is evident that for a given mix, the torque level varied inversely with the programmed temperature profile.

The above rheological variation data are to be used as guidelines for injection molding parameter studies in the future.

(2) Injection molding behavior map.--A series of injection molding experiments were performed to investigate the molding behavior variation of mixes. It was found that when all other molding

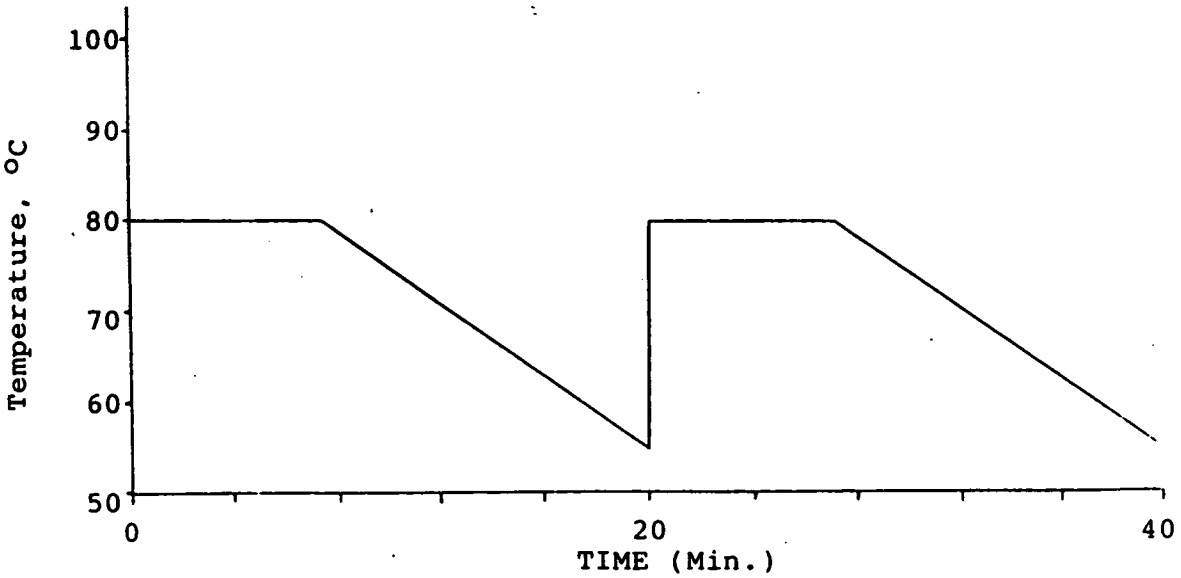

A. Programmed temperature profile for mixing.

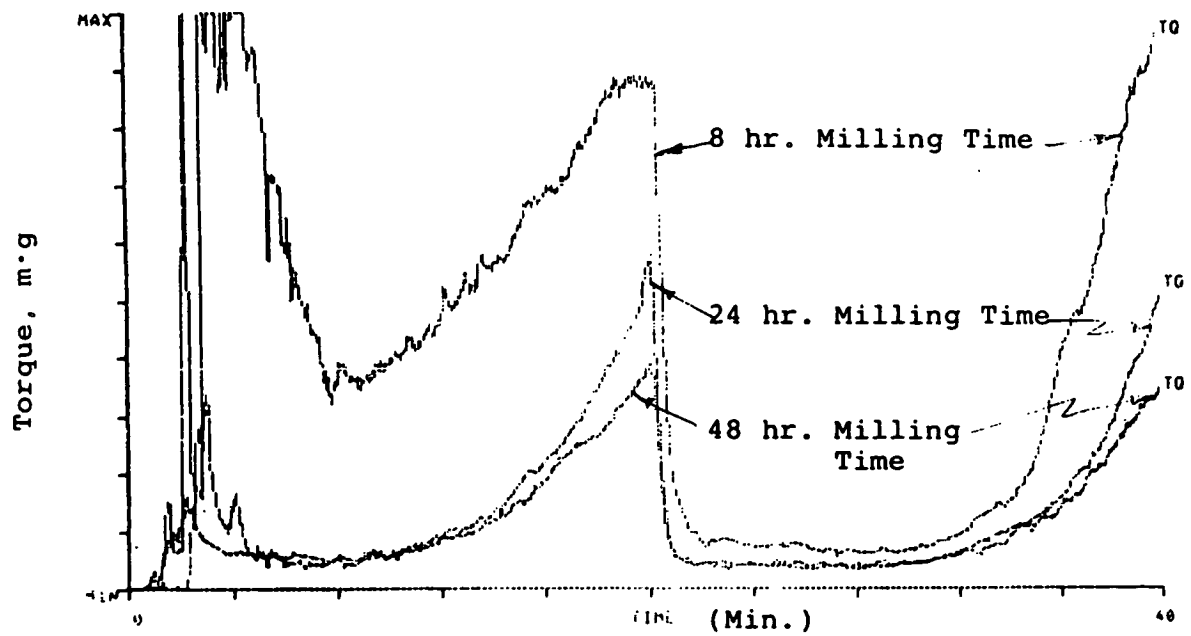

B. Mixing torque curves under the programmed temperature profile at 60 rpm rotor rotation speed.

Figure 59.--Mixing torque curves from powders of various milling times.

parameters were held constant, the material molding temperature required to obtain visually good test bars depended strongly on the PSD of the powder. The molding material temperatures required for 8-, 24-, and 48-hr milled materials were 93°, 77°, and 71°C (200°, 170°, and 160°F), respectively.

The general flow behavior observed for 18 different milling time/molding temperature combinations is illustrated in figure 60. As the graph indicates, high molding temperatures (i.e., greater than 93°C) are required to obtain satisfactory test bars for powder milled for 8 hours. Bars which appeared to be satisfactory by visual and X-radiographic inspection were injected at 71°C material temperature with powders milled for 48 or 96 hours. The following process step, binder removal, resulted in cracks and shrinkage in bars with 48- or 96-hour-milled powder; this was attributed to excess binder.

In figure 60, "insufficient fluidity" describes the condition at which the material does not flow smoothly but tends to break up as it fills and conforms to the die cavity. "Excess fluidity" describes the condition at which leakage within the injection molding machine prevents maintaining full pressure during the forming of the test bar.

(3) Dewax experiments--Four thermal cycles are used for the experiments in this matrix. Weight loss, dimensional change, and surface quality inspection were evaluated and correlated with PSD (or milling time) and injection molding parameters. The observations and results are described in the following paragraphs.

(a) Weight loss analysis--Table XXV shows the treatments in Matrix 3 and the experimental results of the dewax weight loss. The data in table XXV can not be analyzed by using the Latin square or Youden square methods as was originally planned. Rather, data from bars which have been through dewax are point estimated for several selected treatments of dewax cycle, material temperature, and milling time instead of investigated in a three-dimensional space of these variables. Therefore, the statistical analysis is conducted to compare the results between two points (or treatments).

Table XXVI shows the comparison of two groups of treatments with the same dewax cycles, and table XXVII shows the comparison of two groups of treatments with the same molding material temperature. From these results it is observed that:

(1) With the same dewax cycles, the difference in dewax weight loss between treatments is significant in most cases. The difference is more likely influenced by milling time (or PSD) than by material molding temperature.

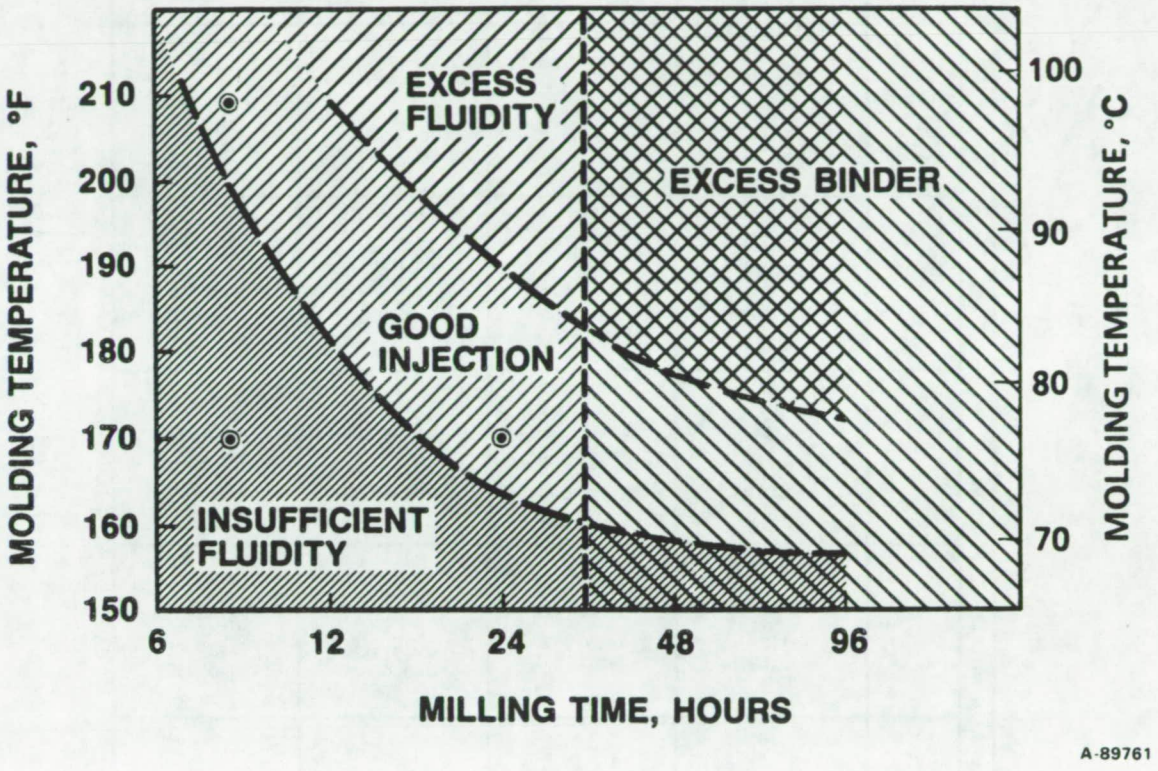

Figure 60.--Flow characteristics of injection molding materials as a function of powder milling time, material temperature during molding, and mixing torque at 65°C (GTE SN-502 powder was used).

TABLE XXV.--MATRIX 3, DEWAX WEIGHT LOSS DATA

MOLDING MATERIAL TEMPERATURE	DEWAX CYCLES: DC1 132 HR 850°F	DC 2 40 HR 850°F	DC3 20 HR 850°F	DC4
155°F	N=4 MILLING TIME 48 HR $\bar{X}$=15.275% σ=0.05			
160°F		12 48 HR $\bar{X}$=15.375 σ=0.0866	12 96 HR #2 $\bar{X}$=15.5 σ=0.0853	16 24 HR #1 $\bar{X}$=15.07 σ=0.0704
170°F	23 24 HR #2 $\bar{X}$=15.37 σ=0.0703	4 24 HR #2 4 96 HR #1 2 8 HR $\bar{X}$=15.45 σ=0.10 $\bar{X}$=15.57 σ=0.058 $\bar{X}$=15.0 σ=0	12 48 HR $\bar{X}$=15.308 σ=0.0996	24 96 HR #1 $\bar{X}$=15.571 σ=0.0751
180°F	8 48 HR $\bar{X}$=15.4 σ=0.0926	12 96 HR #2 $\bar{X}$=15.533 σ=0.065	16 24 HR #1 $\bar{X}$=15.131 σ=0.0602	4 8 HR $\bar{X}$=15.05 σ=0.0577
190°F	12 96 HR #2 $\bar{X}$=15.45 σ=0.0904	10 24 HR #2 $\bar{X}$=15.17 σ=0.0675	8 8 HR $\bar{X}$=14.963 σ=0.0517	
200°F				4 8 HR $\bar{X}$=15.05 σ=0.0577
210°F		4 8 HR $\bar{X}$=14.975 σ=0.0958		

A-81092

N=NUMBER OF SAMPLES

MILLING TIME IN HOURS

$\bar{X}$=MEAN DEWAX WEIGHT LOSS
σ=STANDARD DEVIATION

TABLE XXVI.--MATRIX 3, DEWAX WEIGHT LOSS DATA SUMMARY ARRANGED BY DEWAX CYCLE

DC1 (132 hr to 454°C/850°F)			DC2 (40 hr to 454°C/850°F)			DC3 (20 hr to 454°C/850°F)			DC4 (10 hr to 454°C/850°F)		
Groups	$\bar{X}$	σ	Groups	$\bar{X}$	σ	Groups	$\bar{X}$	σ	Groups	$\bar{X}$	σ
(1) 155°F 48 hr	15.275	0.05	(1) 160°F 48 hr	15.375	0.0704	(1) 160°F 95 hr #2	15.5	0.0853	(1) 160°F 24 hr	15.07	0.0704
(2) 170°F 24 hr #2	15.37	0.07	(2) 170°F 24 hr	15.45	0.10	(2) 170°F 48 hr	15.31	0.0996	(2) 170°F 96 hr #1	15.57	0.075
(3) 180°F 48 hr	15.40	0.093	(3) 170°F 96 hr #1	15.37	0.058	(3) 180°F 24 hr #1	15.13	0.0602	(3) 180F 8 hr	15.05	0.0577
(4) 190°F 96 hr	15.45	0.09	(4) 170°F 8 hr	15.0	0	(4) 190°F 8 hr	14.96	0.0517	(4) 200°F 8 hr	15.05	0.0577
			(5) 180°F 96 hr #2	15.533	0.065						
			(6) 190°F 24 hr #2	15.17	0.0675						
			(7) 210°F 8 hr	14.975	0.096						
Comparison between groups	P-value		Comparison between groups	P-value		Comparison between groups	P-value		Comparison between groups	P-value	
(1) (2)	0.0169		(1) (2)	0.1693		(1) (2)	0.000		(1) (2)	0.000	
(1) (3)	0.0323		(1) (3)	0.0033		(1) (3)	0.000		(1) (3)	0.630	
(1) (4)	0.0027		(1) (4)	0.0001		(1) (4)	0.000		(1) (4)	0.630	
(2) (3)	0.339		(1) (5)	0.000		(2) (3)	0.000		(2) (3)	0.000	
(2) (4)	0.0084		(1) (6)	0.000		(2) (4)	0.000		(2) (4)	0.000	
(3) (4)	0.246		(1) (7)	0.000		(3) (4)	0.000		(3) (4)	1.000	
			(2) (3)	0.1345							
			(2) (4)	0.0039							
			(2) (5)	0.0714							
			(2) (6)	0.000							
			(2) (7)	0.0005							
			(3) (4)	0.0009							
			(3) (5)	0.435							
			(3) (6)	0.000							
			(3) (7)	0.0002							
			(4) (5)	0.000							
			(4) (6)	0.0065							
			(4) (7)	0.745							
			(5) (6)	0.000							
			(5) (7)	0.000							
			(6) (7)	0.0009							

TABLE XXVII.--DEWAX WEIGHT LOSS DATA SUMMARY ARRANGED BY MOLDING TEMPERATURE

71°C (160°F)			77°C (170°F)			82°C (180°F)			88°C (190°F)		
Groups	$\bar{X}$	σ	Groups	$\bar{X}$	σ	Groups	$\bar{X}$	σ	Groups	$\bar{X}$	σ
(1) DC2 48 hr	15.375	0.0866	(1) DC1 24 hr #2	15.37	0.0703	(1) DC1 48 hr	15.4	0.0926	(1) DC1 96 hr #2	15.45	0.0904
(2) DC3 96 hr	15.50	0.0853	(2) DC2 24 hr #2	15.45	0.10	(2) DC2 96 hr #2	15.53	0.065	(2) DC2 24 hr #2	15.17	0.0675
(3) DC4 24 hr #1	15.07	0.0704	(3) DC2 96 hr #1	15.567	0.058	(3) DC3 24 hr #1	15.13	0.0602	(3) DC3 8 hr	14.96	0.0517
			(4) DC2 8 hr	15.0	0.0	(4) DC4 8 hr	15.05	0.0577			
			(5) DC3 48 hr	15.308	0.0996						
			(6) DC4 96 hr #1	15.57	0.0751						
Comparison between groups	P-value		Comparison between groups	P-value		Comparison between groups	P-value		Comparison between groups	P-value	
(1) (2)	0.0017		(1) (2)	0.0572		(1) (2)	0.0013		(1) (2)	0.000	
(1) (3)	0.000		(1) (3)	0.0001		(1) (3)	0.000		(1) (3)	0.000	
(2) (3)	0.000		(1) (4)	0.000		(1) (4)	0.000		(2) (3)	0.000	
			(1) (5)	0.042		(2) (3)	0.000				
			(1) (6)	0.0001		(2) (4)	0.000				
			(2) (3)	0.134		(3) (4)	0.0258				
			(2) (4)	0.0039							
			(2) (5)	0.0275							
			(2) (6)	0.356							
			(3) (4)	0.0009							
			(3) (5)	0.001							
			(3) (6)	0.850							
			(4) (5)	0.0012							
			(4) (6)	0.000							
			(5) (6)	0.002							

(2) With the same material molding temperature, the difference in dewax weight loss between treatments is also significant in most cases. The difference is also more likely influenced by milling time (PSD) than by dewax cycle.

(3) With the same molding material temperature, the influence of different dewax cycles is not significant.

(b) Dimensional change--The thickness of a selected group of dewaxed bars was measured and compared with the thickness of these bars before being dewaxed. These dimensional changes are listed in table XXVIII along with the bars' weight loss as a function of milling time. The dimensional change data are also plotted in figure 61. It is obvious that the dimensional change is a function of milling time (PSD), ranging from an expansion of 0.5 percent to a shrinkage of 1.5 percent. This has a significant implication in understanding the cracking behavior of a dewaxed part. The significance of the increase in weight loss with milling time (table XXVI) observed on the same set of test bars can not be interpreted at the present time.

TABLE XXVIII.--MILLING TIME EFFECT ON BINDER EXTRACTION OF TEST BARS

Milling time, hr	Test bar thickness change[1,2], %	Weight loss[1], %
8	+0.5	15.00
24	+0.2	15.10
48	-0.1	15.35
96	-1.0	15.56

Notes:

1. $\frac{\text{Thickness after binder extraction-thickness before binder extraction}}{\text{thickness before binder extraction}}$

2. Average of a minimum of 10 test bars

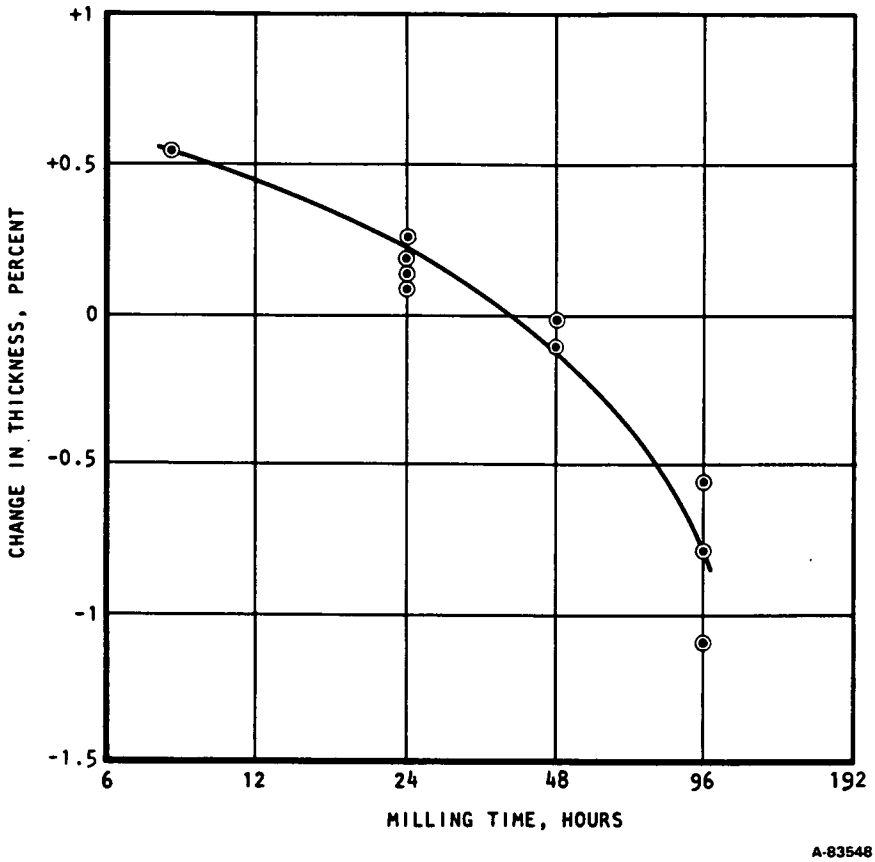

Figure 61.--Dimensional change during binder removal, using a constant binder content and GTE SN-502 powder.

(c) Surface quality--A selected number of samples were examined under a micropscope after dewaxing. It was found that:

(1) Binder-extracted specimens often revealed additional defects not seen on injection-molded test bars. An example is shown in figure 62.

(2) The visual surface quality of the binder-extracted test bars also depends on the injection molding temperature and PSD (milling time) as shown in figures 63 and 64.

(4) Sintering--Sintering was completed on 144 test bars representative of 4 PSD's and 4 dewax cycles. Weight loss was comparable to Task I resintered bars. Higher weight loss bars (located in the outer position of the sintering tray) appeared darker and somewhat grainy. They are relatively free, however of the pitting which was extensive in earlier bars (shown in figure 65 near the bottom edge).

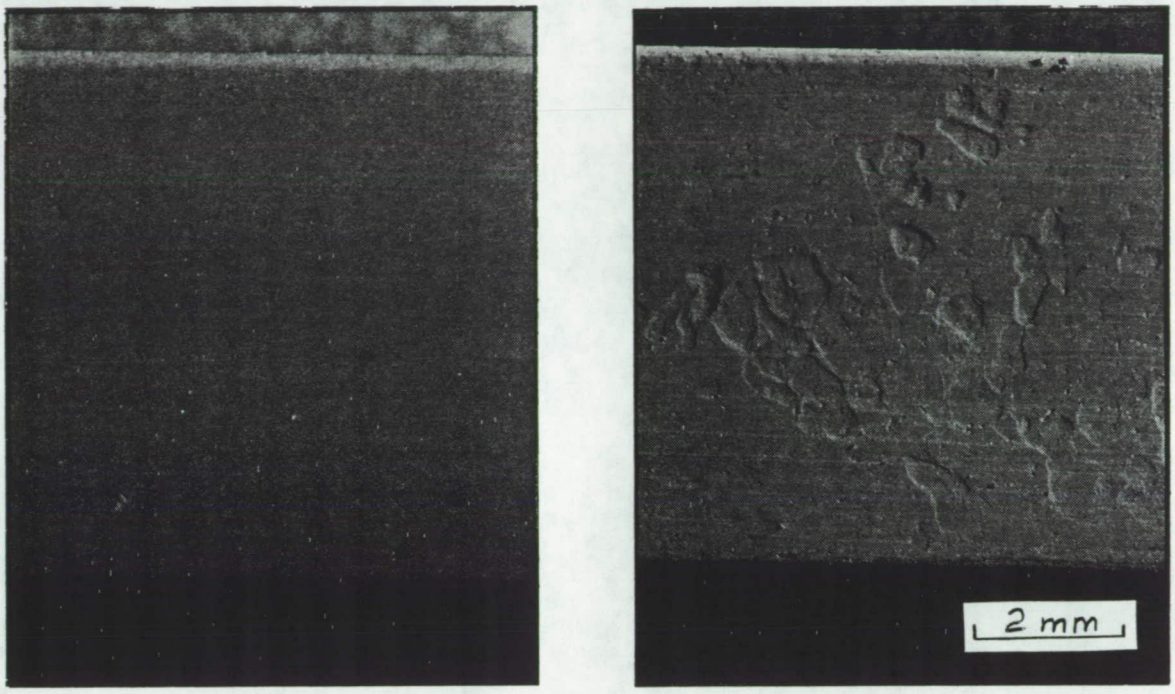

A. Injection molded

B. Dewaxed

Figure 62.--Injection-molded and dewaxed surfaces of test bar no. 904 (76.6°C/170°F injection) using powder milled 96 hours.

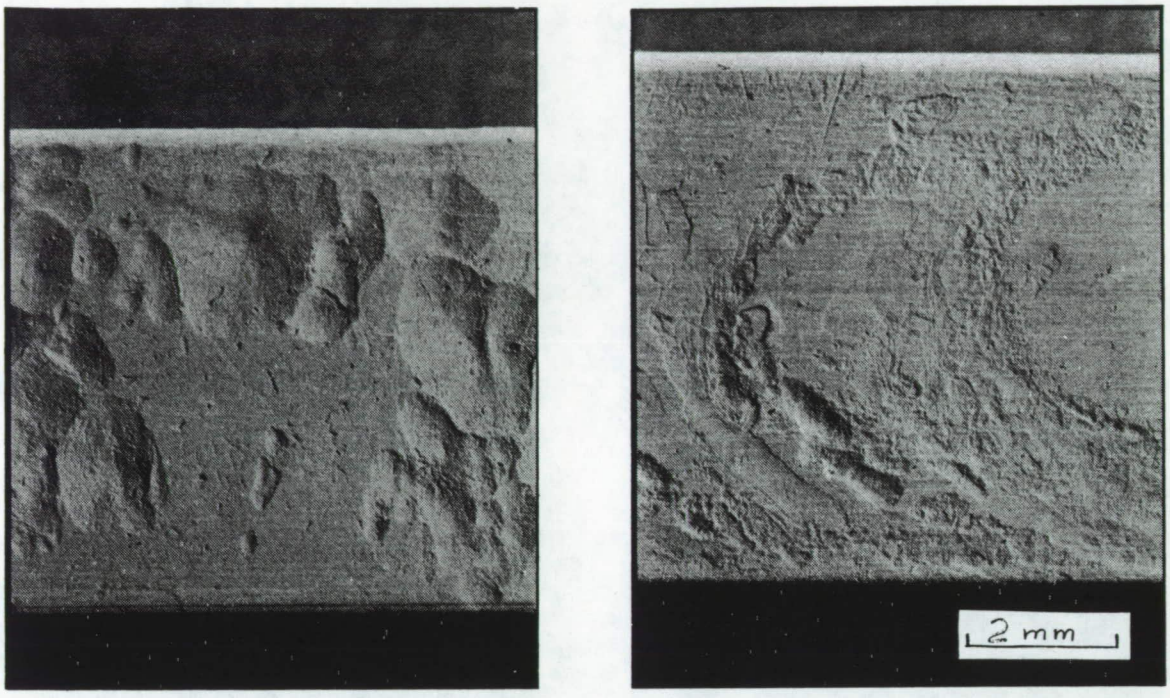

A. Bar no. 1054 (71°C/160°F injection)

B. Bar no. 1072 (77°C/180°F injection)

Figure 63.--Dewaxed test bar surfaces from two molding temperatures using powder milled 96 hours.

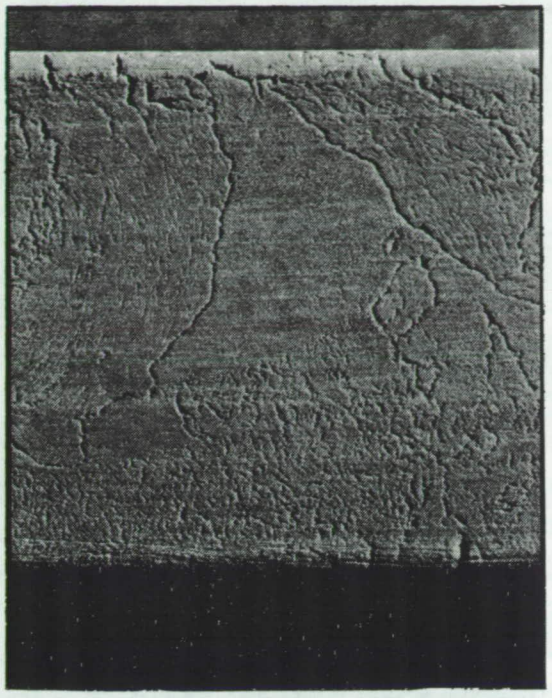

A. Bar no. 910 (77°C/170°F injection

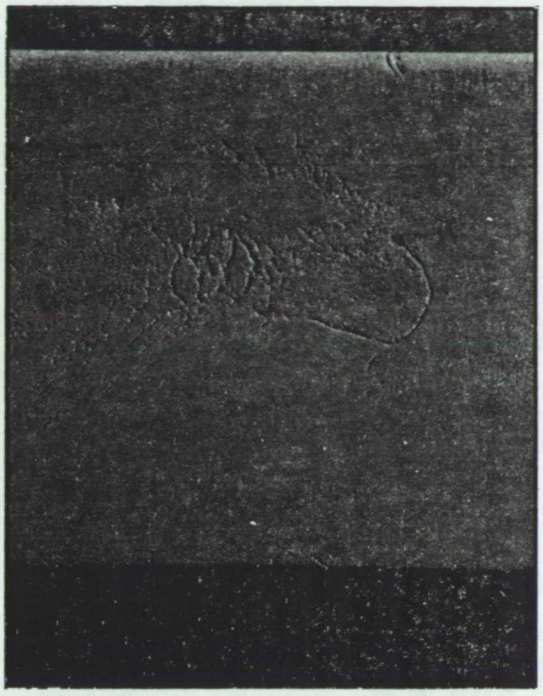

B. Bar no. 951 (88°C/180°F injection

C. Bar no. 942 (93°C/200°F injection)

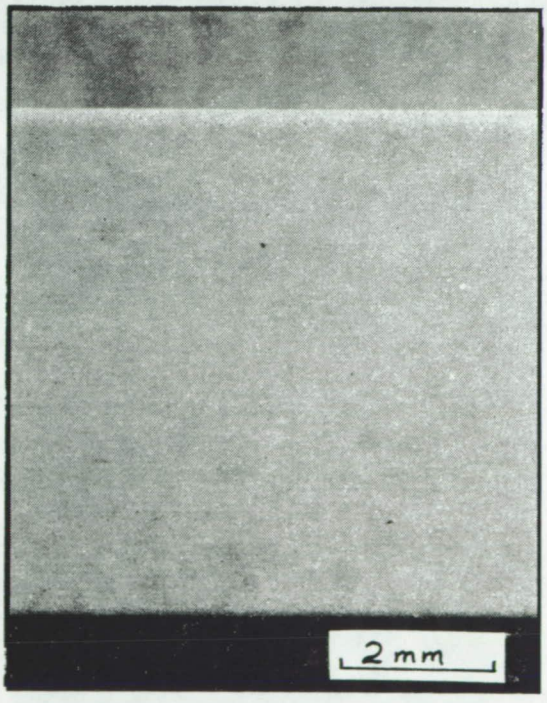

D. Bar no. 948 (99°C/210°F injection) F-47247

Figure 64.--Dewaxed test bar surfaces from four molding temperatures using powder milled 8 hours.

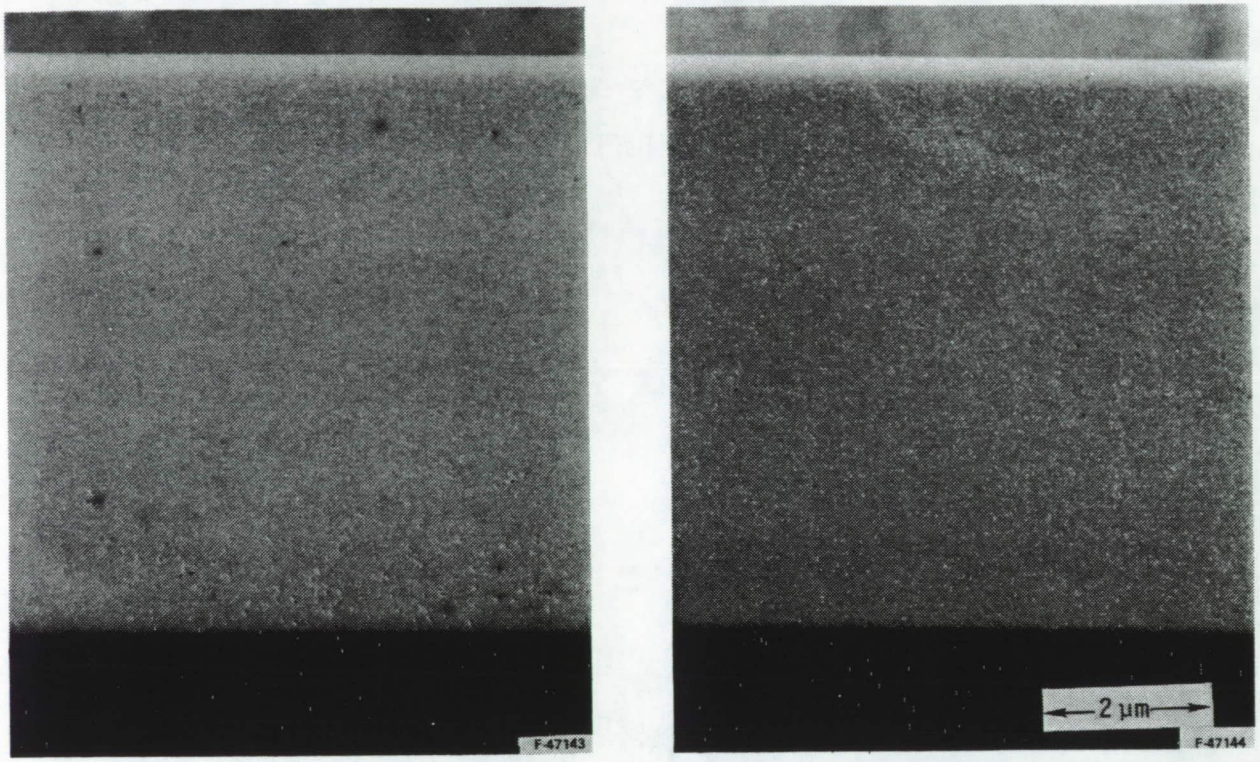

a. Bar no. 48, Task I resintered

b. Bar no. 948, Task VII, Matrix 3

Figure 65.--Sintered test bars with high weight loss.

F-47173

Densities after sintering were generally higher than Task I results. Data are presented in table XXIX.

Some improvements were seen in surface finish during sintering as compared with dewax (see fig. 66). Existing cracks were not healed, however. It is not clear if a smoother surface results in any flaw healing.

Three-way plots of the MOR data vs two process variables at fixed dewax run or molding temperature were made. From these plots the following observations are made.

(1) At a fixed dewax run, or a fixed material molding temperature, each PSD has its own specific dewax weight loss region and that PSD affects MOR significantly. For the same PSD, dewax weight loss does not affect MOR. At this time, it is concluded that PSD has the primary effect.

(2) At a fixed dewax run or a fixed material molding temperature, different PSD significantly affects MOR and sintering weight loss. For some dewax runs and some fixed PSD's, the higher the sintering weight loss, the higher the MOR.

(3) At a fixed dewax run or a fixed material molding temperature, different PSD has a distinguishable but not significant region of density. Different PSD significantly affects MOR. At a fixed PSD, the higher the density, the higher the MOR.

Matrix 4 - sintering aids/sintering cycle.--In order to improve the high temperature strength of the test bars, modification of the type and quantity of sintering aids is planned. In the first iteration, Y_2O_3 and Al_2O_3 levels will be varied with the goal of reducing the Al_2O_3 content. The baseline composition uses 6% Y_2O_3 and 2% Al_2O_3. Alternate levels were selected as follows: 6% and 1%, 6% and 0.5%, and 8% and 1%, Y_2O_3 and Al_2O_3, respectively. Sintering aid, sintering cycle, and heating rate are combined to form Matrix 4, as shown in figure 67. Hot isostatic pressing (HIP) cycle is also included in this Matrix.

Experimental procedures: Baseline powder (GTE SN-502 Si_3N_4) was milled for 24 hr with the appropriate sintering aids. The milled powders were then blended with the baseline binder (B_1) at the baseline level (15.5 percent) using the "HAAKE baseline" procedures.

Results and discussion: Because of the variation in sintering aids, the mixing behavior of the mixes in the HAAKE 600 mixer also varied as reflection by the mixing torque summarized in table XXX. Correspondingly, the injection molding behavior using the baseline parameters also differs as reflected by the surface finish of the injection bars (see the last two columns of table XXX). This suggests that in order to fabricate good quality test bars, with different sintering aids, the injection parameters have to be readjusted.

TABLE XXIX.--MATRIX 3, SINTERING DATA SUMMARY

Milling time, hr	Average density, g/cc	Average weight loss, %	Number of samples weighed
8	3.22	1.44	21
24	3.25	1.65	57
48	3.25	2.14	32
96	3.23	2.17	29

a. Bar no. 882 as-dewaxed

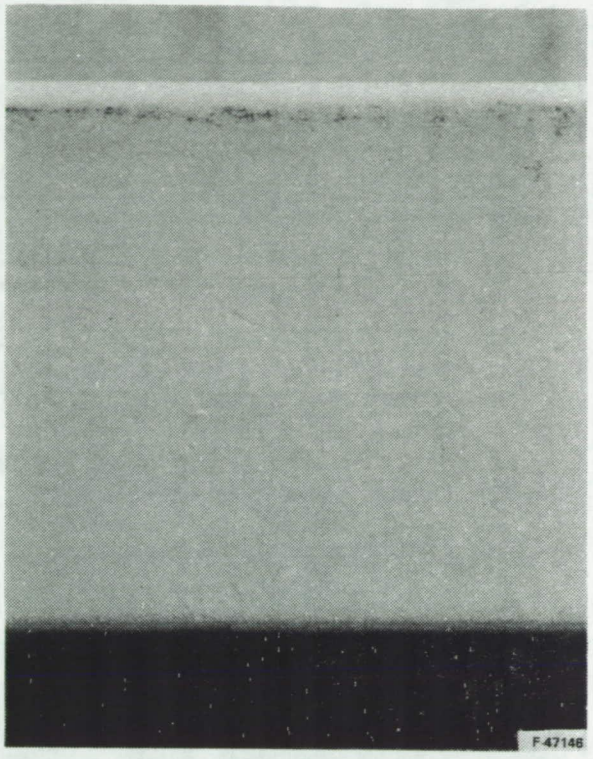

b. Bar no. 882 as-sintered

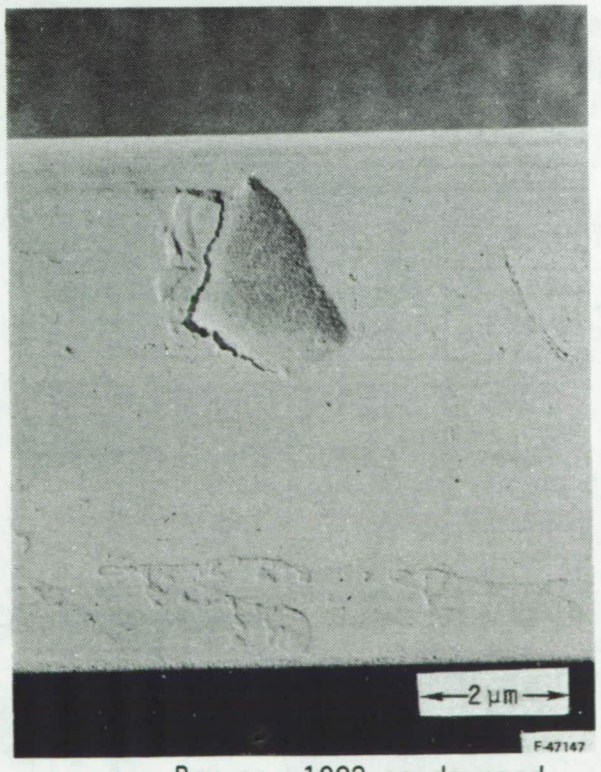

c. Bar no. 1082 as-dewaxed

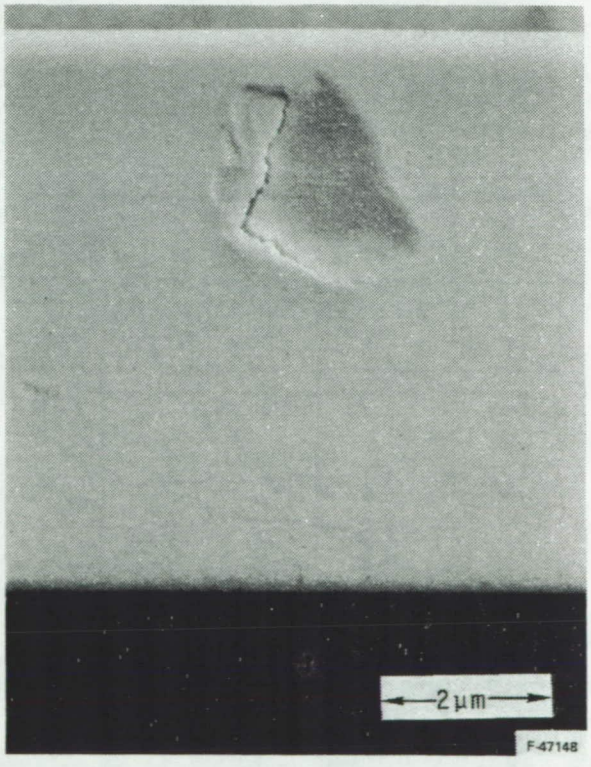

d. Bar no. 1082 as-sintered

Figure 66.--Surface changes in sintering. F-48900

	S1				S2			
	SA1	SA2	SA3	SA4	SA1	SA2	SA3	SA4
HR1								
HR2								
HIP								

S = Sintering peak temperature

HR = Heating rate

SA = Sintering aid

HIP = Hot isostatic pressing

Figure 67.--Matrix 4.

TABLE XXX.--MIXING AND MOLDING BEHAVIORS OF MATERIALS CONTAINING DIFFERENT SINTERING AIDS

Code	Composition, %			Mixing Torque (m·g) at 65°C		Number of bars injected	Surface finish of as-injected test bars
	Si_3N_4	Y_2O_3	Al_2O_3	Average*	Standard deviation		
SA_1	92	6	2	400	40	44	Good
SA_2	93	6	1	507	60	52	Marginal
SA_3	93.5	6	0.5	510	52	32	Bad
SA_4	91	8	1	380	35	32	Some good, some marginal

*Average of 5 or 6 values

Matrix 5 - raw materials, milling time, and milling aid.--Matrix 5 (fig. 68) was designed to provide a range of processing conditions in order to identify appropriate parameters for evaluating new powders and milling aids (MA_1 and MA_2). The results in Matrix 1 indicated that it may be necessary to change the processing parameters when evaluating a new powder.

Based on the results of Matrix 5 efforts, the range of processing conditions was narrowed to provide a limited number of materials for test bar fabrication and evaluation in Matrix 6.

Experimental procedure: Each powder and milling aid combination was milled at a minimum of two different milling time periods. Each of the milled powders was mixed with binder on the torque rheometer, using a fixed binder ratio, to determine the mixing and flow behavior.

Materials M_5 (Starck LC-1), M_6 (KermaNord P95M), and MA_2 had no prior processing history. The experiment plan was modified after finding that MA_2 appeared to yield inconsistent milling results, increased mixing torque, and increased dewax residue. Use of MA_2 was discontinued until benefits are shown in further processing of M_1/MA_2 and M_4/MA_2 combinations.

	MA_0	MA_1	MA_2
M_1	PSD_1PSD_2	PSD_3PSD_4	
M_4	PSD_5PSD_6		
M_5			
M_6			

M = Si_3N_4 raw material

MA_0 = No milling aid

MA_X = Proprietary milling aid

PSD_X = Particle size distribution variations for each powder

Figure 68.--Matrix 5 - milling study on various raw materials.

Results and discussion: Processing conditions evaluated in Matrix 5 are shown in table XXXI. Seventeen batches were milled and mixed on the torque rheometer. Torque results shown were taken from one mixer run for materials not selected for further processing. Materials chosen for further processing required additional mixing and provided up to six mixes for torque data averaging. The standard deviation was typically 10 percent of the average value indicating the level of uncertainty of data based on one run. In nearly all cases where milling time was increased for a given composition, the torque value dropped.

Powder M_1 was initially milled as follows: 48 hours with no milling aid MA_0, 24 hours with milling aid MA_1, and 24 hours with milling aid MA_2. Even with shorter milling times, the use of milling aids provided a finer powder as shown by the data in table XXXI.

New milled batches were prepared using milling aids MA_1 and MA_2. Milling was performed with these materials until the median particle size (50 percent on the cumulative volume curve) matched that of the baseline at 0.87 μm. Inconsistent milling behavior was observed when MA_1 was used; this is not yet understood. The longer milling time resulted in a coarser powder as indicated by the PSD measurement and supported by the torque behavior.

Powder M_4 (Starck H-1) is finer than M_1 and has a greater surface area. Shorter milling times--2 and 8 hours--were selected for evaluation. The median particle size for all 8-hour-milled powders ranged from 0.92 to 0.95 μm in diameter. The 8-hour-milled powders were selected for test bar fabrication in Matrix 6.

Material M_5 (Starck LC-1) was reported by the manufacturer to be physically similar to M_4. The milling parameters chosen for M_5 were based on M_4 results. The eight-hour-milled powders were selected for further processing in Matrix 6.

Initially, material M_6 (KemaNord P95M) was milled eight hours and mixed. However, very high torque values indicated that more milling was required. The milling time was increased to 48 hours and a significant reduction in mixing torque was observed. The effect of MA_1 observed with powder M_1 was assumed to provide a similar effect with powder M_6. Powders milled for 48 hours with no milling aid and 24 hours with a milling aid were selected for further processing.

Increased milling time for all M/MA combinations generally showed reduced mixing torque. Exceptions to this were small (M_4/MA_0) or from a milling anomaly (M_1/MA_2) and could also result in the uncertainty of the torque rheometry reading. This behavior is consistent with Matrix 3 results.

TABLE XXXI.--PROCESSING RESULTS--RAW MATERIALS AND MILLING VARIATIONS

Material	Milling aid	Milling time, hr	Particle size at 50%, μm	Mixing torque[1] at 65°C m·g	Bars molded[2] for Matrix 6
M_1	MA_0	48	0.87	281	Yes
	MA_1	24	0.80	290	
	MA_1	14	0.87	481	Yes
	MA_2	24	0.80	310	
	MA_2	26	0.87	479	Yes
M_4	MA_0	2	1.05	416	
	MA_0	8	0.95	452	Yes
	MA_1	2	1.05	1107	
	MA_1	8	0.93	569	Yes
	MA_2	2	1.03	1771	
	MA_2	8	0.92	1264	Yes
M_5	MA_0	2	1.06	946	
	MA_0	8	0.93	765	Yes
	MA_1	8	0.92	1083	Yes
M_6	MA_0	8		1900	
	MA_0	48	1.03	660	Yes
	MA_1	24		1500	Yes

Notes:

1. Cooling rate 2°C/hr

2. The mixing torque data for materials selected for bar production is an average of five mixer runs

Milling aids proved to accelerate the particle reduction rate during milling for powders M_1 and M_4. The use of milling aids, however, resulted in a higher torque, at the same or finer PSD, than for those mixes with no milling aid. Milling with an effective milling aid is not equivalent to increasing the milling time.

Matrix 6 - raw materials, molding parameters, binder removal, and sintering.-Matrix 6 was designed to provide a range of processing conditions in order to identify appropriate parameters for evaluating new materials (M_4, M_5, and M_6) and milling aids (MA_1 and MA_2). Powders were milled and evaluated for suitable processing behavior in Matrix 5. Materials that did not process well in Matrix 1 (M_2 blistered in sintering and M_3 mixed with great difficulty) were not studied here. Processing which appeared detrimental in Matrix 1 was avoided (M_4 cracked upon dewax similar to excessively milled GTE SN-502 in Matrix 3).

Experimental procedure: A statistically designed experiment was planned to include five variables: four Si_3N_4 powders, three milling aids, two molding temperatures, two binder removal cycles, and two sintering cycles. The large matrix was a combination of four 1/2 replicate 2^5 fractional designed matrixes. The detailed original plan was presented (Monthly Report No. 7) and is not shown here due to required modifications.

The revised matrix is shown in figure 69. Modifications were required after recognizing the sintering temperature required for densification was similar for M_1 and M_6 and similar for M_4 and M_5 but is very different for the two pairs. The configuration of the submatrixes was reduced by the elimination of M_5/MA_2 and M_6/MA_2 as discussed in Matrix 5.

Results and discussion: Molding temperatures were selected based on visual examination of molded test bars. A good correlation exists between mixing torque and required molding temperature as seen in table XXXII. Combination M_4/MA_2 had high mixing torque but was injected prior to establishing the torque molding temperature relationship. The 77°C (170°F) molded M_4/MA_2 bars did show evidence of insufficient flow.

Inspection of dewaxed bars showed no effect from the two different binder removal (dewax) cycles. This is consistent with Matrix 3 results (Matrix 6, DC_1, and DC_2 are the same as Matrix 3, DC_2 and DC_3, respectively). Cycle DC_1 is currently being used in the program as the standard cycle. Matrix 6 cycle DC_2 doubles the heating rate, apparently with no damage to thin section test bars.

Dewax weight loss indicated that a significant residue resulted from the use of MA_2. Sintering trails have been run on spare bars representing Matrix 6 materials. (Spare bars resulted from molding trials for identifying proper molding temperatures which resulted in less-than-optimum surfaces.) A sample run included 27 test bars and the data are presented in table XXXIII. Run parameters were approximately 1975°C for 4 hours. M_1 baseline material went to 100 percent theoretical density

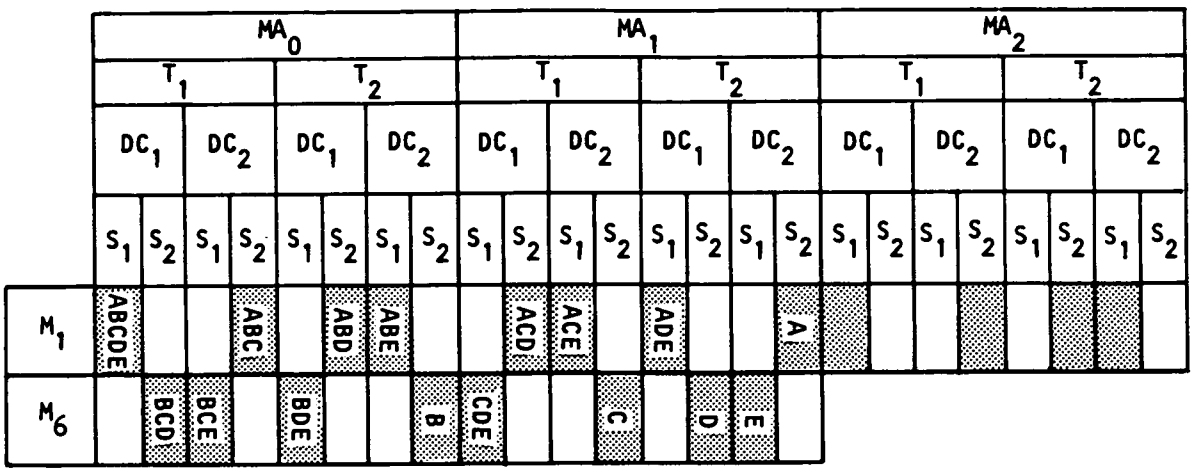

a. M1 AND M6

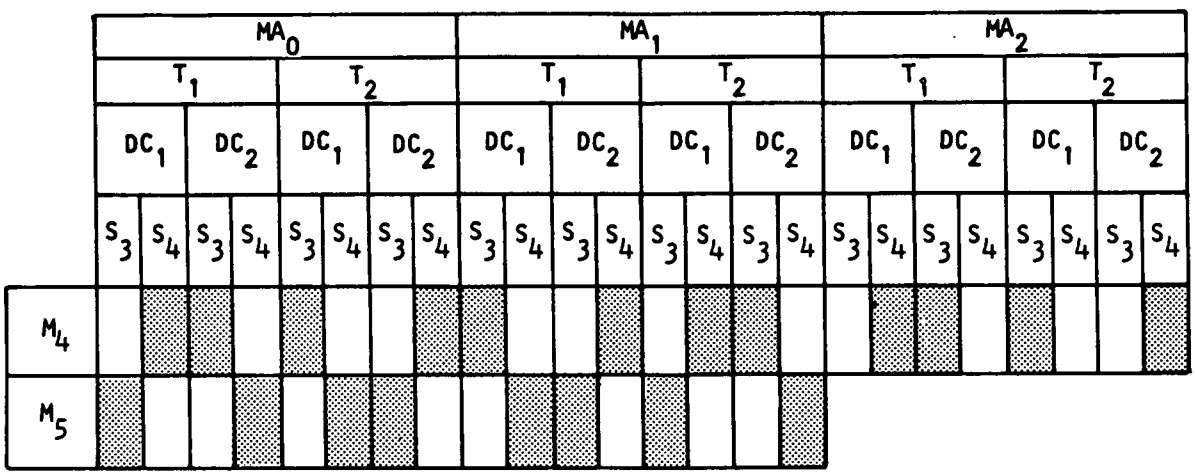

b. M4 AND M5

NOTES:

1. M = Si_3N_4
2. MA = MILLING AID
3. T = MOLDING TEMPERATURE
4. DC = DEWAX CYCLE
5. S = SINTERING CYCLE

A-87181

Figure 69.--Matrix 6 submatrixes; shaded areas to be performed.

TABLE XXXII.--TORQUE AT 65°C (150°F) AND MOLDING TEMPERATURES FOR MATRIXES 5 AND 6

	MA_0		MA_1		MA_2	
	Torque at 65°C, m·g	Molding temperature, °C (°F)	Torque at 65°C, m·g	Molding temperature, °C (°F)	Torque at 65°C, m·g	Molding temperature, °C (°F)
M_1	281	77, 82 (170, 180)	481	77, 82 (170, 180)	479	82, 88 (180, 190)
M_4	452	77, 82 (170, 180)	569	77, 82 (170, 180)	1264	77, 82 (170, 180)
M_5	765	82, 88 (180, 190)	1083	82, 88 (180, 190)		
M_6	660	82, 88 (180, 190)	1500	88, 93 (190, 200)		

Notes:

1. Mixer cooling rate was 2°C (3.6°F) per minute.
2. Torque values given are averages from 5 mixer runs.

M = Si_3N_4 raw material

MA = Milling aid

m·g = meter·gram

TABLE XXXIII.--MATRIX 6--SINTERED DENSITIES FROM TRIAL RUN[1]

Material	Number of bars	Density range[2], g/cc	Weight loss range[2], %
M_1	10	3.25-3.26	3.1-4.0
M_4	10	3.06-3.16	2.3-2.8
M_5	3	3.16-3.23	2.5-2.7
M_6	4	3.15-3.26	0.8-2.0

Note:

1. Bars were sintered at 1950°C/4 hr/0.68 MPa (100 psi).
2. Broad range is due to variables including BN powder bed, sintering position, milling time, and binder residue.

but demonstrated significant weight loss. M_6 yielded one 100 percent theoretically dense sample and indicated low weight loss. This material will be further evaluated in subsequent experiments.

Silicon nitride M_4, Starck H-1, also showed lower weight loss. Higher temperatures or pressures are required to fully densify M_4-based samples. These data provide useful input to establishing processing conditions for Task II, Matrix 1. Successful processing of M_4 powder was achieved in Matrixes 5 and 6 because of understanding gained in Matrix 3 and the iterative approach used here. The same material in Matrix 1 yield poor results.

Matrix 7 - Dewax load size.--The requirements of processing large numbers of bars in Task II suggested the need to evaluate the effect of increasing the number of test bars within the closed system of the binder removal cycle. As many as 100 test bars had been processed in a single cycle (Matrix 1) with no detrimental effects attributed to the large furnace load. However, the furnace that was used had a processing capacity that was significantly larger.

Experimental procedure: Test bars were injected in parallel with Matrix II-1 (Task V) for use in optimization experiments. Dewax run 101 consisted of 36 bars, while run 102 contained 216 bars. Bars from each of the eight groups injected in Matrix II-1 were distributed uniformly throughout the furnace in run 102. These included bars with 14.5 percent and bars with 15.5 percent binder. Only three groups were used in run 101 to provide a statistically significant number of bars in each group.

Evaluation was performed on load size, tray stacking, and location within a tray. A three-day dewax cycle was used, which proved acceptable in Matrixes 3 and 6, instead of the Task I, baseline seven-day cycle.

Results and discussion: Table XXXIV shows the dewax weight loss from three sets of similar bars from dewax runs 101 and 102. The t test was used to compare individual sets of bars and indicated a difference between like sets of bars in different runs. Some sets, however, indicate more residue in run 101 while others indicate more residue in run 102. When combining the data from all sets, the difference is actually beyond the range of precision of the balances used for obtaining the data. Very little difference, if any, can be detected between the runs based on dewax weight loss data.

TABLE XXXIV.--DEWAX WEIGHT LOSS - EVALUATION OF LOAD SIZE

Run 101 (36 bars, one layer)				Run 102 (216 bars, 3 layers)			
Bar number	N	Ave. weight loss, %	σ	Bar number	N	Ave. weight loss, %	σ
1548-1559	12	15.39	0.05	1560-1579	20	15.32	0.07
2343-2354	12	14.32	0.07	2383-2402	10	14.41	0.03
2943-2954	11	14.44	0.05	2974-2993	20	14.40	0.04
All bars (sets)	3	14.72		All bars (sets)	3	14.71	

No test bar location was identified in run 102 with three layers of test bars. Figure 70 shows the average residue measured for eight bars in each location shown. All groups of eight bars consist of one bar from each of the eight groups processed in Matrix II-1. The observed range is 0.08 to 0.16 percent, but this does not appear to correspond to any trend related to location.

Twelve bars from each of the dewax runs were sintered. A total of 24 bars, consisting of 4 bars from each of the groups identified in table XXXIV, yielded the sintering results shown in table XXXV. Only a small difference is indicated in density and no difference in weight loss. The low densities shown here result from a nonoptimum sintering cycle, and are especially noticeable for bars with a reduced level of sintering aids.

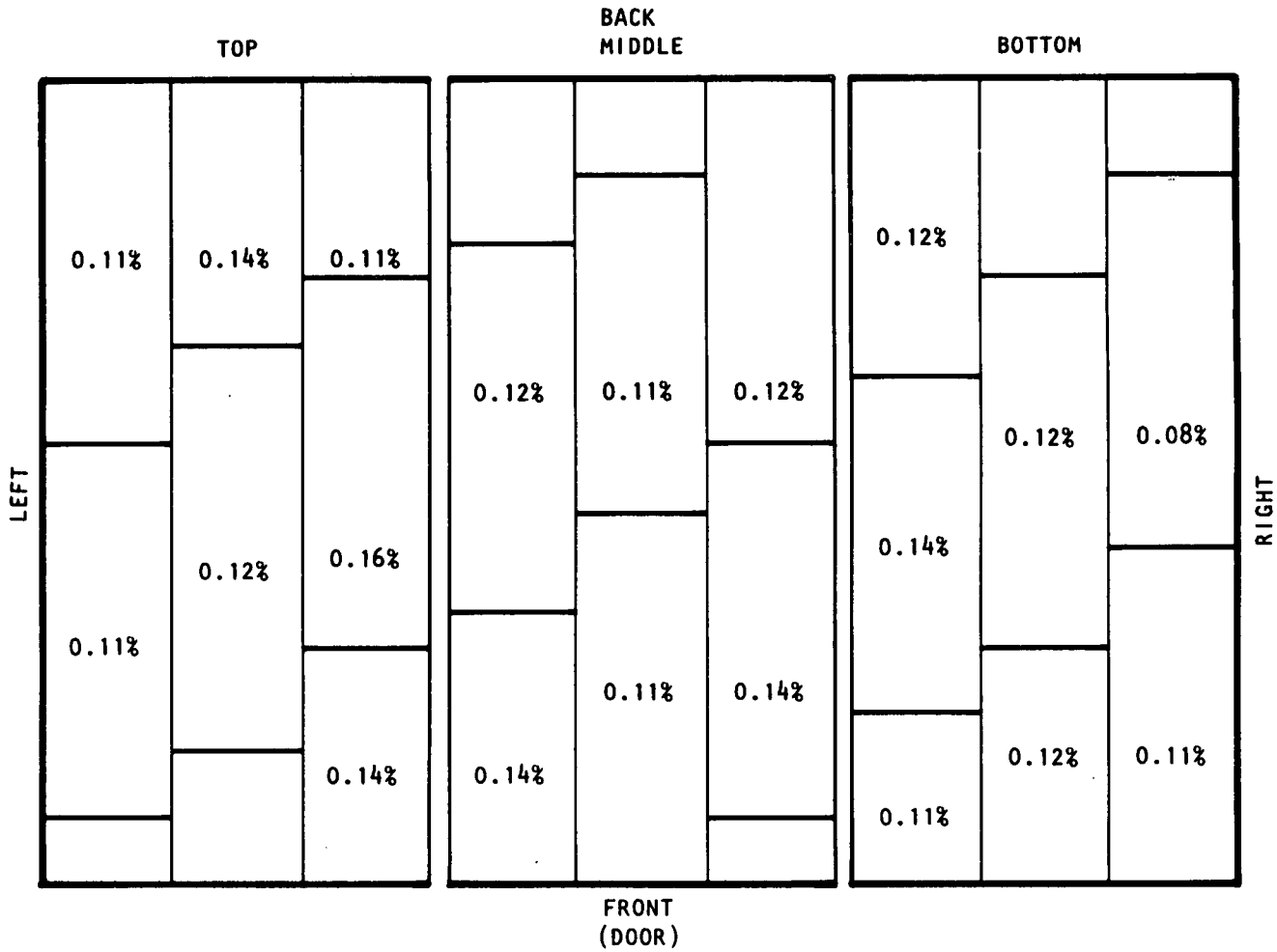

Figure 70.--Residue after dewax in run 102.

TABLE XXXV.--SINTERING RESULTS - EVALUATION OF DEWAX LOAD SIZE

Parameter	Dewax run 101		Dewax run 102	
Density, g/cc	2.93	σ = 0.04	2.96	σ = 0.04
Weight loss, %	2.0	σ = 0.3	2.0	σ = 0.2

APPENDIX A

PROCESSING STUDY OF INJECTION MOLDING OF SILICON NITRIDE FOR ENGINE APPLICATIONS *

By Michael E. Rorabaugh & Hun Yeh

AiResearch Casting Company, Torrance, CA

June 1985

ABSTRACT

PROCESSING STUDY OF INJECTION MOLDING OF SILICON NITRIDE FOR ENGINE APPLICATIONS

By Mike Rorabaugh & Hun Yeh
AiResearch Casting Company, Torrance, CA

Silicon nitride is a high temperature structural material currently considered for gas turbine engine applications. Due to the high cost of machining ceramics, net (or near net) shape forming capability of this new high performance material is the key to the ultimate use of this material in engines. Injection molding is one of the most promising forming processes being considered.

The integrity and properties of an injection molded Si_3N_4 part strongly depend on the processing parameters used. To successfully fabricate reliable high performance parts, it is essential to understand the interrelationships between processing variables and the resulting microstructure and properties of the finished parts. This paper summarizes some of the initial results from an on-going NASA funded program to improve Si_3N_4 materials (NASA Contract No. NAS3-24385). The quality of injection molded test bars at various stages of processing will be correlated with selected processing variables.

1. INTRODUCTION

To increase the efficiencies of gas turbine engines it is necessary to increase the gas inlet temperature of the engine. The current supper alloys used in turbine engine component fabrication limit the inlet temperature to about 1800°F. Silicon nitride, a candidate material under evaluation, has the potential to increase the inlet temperature to 2500°F.

Due to the high hardness of silicon nitride, the cost of machining this material to engine component configurations is prohibitive. Consequently, near net shape forming techniques, such as injection molding, are essential in the manufacturing of silicon nitride engine components. Ceramic materials such as silicon nitride currently do not have high reliability chiefly due to the lack of understanding the relationship between processing parameters and mechanical properties as measured by modulus of rupture (MOR).

A 5-year R&D program at AiResearch Casting Company (ACC), sponsored by DOE/NASA, is aimed at increasing the MOR of existing baseline ACC injection molded silicon nitride by 20% and the Weibull modulus (reliability) by 100% through process optimization using statistical experimental design and analysis. The major processing parameters investigated include raw materials, particle size distribution (milling), binder system, injection molding parameters, dewax cycle and sintering cycle. This paper discusses some of the initial results of the program demonstrating the effects of some of the processing parameters on the flexural strength of the test bars (MOR).

2. TEST BAR FABRICATION PROCEDURES

Figure 1 is a flow chart showing the major steps involved in a typical ceramic injection molding process. Although several raw Si_3N_4 materials are included in the program, the work described in this paper is limited to GTE SN 502 sizing with 6 wt.% Y_2O_3 and 2 wt.% Al_2O_3 as sintering aids. The as-received SN 502 Si_3N_4 was air-classified to remove the coarser fraction of the powder before being mixed with Y_2O_3 and AL_2O_3 through milling. Milling time was varied from 8 to 96 hours to produce a range of particle size distributions (PSD) for investigation. Steel mill jars with rubber

*Presented at 1985 SAE AEROSPACE TECHNOLOGY conference and exposition, Oct. 14-17, Long Beach CA

lining and Si_3N_4 milling media were used to minimize contamination. A Leeds and Northrup Microtrac particle size analyzer was used to characterize the milled powders.

An ACC proprietary binder system at 15.5 wt% was blended with the milled powder. A sigma mixer at a controlled temperature, rpm and time cycle was used to form an injection mix. The blended material was then pelletized before being fed into an injection molder. An Arburg, screw-type injection molder was used in this program, which has the capability of temperature and pressure variation. The material was injection molded into a four cavity test bar die producing bars nominally 6.1 x 0.73 x 0.37 cm (2.4" x 0.291" x 0.146"). The binder was removed from the test bars in a nitrogen furnace pressurized at 69 kPa (10 psi) gauge pressure using a proprietary thermal cycle. Binder removal of more than 99% complete was normally accomplished.

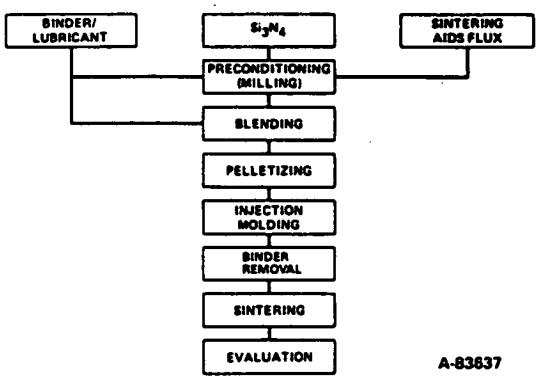

Figure 1. Injection Molding Process Flow Chart

Sintering of the dewaxed test bars was carried out in a 690 kPa (100 psi) N_2 furnace using a thermal cycle with a peak temperature of 1850°C (3362°F).

Visual inspection up to 40x under a binocular microscope was performed on each bar after injection molding, dewaxing, and sintering, respectively. Based on the inspection, a quality grade on a scale of 0 to 5, 0 being the best, was assigned. In addition, conventional x-ray radiographic inspection was made on the bars after each step of processing. Weight change of the test bar at each processing step was also monitored.

The room temperature 4-point flexural strength (MOR) of sintered test bars was measured on an Instron testing machine at a cross head speed of 0.5 mm/min (0.02"/min).

3. RESULTS AND DISCUSSIONS

(a) Baseline Test Bars

The baseline test bars were processed using the 24 hr milled powder and injection molded at 77°C (170°F) material temperature and 9.6 MPa (1400 psi) injection pressure. The resulting sintered baseline test bars, a total of 66, yielded test bars having surface quality ranging from grades 0 to 4, with grade 3 being the most frequent as shown in Figure 2. The strengths (MOR's) of the bars are plotted on a Weibull statistic graph, Figure 3, to obtain the Weibull modulus (a measure of reliability). From this plot and a computer program, the Weibull modulus was determined to be 7.9 and the average strength was 547 MPa (79.3 ksi). To illustrate the relationship between test bar surface quality and strength, the visual surface quality grade and test bar serial number are marked next to each datum point, as shown in Figure 3. There is a clear trend that the lower the MOR the higher is the surface quality grade (i.e. more surface defects). This observation indicates that the surface quality is one of the most important factors in influencing the strength of test bars under flexure test conditions, when sample density, composition and micro-structure were not intentionally varied. It is possible that the degree of sub surface defects, which are often found to be the failure origins under bending, are directly proportional to the degree of defects on the surface.

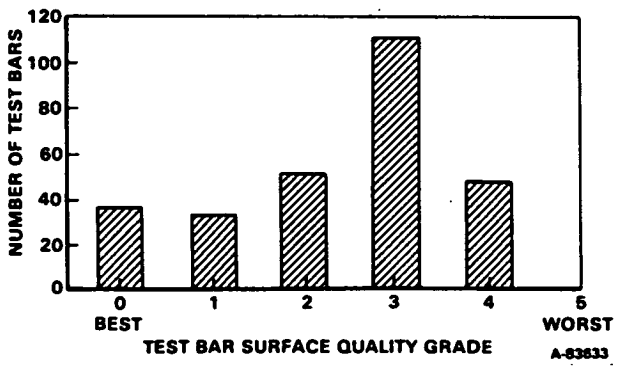

Figure 2. Distribution of Sintered Test Bars as a Function of Surface Quality

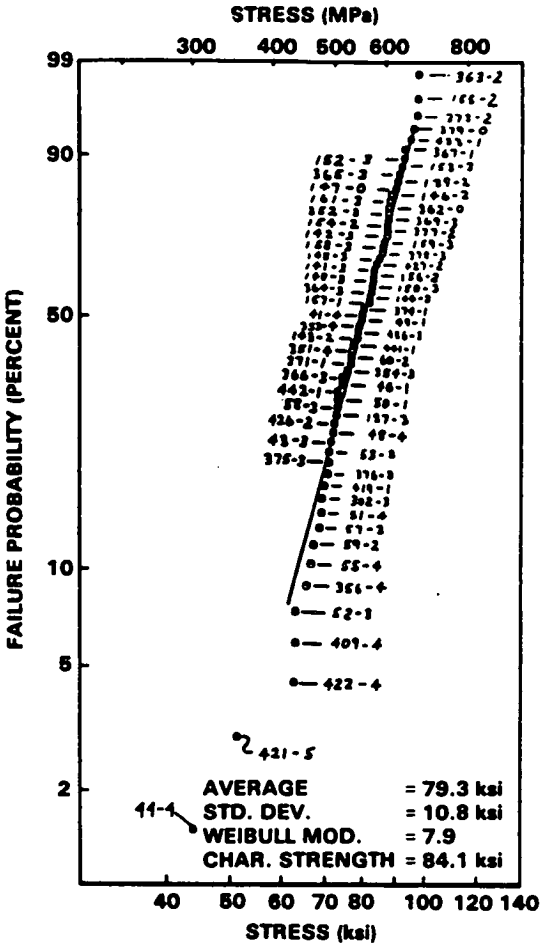

Figure 3. Weibull Plot on Baseline Bars

(b) Milling Time (or Particle Size Distribution) and Molding Temperature Effects

GTE SN 502 Si_3N_4 plus 6% Y_2O_3 and 2% Al_2O_3 were milled for 8, 24, 48 and 96 hrs to produce a range of particle distributions. Figure 4 shows the progressive reduction in particle size with increased milling time until 48 hrs, beyond which the reduction is particle size is not clear. The scatter in particle size at 24 hr milling time could be due to variation in as-received Si_3N_4.

Injection molding mixes prepared from the powders milled for different length of time were characterized on a Haake torque rheometer. The operating parameters (temperature and rpm) were chosen to represent the range of operating conditions used on the injection molding machine to fabricate

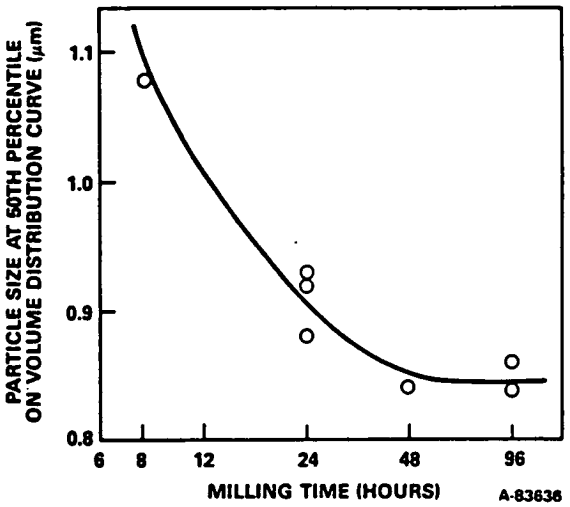

Figure 4. Median Particle Size Resulting from Ball Milling

the test bars. The output of the rheometer, mixing torque, correlates with the test bar molding behavior. Figure 5 shows a systematic variation of the mixing torque output of the rheometer. The rheometer was operated under the chosen thermal cycle, as indicated in the figure, at 60 rpm. It also shows the mixing torque decreases as the particle size decreases with increased milling time (1).* Lower material viscosity, indicated by lower mixing torque, results in easier flow in injection molding. Excessively high and low viscosities have adverse effects on the molded parts as to be discussed later.

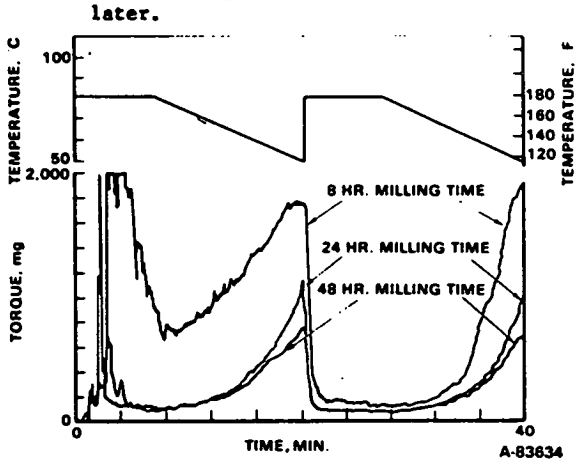

Figure 5. Mixing Temperature Profile and Mixing Torque Response for Powders Milled 8, 24, and 48 Hours

*Number designates reference at the end of the paper.

Based on a series of controlled injection molding experiments, a molding quality diagram as a function of molding temperature and powder milling time (or PSD) is constructed as shown in Figure 6. Test bars molded in the "insufficient fluidity" region, Figure 6, show severe surface defects while testbars molded in the "excess fluidity" region require lower molding pressures which results in internal defects (voids). The "good injection" region produces test bars with acceptable surface quality (grades 0 to 1), with no detectable internal voids in the as-molded condition.

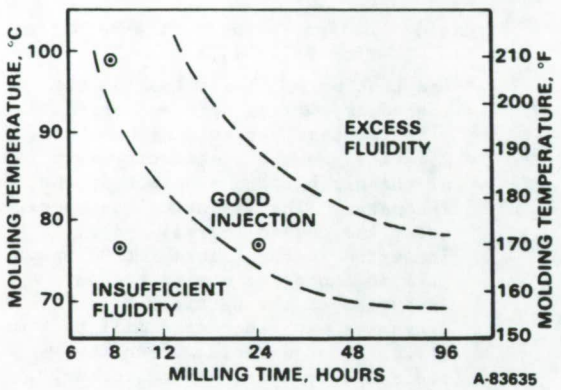

Figure 6. Flow Characteristics of Injection Molding Materials as a Function of Injection Milling Time and Material Temperature During Molding

Figure 6, illustrates that a given powder, such as the 8 hr milled powder, can be molded with different quality depending on the injection condition. A good quality test bar was made with the 8 hr milled powder, (Figure 7a) at 99°C (210°F), while a very poor test bar was molded with the same powder at 77°C (170°F), (Figure 7b). However, a good test bar can be molded at 77°C (170°F) if a finer PSD powder (24 hr milled powder) is used as shown in Figure 7c. Figure 8 shows typical defects on surface of dewaxed test bars produced from materials subjected to 48 or 96 hours of milling. This type of defect, sink marks, probably resulted from the excess quantity of wax (more than required to provide good as-injected test bars) which, upon removal, produces unfilled space (voids) under the surface. The relatively low temperatures required for good injection of 48 to 96 hour powders also suggests that excess binder is present.

(c) Sintering Effects

The defects found on the surface of as-dewaxed test bars normally remain but become less prominent upon sintering. The surface appearance of test bars #910 and #1068 after sintering are shown in Figure 9a and 9b, showing the changes from the appearance of the same bars before sintering as shown in Figure 7b and Figure 8. The surface quality grades and room temperature MOR's of these two sintered test bars are also indicated in Figure 9, again the lower the surface quality the lower the strength.

a. 8 Hr. Milled Powder 210°F Molding Temperature

b. 8 Hr. Milled Powder 170°F Molding Temperature

c. 24 Hr. Milled Powder 170°F Molding Temperature

Figure 7. Photographs of As-Injected Test Bars Showing Effects of Injection Temperature and PSD

Figure 8. Dewaxed Test Bar Made With Powder Milled 96 Hours

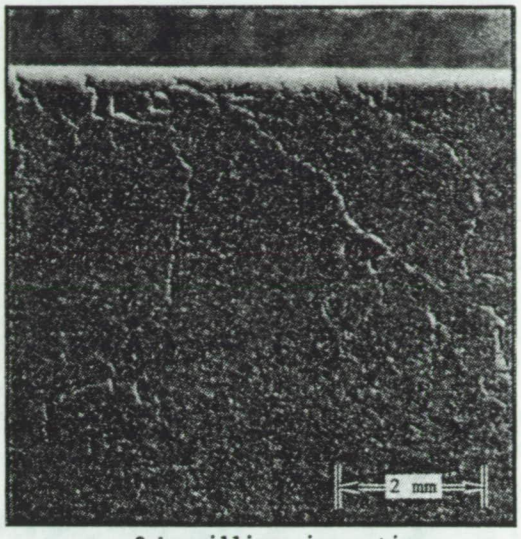

a. 8 hr milling, inspection grade 5, 35 ksi bend strength

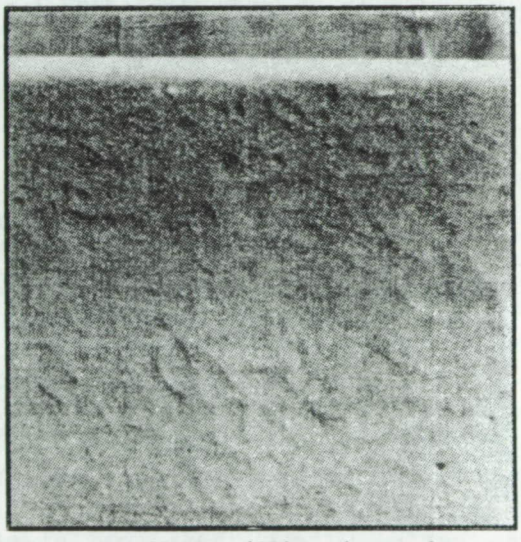

b. 96 hr. milling, inspection grade 4, 58 ksi bend strength

Figure 9. As-Sintered Test Bars Showing Improved Surfaces Compared To Earlier Processing Steps

4. CONCLUSIONS

(a) The as-sintered room temperature average strength and Weibull modulus of a baseline silicon nitride material are 547 MPa (79.3 ksi) and 7.9, respectively.

(b) In general the strength of the baseline test correlates with the surface quality observed at 40x.

(c) Torque rheometer is an effective tool to characterize the flow behavior of a ceramic injection mix and mixing torque output can be correlated with injection molding behavior of test bars.

(d) At a given injection pressure, quality of injection molded test bars can be varied by adjusting injection temperature and powder particle size distribution.

(e) Additional surface defects appear on test bars made from powders having very fine particle size distributions or made using excess binder.

(f) The mechanical properties of as sintered injection molded test bars, strongly depend on processing parameters such as particle size distribution, injection molding parameters, and binder systems.

References

1. J. A. Mangels, "Development of Injection Molded Reaction Bonded Si_3N_4," Ceramics for High Performance Applications -II, Editors J. J. Burke, E. N. Lenoe and R. N. Katz, Metals and Ceramics Information Center, Columbus, Ohio, 1977, p. 113-130.

APPENDIX B

TASK II TEST MATRIX AND EXPERIMENTAL TEST PLAN (REVISED) JULY 23, 1985

1. INTRODUCTION

The objective of Task II is to conduct a series of test matrixes to establish optimized materials and processing parameters to achieve the initial program goal of improving the test bar properties. Figure B-1 shows the estimated overall schedule for Task II.

The initial two test matrixes, 1st Iteration, are designed based on prior experiences and the results obtained in Tasks I and VII. They are to be completed in the first seven months of this task. Subsequent test matrixes in the 2nd Iteration, and the optimization experiments, are to be designed based on the results of the 1st Iteration and the continuing Task VII studies. At the end of Task II, a set of optimized material/processing parameters are to be selected for Task III, Optimized MOR Bar Study, to demonstrate reproducibility and to fabricate test bars for evaluation at NASA-Lewis.

In figure B-1, the two test matrixes in the 1st Iteration are termed 1st and 2nd test matrixes, and the two in the 2nd Iteration are 3rd and 4th test matrixes.

A proposed matrix design and experimental procedures for the 1st Iteration are described in this plan. Upon the completion of the 1st Iteration, a plan for the 2nd Iteration and the parallel optimization experiments will then be formulated and submitted for approval.

2. SELECTION OF KEY VARIABLES

The fractographic analyses conducted in Tasks I and VII indicated that surface, subsurface and internal flaws and foreign inclusions were the major failure origins of the MOR test bars tested. In addition, MOR test results suggest that strengths of sintered bars are related to test bar bulk densities and surface quality grades. To improve the strength (both room and high temperature) and reliability of the test bars, it is necessary to reduce/eliminate the above-mentioned defects in the test bars.

Based on prior experience and results obtained in the first nine months in this program, the following six variables are considered most important and thus are selected for initial evaluation in the 1st Iteration in this task. A brief discussion of each of these variables follows.

- Raw Materials: It was found in Task VII that the starting raw material has a strong influence on the processing behavior. The interaction between starting powder and several of the processing steps results in parameters which may be optimum for one material but unsatisfactory for another. It is desirable to evaluate more than one material in the test matrix study of Task II.

  Task I baseline powder, GTE SN-502, is not included in the first iteration of Task II. Lot-to-lot variations, identified in Tasks I and VII, led to variable results from the same processing. The version of GTE SN-502 Si_3N_4 used in Task I is no longer available.

  Two Si_3N_4 materials, Starck H-1 and Denka 9FW, are more consistent in properties, compatible with the injection molding process, and available in quantities required for this program. These two materials are recommended for evaluation in parallel in the 1st Iteration, Task II, as test Matrix 1 and test Matrix 2, respectively.

  Task VII will continue to evaluate/monitor the evolution of GTE SN-502 Si_3N_4 properties. We will reconsider GTE SN-502 Si_3N_4 for future Task II evaluations when the GTE production process reproducibly yields a suitable, injection-moldable grade power.

- Consolidation Method: A new sinter/HIP cycle has been developed recently at ACC which produces higher-density parts than the 0.68 MPa (100 psi) N_2 sintering. Therefore, two levels of consolidation methods, sintering and sinter/HIP, are included in the test matrix.

- Consolidation Environment: Covering Si_3N_4 samples in a high temperature powder such as Si_3N_4 or BN in sintering usually improves the surface quality of the sintered test bars. Comparison will be made between with and without powder bed in sintering and sinter/HIP. The powder chosen for initial study is BN.

- Mixing (Blending): Some of the internal flaws in the test bars most likely resulted from nonuniform mixing of the injection mix. The baseline sigma mixing will be compared with sigma mixing plus extrusion.

- Sintering Aid: To improve the high temperature strength of the test bars, it is necessary to reduce the sintering aid level. The results from Task VII suggest that 6% Y_2O_3 + 1% Al_2O_3 is a promising initial candidate for evaluation in comparison with the baseline 6% Y_2O_3 + 2% Al_2O_3.

- o Binder Concentration: The baseline binder still appears to be an acceptable binder until an improved binder is developed. However, results from Task VII suggest that a lower binder content may minimize dewax defects. 15.5% (baseline) and 14.5% are included in the evaluation.

3. EXPERIMENTAL DESIGN (1ST ITERATION)

To include all six variables previously mentioned, two five-factor matrixes will be conducted. One matrix applies to Starck H-1 and the other to Denka 9FW Si_3N_4. These first two matrixes are identical in design except that the raw materials used are different.

The matrix design is a half replicate of a 2^5 fractional factorial design as shown in figure B-2. A brief discussion of this design follows:

For an experiment of five factors, each in two levels, the full-factorial design consists of 32 treatment* combinations (2^5). In the first iteration of Task II, (months 1 through 7), only half replicate of the full design is used. The full matrix is then divided into two blocks of confounding ABCDE interaction, each block will include 16 treatments, and the following block of treatment combinations is chosen as the first iteration of the Task II experiment:

1, ab, ac, bc, ad, bd, cd, abcd, ae, be, ce, abce, de, abde, acde, bcde

The "1" denotes the treatment combination in which every factor is at its lower level; treatment "ab" represents the higher levels of factors A and B and the lower level of all other factors; treatment "abed" is the higher levels of all four factors and so on. These treatment combinations are indicated in the shaded areas of figure B-1.

By conducting only a half replicate of a factorial design, each effect will be confused with another effect, that is, the effects occur in pairs which are termed "aliases". It is imperative to determine the aliases for any fractional design in order to avoid confusion of important effects. The alias structure of the fractional factorial experiment in figure B-1 is shown in table B-1. The symbol "=" in table B-1 implies "alias with." In table B-1, it is indicated that all the main effects and two factor interactions can be evaluated if three and more factor interactions are negligible. Thirty bars will be tested in each treatment. It is realized that this is only one sample. To repeat the experiment to obtain more replications (obtain several samples) is prohibited by time and budget. However, in the case of ceramic materials, the within-sample variation is so large compared with

*Treatment is a statistical term referring to a unique combination of experimental parameters. In the original proposal and elsewhere in this plan the term "treatment" is used interchangeably with "experiment".

the variation of between-sample that the repeat sampling is statistically less important, but the power for detecting differences in the analysis of variables will be reduced.

An important feature of most industrial experiments is that the observations are made in sequence, either singly or in sets of a few at a time, so that the results of one set become available before the next set need be started. Following this procedure when investigating a number of factors, even when a full factorial design may ultimately be required, requires dividing the factorial design into blocks confounding higher order interactions and dealing with these blocks in succession, examining each as soon as it is completed.

It may happen that the first block will give all information required. In this case the other blocks need not be examined. If one or more of the factors demonstrates a large effect, all further work will be confined to the more favorable levels of such factors. The experiment is then redesigned with fewer factors, or, if required, with other factors to replace the ones dropped as a result of the first trial.

In the Task II experimental design, (1st Iteration, months 1-7), the factors are investigated at two levels. This does not necessarily restrict the range over which the factors are examined, because the experiment in Task II consists of a series of fractional replicates in which each of the factors are examined at two levels, but not necessarily at the same two levels in the whole series.

4. TEST BAR FABRICATION AND CHARACTERIZATION

Both in-process and post-process characterizations will be conducted for each experiment (or treatment) as outlined in figure B-3.

The characterization procedures are somewhat modified from the one in the proposal based on the experience learned in the first nine months of the program. Post process characterization now includes high-temperature MOR testing on a minimum of three test bars from each experiment.

5. SCHEDULE - 1ST ITERATION

Figure B-4 is the proposed schedule showing the activities for both Matrixes 1 and 2 covering the period July 1985 through January 1986.

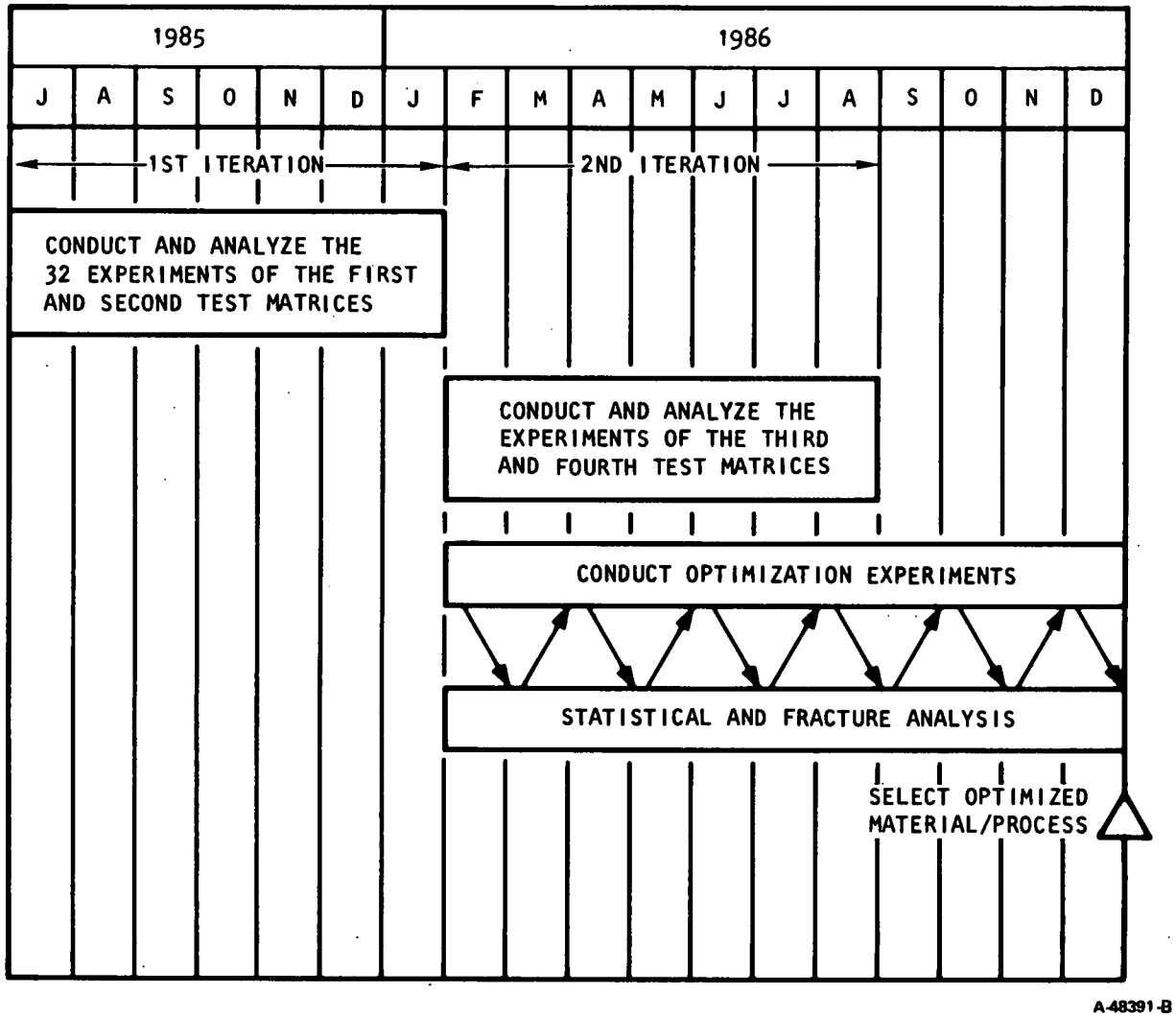

Figure B-1.--Estimated Schedule for Task II.

1/2 REPLICATE OF A 2^5 FRACTIONAL FACTORIAL DESIGN

		C+				C-			
		D+		D-		D+		D-	
		E+	E-	E+	E-	E+	E-	E+	E-
	B+		abcd	abce		abde			ab
	B-	acde			ac		ad	ae	
A-	B+	bcde			bc		bd	be	
	B-		cd	ce		de			1

A = CONSOLIDATION METHODS — SINTERING (A-) VS SINTER/HIP (A+)

B = CONSOLIDATION ENVIRONMENT — WITHOUT POWDER BED (B-) VS WITH POWDER BED (B+)

C = MIXING — SIGMA MIXER (C-) VS SIGMA MIXER PLUS EXTRUDER (C+)

D = SINTERING AIDS — (6% Y_2O_3 + 2% Al_2O_3) (D-) VS (6% Y_2O_3 + 1% Al_2O_3) (D+)

E = BINDER CONTENT — 15.5% (E-) VS 14.5% (E+)

A-82151

Figure B-2.--Experimental Design.

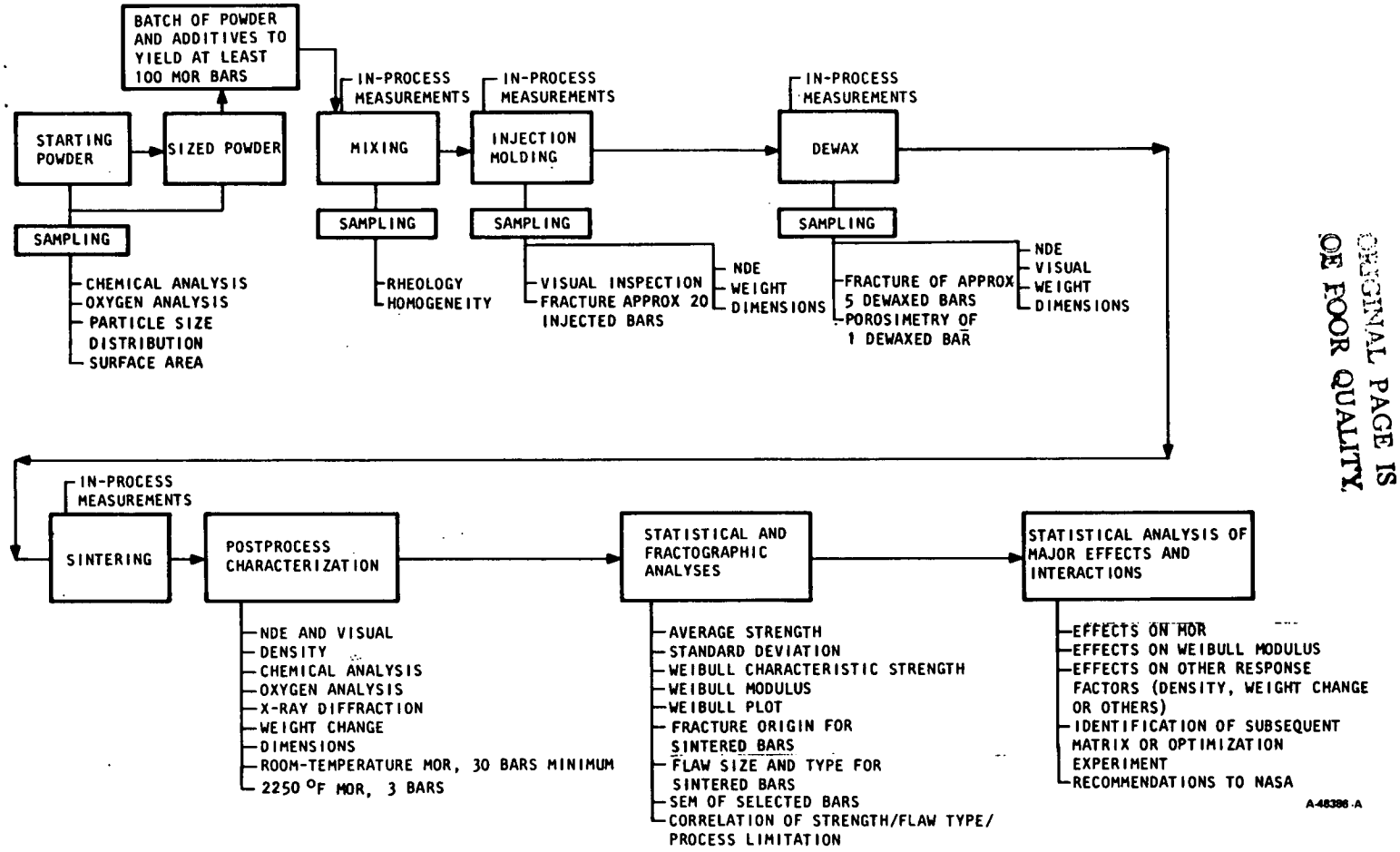

Figure B-3.--Process Flowchart Showing In-Process and Post-Process Characterization.

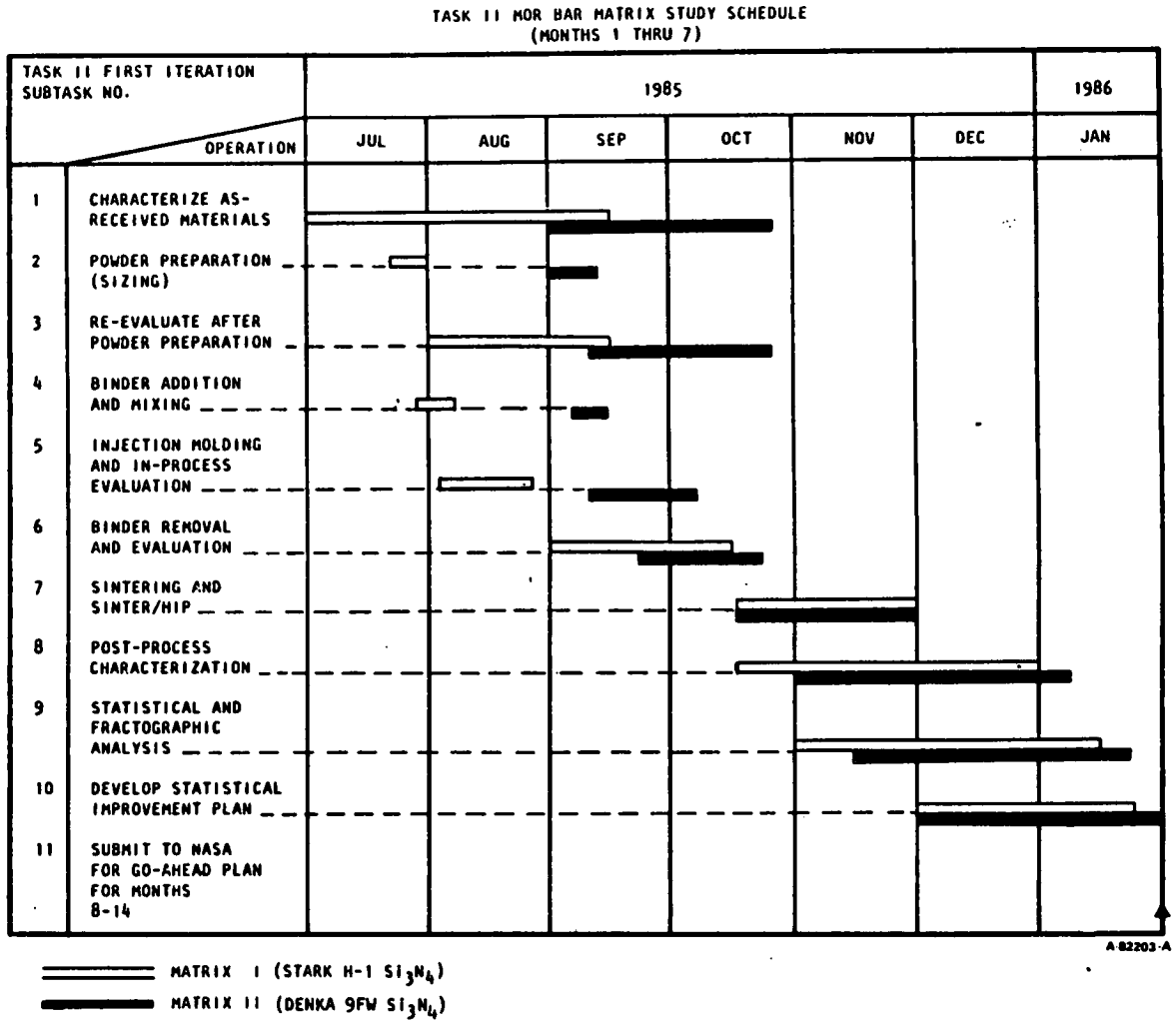

Figure B-4.--Proposed Schedule for Matrixes 1 and 2.

TABLE B-1

ALIAS STRUCTURE OF THE HALF REPLICATE OF A 2^5 FRACTIONAL FACTORIAL DESIGN CONFOUNDING ABCDE

A = BCDE	AD = BCE
B = ACDE	BD = ACE
C = ABDE	CD = ABE
D = ABCE	AE = BDC
E = ABCD	BE = ACD
AB = CDE	CE = ABD
AC = BDE	DE = ABC
BD = ADE	

APPENDIX C

GLOSSARY

ACC	AiResearch Casting Company
A/C	Air classified
AR	As-received
BET	Brunauer-Emmett-Teller Surface Area Measurement Method
BSE	Back scatter electron imaging in SEM
EDX	Energy dispersive X-ray analysis
GTE	General Telephone and Electronics, Inc.
GTEC	Garrett Turbine Engine Company
HIP	Hot isostatic pressing
IRT	IRT Corporation, San Diego, CA
ksi	Thousand pounds per square inch
L/N	Leeds and Northrup
MOR	Modulus of rupture
NASA	National Aeronautics and Space Administration
PSD	Particle size distribution
RBSN	Reaction-Bonded Silicon Nitride
RPM	Revolutions per minute
SEM	Scanning electron microscope
USP	Ultrasonic probe dispersion time